Abstract

Four rocket observations of the NO $\gamma(1, 0)$ 2148 Å band airglow and ground observations of the NI 5200 Å emission in the auroral zone are presented.

A radiometer was developed to measure the NO $\gamma(1, 0)$ band airglow in the mesosphere and thermosphere. It can extract the $\gamma(1, 0)$ band airglow from intense background radiations by making use of a self-absorbing gas cell. NO density profiles were deduced from the $\gamma(1, 0)$ band emission rates measured at Uchinoura (31°N), Thumba (9°N) and Syowa Station (69°S). The NO densities in the thermosphere obtained at middle and low latitudes are found to vary with solar activity. In view of a considerable temperature dependence of the production rate of NO in the thermosphere, the variation may be attributed to change in thermospheric temperature, which is closely related to solar activity. Change in the solar extreme ultraviolet radiation flux may also be responsible for the variation. The NO density in the mesosphere and the lower thermosphere obtained in the auroral zone is found to be larger than those obtained at middle and low latitudes under the conditions of similar solar activity. Because of a long life time of NO in the altitude region, the observed enhancement may be due to the after-effect of a particle precipitation event which occurred within a day before in despite of no polar disturbance during the flight.

The emission rate of the NI 5200 Å doublet in the aurora was measured with a tilting-filter photometer at Syowa Station from March to September 1977. The N_2^+ 1NG(0, 1) 4278 Å band emission was measured simultaneously with the 5200 Å emission for comparison. Examining nighttime variations of the emissions obtained in thirteen clear and moonless nights, the 5200 Å emission is found to be one of the common spectral features of the aurora. A simple model calculation is performed to investigate the excitation mechanism for the 5200 Å emission in the aurora, and dissociative recombination of NO^+ is found to be insufficient to explain the observations. Alternatively, impact dissociation and excitation of N_2 by auroral electrons may be the major excitation process. The ratio of measured 5200 Å emission rate to the 4278 Å emission rate decreases as the 4278 Å emission rate increases. This tendency may be qualitatively explained by the combined effect due to the highly forbidden nature of the 5200 Å emission and the characteristics of the precipitating particles in that their mean energy generally increases with their total energy.

General Introduction

The earth's atmosphere is known to radiate optical emissions called the airglow, and at high latitudes a remarkable phenomenon, the aurora, has long been recognized. These emissions have been conveniently used to investigate physical and chemical processes occurring in the upper atmosphere. Of these emissions, the NO $\gamma(1, 0)$ 2148 Å band dayglow and the NI 5200 Å doublet emission in the aurora are investigated in the present study. From a rocket measurement of the γ-band dayglow, the NO density in the mesosphere and thermosphere can be deduced. The 5200 Å doublet is spontaneously emitted from the metastable atomic nitrogen $N(^2D)$, whose reaction with O_2 is believed to be the major source for NO in the thermosphere.

NO is a minor constituent in the upper atmosphere; however, as seen in the case of O_3 in the stratosphere such minor constituents sometimes play important roles in the upper atmosphere in spite of their small relative abundance. The importance of NO in the upper atmosphere was first recognized by NICOLET (1945). He pointed out that NO may be photoionized by the solar Lα radiation in the ionospheric *D* region, and NO^+ may be the dominant positive ion in the lower ionosphere. The solar Lα radiation whose wavelength is accidentally coincident with one of the atmospheric windows can penetrate deep into the upper atmosphere and ionizes NO, but cannot ionize major constituents of the upper atmosphere. The chemistry in the lower ionosphere cannot be discussed without a knowledge of the NO density distribution.

The NO density distribution in the lower thermosphere was first successfully estimated by BARTH (1964) from a measurement of the γ-band airglow with a scanning spectrometer on board a sounding rocket. The value for the NO density deduced from his experiment was much larger than that theoretically predicted by NICOLET (1960). The chemical reactions considered to be important in producing NO in the lower thermosphere at that time were $N(^4S)+O+M\rightarrow NO+M$ and $N(^4S)+O_2\rightarrow NO+O$ (NICOLET, 1965a). Another producing reaction of NO in the lower thermosphere had to be looked for.

Some new reactions were proposed by NICOLET (1965b), BARTH (1966a) and HUNTEN and MCELROY (1968); however, their proposals were found to be incapable

of explaining the observation by BARTH (1964). The missing producing reaction of NO was finally found by NORTON and BARTH (1970). They pointed out that the reaction $N(^2D)+O_2 \rightarrow NO+O$ is important in producing NO in the lower thermosphere. The observations of the NO density by BARTH (1964, 1966b) were roughly explained by this reaction, where $N(^2D)$ is supplied by dissociative recombination of NO^+, N_2^+ and the reaction of N_2^+ and O (NORTON and BARTH, 1970). The $N(^2D)$ density distribution has been deduced from a rocket or a satellite measurement of the 5200 Å airglow (WALLACE and MCELROY, 1966; RUSCH *et al.*, 1975; TORR *et al.*, 1976; FREDERICK and RUSCH, 1977).

Rocket measurement of the NO γ-band airglow and deduction of NO density distribution in the mesosphere and lower thermosphere were successfully made by MEIRA (1971), TISONE (1973), TOHMATSU and IWAGAMI (1975, 1976) and BAKER *et al.* (1977), and their measurements show that the NO density profile usually has its peak of about 3×10^7 cm^{-3} at around 110 km. Satellite measurements of the γ-band have been carried out by RUSCH (1973), RUSCH and BARTH (1975), GÉRARD and BARTH (1977) and CRAVENS and STEWART (1978), and latitudinal and seasonal variations of the NO total content in the thermosphere have been investigated. These satellite measurements show that the thermospheric NO content is larger at high latitude than at low latitude by a factor of 2 to 4, and represent rather small seasonal variation of a few tens percent. This latitudinal dependence of the NO total content may be caused by a horizontal transport of NO produced in the auroral zone (RUSCH and BARTH, 1975; CRAVENS and STEWART, 1978).

In response to these observations, theoretical models of minor constituents in the mesosphere and thermosphere were developed by many investigators. The diurnal variation of the odd nitrogen species (NO, $N(^4S)$ and $N(^2D)$) was calculated by STROBEL (1971) by solving time-dependent continuity equations. And the theoretical models were developed farther by ORAN *et al.* (1975) and OGAWA and SHIMAZAKI (1975). Recent theoretical model calculations performed by KONDO and OGAWA (1977) and OGAWA and KONDO (1977) show that the thermospheric NO density distribution strongly depends on thermospheric temperature, which is dependent on solar activity and local time. This is mainly due to the fact that the rate coefficient of the most important producing reaction of NO above 130 km, $N(^4S)+O_2 \rightarrow NO+O$, increases rapidly with temperature. Though the diurnal variation of the thermospheric NO total content of a factor of about 2 has been inferred from a satellite observation (STEWART and CRAVENS, 1978), the dependence of the thermospheric NO density on solar activity has not been confirmed. It is due to the fact that most of the observations mentioned before were made during a period of rather low solar activity, and that the observations of NO density distribution above 130 km, where the temperature dependence is expected, were few. Rocket observations of the NO density distribution above 130 km were first reported by TOHMATSU and IWAGAMI (1976) and recently by TRINKS *et al.* (1978) and THOMAS

(1978), but the last instance may be ascribed to a background contamination.

At the same time, much attention has been paid to the NO density in the polar upper atmosphere since an incredibly large NO density in an auroral arc was inferred from mass-spectrometric measurements (ZIPF *et al.*, 1970; DONAHUE *et al.*, 1970). In addition, a strong emission was observed at the wavelength very close to that of the NO $\gamma(1, 0)$ band in an auroral spectrum (DUYSINX and MONFILS, 1972; FELDMAN, 1976; BEITING and FELDMAN, 1978). However, this auroral emission is now considered to be due to the NII 2140/2144 Å doublet (DICK, 1978; SHARP, 1978).

NO density profiles in the polar upper atmosphere were obtained from airglow measurements by WITT *et al.* (1976) and IWAGAMI and OGAWA (1980), but the former result may be ascribed to large uncertainty due to the intense Rayleigh scattered continuum. Satellite observations by the use of the $\gamma(1, 0)$ band airglow found 2 to 4 times larger NO content at high latitude even under geomagnetically quiet conditions than at middle latitude (RUSCH and BARTH, 1975; GÉRARD and BARTH, 1977; CRAVENS and STEWART, 1978). They also found a high variability of NO content and its strong correlation with geomagnetic disturbance.

Behaviors of the odd nitrogen species under an auroral perturbation have been theoretically investigated by KONDO and OGAWA (1976), ROBLE and REES (1977), HYMAN *et al.* (1976) and REES and ROBLE (1979). They show that an enhancement of the NO density in the polar upper atmosphere may be caused by the efficient production of $N(^2D)$ by auroral processes. However, behavior of $N(^2D)$ associated with an auroral event is little known since a quantitative and persistent observation of the 5200 Å emission in the aurora is scarce.

Considering these circumstances, it seems necessary to obtain NO density distribution in the upper atmosphere at high latitude as well as at middle latitude, and to observe the 5200 Å emission in the aurora.

PART 1. ROCKET OBSERVATION OF THE NO γ-BAND AIRGLOW AND DEDUCTION OF NO DENSITY

1.1. Introduction

Rocket and satellite measurements of the NO γ-band($X^2\Pi$–$A^2\Sigma^+$) fluorescence can be used to deduce NO density in the mesosphere and thermosphere. In the mesosphere the measurement is influenced by a background noise due to the Rayleigh scattering of solar radiation by atmospheric molecules. The satellite measurements can provide useful data of only above 90 km, where the Rayleigh scattered sunlight is weak (RUSCH, 1973; RUSCH and BARTH, 1975; GÉRARD and BARTH, 1977; CRAVENS and STEWART, 1978; STEWART and CRAVENS, 1978). Again they have provided total content of NO, but have not provided a height profile of NO density. A rocket measurement is necessary to obtain a vertical NO density profile.

A number of vertical NO density profiles in the mesosphere and lower thermosphere have been inferred from rocket-borne spectrometer measurements of the $\gamma(1, 0)$ 2148 Å band fluorescence (BARTH, 1964, 1966b; MEIRA, 1971; TISONE, 1973). In the mesosphere the subtraction of the large Rayleigh scattering component from the measured signal is necessary to pick up the $\gamma(1, 0)$ band airglow component. This necessity can be satisfied by the use of a spectrometer; however, a spectrometer has some weak points in measuring the γ-band airglow. One is a difficulty in subtracting the Rayleigh scattering component because of a complicated structure of the solar flux in the vicinity of the band, and the other is its small throughput. Due to the latter reason, it seems difficult to measure the γ-band airglow above 130 km by using a spectrometer.

A small and simple radiometer having much larger throughput than a spectrometer has been developed by TOHMATSU and IWAGAMI (1975, 1976) for rocket-borne NO $\gamma(1, 0)$ band measurements. By this radiometer, it is possible, in principle, to obtain accurately both the $\gamma(1, 0)$ band emission and the Rayleigh scattering component.

The purpose of Part 1 of this study is to describe this radiometer system and the principle of data deduction, and to present four rocket measurements of the $\gamma(1, 0)$ band airglow at Uchinoura (31°N), Thumba (9°N) and Syowa Station (69°S).

1.2. Instrumentation

A remarkable feature of the radiometer used for the present study is that it makes use of the self-absorption by NO molecules to extract the NO γ-band emissions from the intense background continuum radiations such as the Rayleigh scattered sunlight. This type of a radiometer was first proposed by TOHMATSU and IWAGAMI (1975). Compared with a grating spectrometer this particular radiometer is smaller in size, less in weight and simpler in its optics. These facts are very favorable for an airglow measurement on board a small sounding rocket. Moreover, this radiometer has a larger ability to measure a faint emission than that of the grating spectrometer because of its non-dispersive optics.

The optical arrangement of the radiometer used for the experiments on board the sounding rockets S-210-9, ISRO 05-31 and S-210JA-27 is shown in Fig. 1.1. The radiometer consists of a light baffle, a honeycomb collimator with a field of view of 5° in full-angle, an interference filter, two fused silica cells and a solar blind photomultiplier HTV–R431S with CsTe photocathode. The interference filter has a peak transmittance of about 15% at around 2148 Å, and a FWHM band width of about 140 Å. One of the two fused silica cells is filled with 200 Torr ($\sim$0.26 atm) NO gas, whereas the other is blank. The transmittance of the blank cell at 2148 Å is about 70%. The photomultiplier is sensitive only between wavelengths of 1600 Å and 3000 Å.

The NO-filled cell can selectively absorb the (v', 0) band emissions of the NO

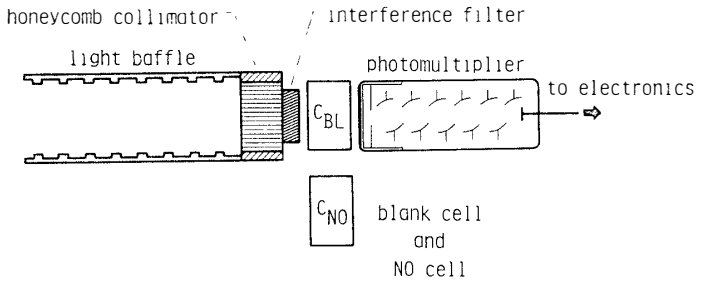

Fig. 1.1. Optical arrangement of the radiometer.

γ-bands. The two cells are alternatively placed in front of the photomultiplier, so as to extract the NO γ-band emissions from the Rayleigh scattered sunlight and other background continuum radiations. The selective absorption by a NO-filled cell is demonstrated in Fig. 1.2. It can be seen that the $v''=0$ progression bands of the $\gamma(v', v'')$ bands such as (0, 0), (1, 0) and (2, 0) are completely absorbed by the NO-filled cell, whereas the $v''\neq 0$ progression bands such as (2, 2), (1, 1) and (0, 1) are not absorbed. A completeness of the self-absorption by the NO-filled cell during the rocket experiments will be discussed in Subsection 1.6.3.

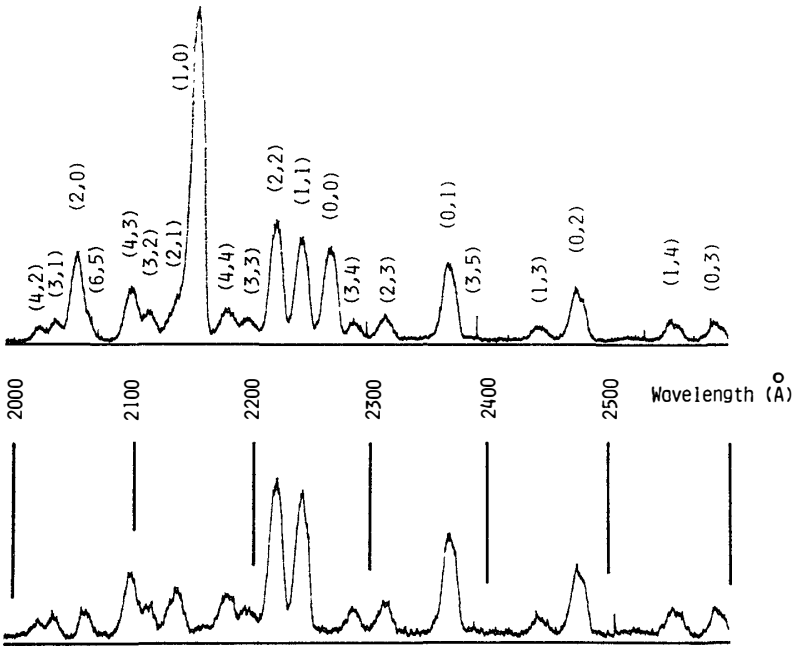

Fig. 1.2. Laboratory spectra of the NO γ-band fluorescence. Upper and lower figures are the spectra obtained with blank and NO cells, respectively.

The optical arrangement of the radiometer used for the S-310-6 experiment is a little different from others, since it was designed to measure the fainter γ-band emissions in the higher altitudes than other experiments. It consists of a fused silica lens with an effective diameter of 4.8 cm and a field stop in order to define the field of view, which is 12° in full-angle, instead of a honeycomb collimator. The radiometer for the S-310-6 experiment has about 25 times larger throughput than that of others.

A block-diagram of the radiometer is shown in Fig. 1.3. An output signal from the photomultiplier is dealt with by operational amplifiers and sent to the telemetry system of the sounding rocket. A high voltage supply feeds a stabilized voltage of 1 kV to the photomultiplier. A cell change controller consists of a micromotor, a gear-system and two microswitches, and drives the cells according to a clock signal.

Normal operation of the radiometer was checked before and after assembling

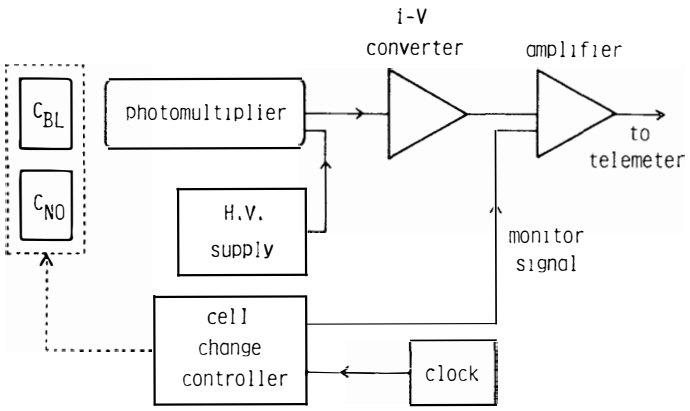

Fig. 1.3. Block-diagram of the radiometer.

payloads with a special care to find any unexpected small gaps, which may cause a contamination in the airglow signals, on the radiometer's body. These small gaps were, if found, filled carefully, however, the contamination due to these gaps was sometimes found in the airglow signals. The radiometer was mounted at the top portion of payloads with its optical axis parallel to the spinning axis of the rocket.

1.3. Principle of Measurement

1.3.1. Extraction of the $\gamma(1, 0)$ band emission

As mentioned in the previous section, extraction of the NO γ-band emission is made by making use of the self-absorption by the NO molecules filled in a cell. Since the radiometer is designed to be sensitive only around the $\gamma(1, 0)$ band, which is the strongest of all the γ-bands, the major component other than the $\gamma(1, 0)$ band emission to be detected by the radiometer is the Rayleigh scattered sunlight around the wavelength of the $\gamma(1, 0)$ band. The Rayleigh scattered sunlight can pass through the NO cell, whereas the $\gamma(1, 0)$ band emission cannot pass through it. Therefore, the following formulae can be well approximated:

$$S_{BL}=C'(I_{10}+I_R+I_B) \tag{1.1}$$

and

$$S_{NO}=C'(I_R+I_B)\,, \tag{1.2}$$

where S_{BL} and S_{NO} are the output signals with the blank and NO cells, respectively; I_{10} is the intensity of the $\gamma(1, 0)$ band; I_R and I_B are the equivalent intensities of the Rayleigh scattered sunlight and other background radiations including instrumental contaminations, respectively; C' is an instrumental constant. The equivalent intensities I_R and I_B have the following meanings:

$$I_R=\int \eta_\lambda J_R(\lambda)\mathrm{d}\lambda \tag{1.3}$$

and

$$I_B=\int \eta_\lambda J_B(\lambda)\mathrm{d}\lambda\,, \tag{1.4}$$

where λ is the wavelength; η_λ is the spectral response of the radiometer normalized to its value at 2148 Å; J_R and J_B are the intensities of the Rayleigh scattered sunlight and other background radiations, respectively, per unit wavelength. Equations (1.1) and (1.2) can easily be transformed to the following formulae:

$$I_{10}=(S_{BL}-S_{NO})/C' \tag{1.5}$$

and

$$I_R+I_B=S_{NO}/C'. \tag{1.6}$$

By using eqs. (1.5) and (1.6) I_{10} can be determined within a precision of a few tens percent. These equations were used in data analysis of the S-210-9 experiment.

The following corrections were introduced to improve the approximation:

(a) other $\gamma(v', 0)$ band emissions than the (1, 0) band are also absorbed by a NO cell,

(b) other γ-band emissions than the $(v', 0)$ band can pass through a NO cell,

(c) transmission of a fused silica cell usually differs slightly from each other,

(d) the Rayleigh scattered sunlight and other background continuum radiations are partly absorbed by a NO cell at the wavelengths of the $\gamma(v', 0)$ bands.

Correction factors for (a), (b), (c) and (d) can be determined from a laboratory calibration as well as from the molecular constants of NO. Taking into account above corrections, eqs. (1.1) and (1.2) are reformed to the following:

$$S_{BL}=C[I_{10}+\sum_{v'\neq 1}\eta_{v'0}I_{v'0}+\sum_{v'}\sum_{v''>0}\eta_{v'v''}I_{v'v''}+(I_R+I_B)] \tag{1.7}$$

and

$$S_{NO}=Cf[\sum_{v'}\sum_{v''>0}\eta_{v'v''}I_{v'v''}+(1-w)(I_R+I_B)]\,, \tag{1.8}$$

where

C: instrumental constant to be given experimentally,

$\eta_{v'v''}$: spectral response of the radiometer at the wavelength of the (v', v'') band normalized to its value at 2148 Å,

f: wavelength-averaged ratio of the transmittance of the NO cell to that of the blank cell at the wavelengths of no selective absorption,

w: ratio of the total equivalent absorption band width of the NO cell to the equivalent band width of the radiometer's sensitivity,

$I_{v'v''}$: intensity of the (v', v'') band.

The second and third terms of eq. (1.7) and the factors f and w correspond to the corrections (a), (b), (c) and (d), respectively.

The second and the third terms in eq. (1.7) and the first term in eq. (1.8) can be easily simplified by using the relation:

$$I_{v'v''}=(g_{v'v''}/g_{10})I_{10}\,, \tag{1.9}$$

where $g_{v'v''}$ is the specific emission rate factor of the (v', v'') band, and is almost constant. Evaluation of $g_{v'v''}$ will be described in Subsection 1.6.1. Substituting eq. (1.9), eqs. (1.7) and (1.8) are transformed to the following:

$$S_{BL}=C[(1+\alpha+\beta)I_{10}+(I_R+I_B)] \tag{1.10}$$

and

$$S_{NO}=Cf[\beta I_{10}+(1-w)(I_R+I_B)] \tag{1.11}$$

with

$$\alpha=(\sum_{v'\neq 1}\eta_{v'0}g_{v'0})/g_{10} \tag{1.12}$$

and

$$\beta=(\sum_{v'}\sum_{v''>0}\eta_{v'v''}g_{v'v''})/g_{10}\,. \tag{1.13}$$

The factors α and β represent physically the portion of the output signals due to the γ-bands other than the (1, 0) band. Other correction factors, f and w, as well as η_λ and $\eta_{v'v''}$ are determined by a laboratory calibration (see Section 1.4). Typical values of α, β, f and w are about 0.1, 0.3, 0.98 and 0.04, respectively. Since there remain only two unknown variables, I_{10} and (I_R+I_B), in eqs. (1.10) and (1.11), it is possible to solve these equations for these two variables. The explicit expressions for them are

$$I_{10}=\frac{(1-w)fS_{BL}-S_{NO}}{Cf[(1+\alpha)(1-w)-w\beta]} \tag{1.14}$$

and

$$I_R+I_B=\frac{(1+\alpha+\beta)S_{NO}-f\beta S_{BL}}{Cf[(1+\alpha)(1-w)-w\beta]}\,. \tag{1.15}$$

Equations (1.14) and (1.15) were used in the data analyses of the ISRO 05-31, S-210-JA-27 and S-310-6 experiments.

1.3.2. Evaluation of the γ(1, 0) band emission rate

By using eqs. (1.14) and (1.15) relative height profiles of I_{10} and (I_R+I_B) can be drawn. However, their values cannot be known until the instrumental constant C is determined. Though a calibration of a radiometer's sensitivity is generally made by using a suitable standard light source, another method was adopted in the present study.

Our present method makes use of the Rayleigh scattered sunlight measured simultaneously with the γ-band airglow. The instrumental constant C is determined so as to fit the measured intensity of the Rayleigh scattered sunlight to the theoretically calculated one. Before this procedure I_R must be separated from (I_R+I_B), which can be made assuming a constancy of I_B. This assumption is well approximated as far as the data in the lower altitudes (below 90 km) are concerned, where I_R is expected to be much larger than I_B. A variation of I_B may affect the value of C little. The major components of I_B are instrumental contaminations such as leaked solar radiation and/or scattered earth shine. Contribution from stellar sources is found to be almost negligible (*i. e.*, less than a few Rayleighs), as far as the G2 type stars are concerned. This particular method may give higher accuracy than that by the standard light source method. Because a laboratory calibration of a radiometer's sensitivity is not easy to attain a high accuracy, whereas the values for the constants and parameters of the Rayleigh scattering of the sunlight in the atmosphere are rather well defined. And our present method has another advantage that a value of NO

density determined cannot be affected by a variation of the solar flux (see Subsection 1.6.4).

The apparent emission rate (4π times the intensity) of the Rayleigh scattered sunlight per unit wavelength in the zenith direction can be formulated as

$$4\pi J_{\mathrm{R}}(z, \lambda)=\frac{3}{4}(1+\cos^2 \xi) \int_z^{\infty} \sigma_{\mathrm{R}}(\lambda)\Phi_{\lambda} n(\mathrm{M}, z')\mathrm{d}z' , \tag{1.16}$$

where z is the altitude; λ is the wavelength; ξ is the scattering angle; σ_{R} is the cross section of the Rayleigh scattering; Φ_{λ} is the solar flux density and $n(\mathrm{M}, z')$ is the total number density of the scattering particles in the atmosphere. Equation (1.16) is based upon a single scattering approximation since attenuation of the solar radiation along the ray-path can usually be neglected even under the twilight conditions. The cross section of the Rayleigh scattering is calculated by the empirical formula given by DALGARNO (1962):

$$\sigma_{\mathrm{R}}=(3.776\times 10^{-28}/\lambda_{\mu}^4)(1+0.00567/\lambda_{\mu}^2) , \qquad (\mathrm{cm}^2) \tag{1.17}$$

where λ_{μ} is the wavelength (μm). To evaluate eq. (1.16) numerically, $n(\mathrm{M}, z')$ was taken from CIRA (1972) and Φ_{λ} from BRINKMAN *et al.* (1966) ($\lambda<3000$ Å) and from THEKAEKARA (1974) ($\lambda>3000$ Å). Actual procedures for the determination of C by this method will be shown in Subsection 1.5.2.

Besides the method discussed above, another way to determine the instrumental constant is available by making use of a measured response of the photomultiplier. The measurement was made by the manufacturer. In this case the instrumental constant C^* in ampere per Rayleigh unit is given in the form:

$$C^*=10^6(\omega/4\pi)SeA_{\mathrm{p}}T_{\mathrm{l}}T_{\mathrm{c}}T_{\mathrm{f}} , \tag{1.18}$$

where ω is the solid angle of the radiometer's field of view; S is the effective detecting area; e is the charge of an electron; A_{p} is the response of the photomultiplier at 2148 Å (electrons photon^{-1}); T_{l}, T_{c} and T_{f} are the transmittance of the lens, cell and interference filter, respectively, at 2148 Å. The values of C and C^* have been found to agree with each other within a factor of two. Since the intensity of the Rayleigh scattered sunlight at the altitudes below 110 km failed to be measured in the S-310-6 experiment, C^* was adopted in the S-310-6 data analysis.

1.4. Laboratory Calibration

A purpose of laboratory calibration of the radiometer is to determine the optical parameters such as η_λ, $\eta_{v'v''}$, f and w which are necessary for evaluating I_{10} and I_R. Spectral calibration for the radiometer was made by the procedures A and B schematically shown in Fig. 1.4. A light source is a deuterium (D_2) discharge lamp, which produces continuum radiation in the ultraviolet and visible wavelength region. It is followed by a grating monochromator through which the radiation with a spectral purity of about 1 Å comes out. The monochromators used are Hitachi Parkin-Elmer 139 (for the S-210-9, ISRO 05-31 and S-210JA-27 experiments) and Nikon P–250 (for the S-310-6 experiment). Since the width of the $\gamma(1, 0)$ band is about 10 Å, a spectral purity of 1 Å is adequate to determine optical characteristics of the radiometer. The detector used in the procedure A is the γ-band radiometer which is to be used in the rocket experiment.

S_A, the output signal obtained in the procedure A, can be expressed as

$$S_A(\lambda)=C_A L_\lambda M_\lambda \eta_\lambda , \tag{1.19}$$

where C_A is a constant; L_λ is the spectral distribution of radiation emitted by the D_2

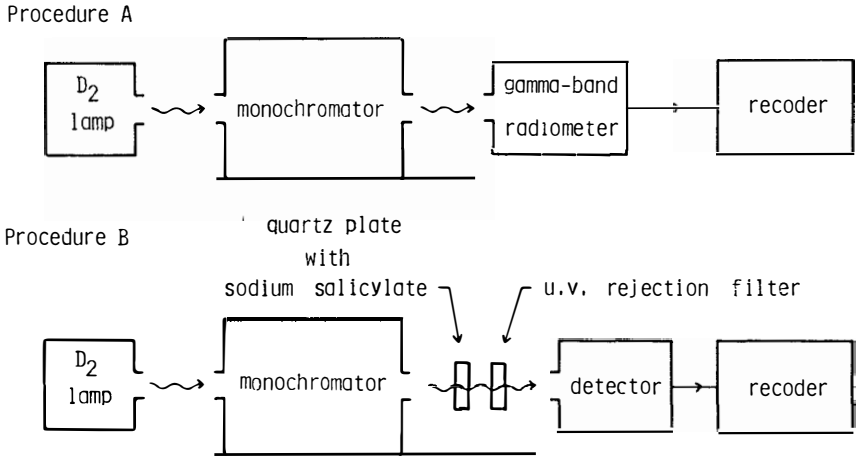

Fig. 1.4. Diagram of the laboratory calibration. Two procedures A and B are necessary for determining the spectral response of the radiometer.

lamp; M_λ is the spectral response of the monochromator and η_λ is the spectral response of the γ-band radiometer. Relative values of η_λ cannot be known until the product of L_λ and M_λ is determined. In order to determine $L_\lambda M_\lambda$ a fluorescence plate of sodium salicylate was adopted in the procedure B. The fluorescence quantum efficiency of sodium salicylate crystalline powder is almost constant over the wide wavelength range from 300 to 3400 Å (SAMSON, 1967), and the fluorescence spectrum, which has its peak intensity at 4200 Å, is independent of incident ultraviolet wavelength. Therefore, S_B, the output signal obtained in the procedure B being independent of the spectral response of the detector used can be written as

$$S_B(\lambda)=C_B L_\lambda M_\lambda\,, \tag{1.20}$$

where C_B is a constant. From eqs. (1.19) and (1.20), η_λ can be determined as

$$\eta_\lambda=C_{AB}[S_A(\lambda)/S_B(\lambda)]\,, \tag{1.21}$$

where C_{AB} is a constant being adjusted so as to fit $\eta_{2148\text{Å}}$ to unity.

A photomultiplier installed in the monochromator was used as the detector in the procedure B. The ultraviolet rejection filter is used to remove the ultraviolet radiations which failed to be absorbed by the sodium salicylate powder.

An example of S_A is shown in Fig. 1.5. The cells of the γ-band radiometer were alternately placed in front of the photomultiplier during the procedure in order to determine the optical parameters f and w. Therefore, S_A appears to consist of output signals with the blank cell (S_{BL}) and the NO cell (S_{NO}), and the former is defined to be proportional to $L_\lambda M_\lambda \eta_\lambda$. An example of η_λ calculated by using eq. (1.21) is shown in Fig. 1.6. The profile of η_λ is found to be almost identical to that of the

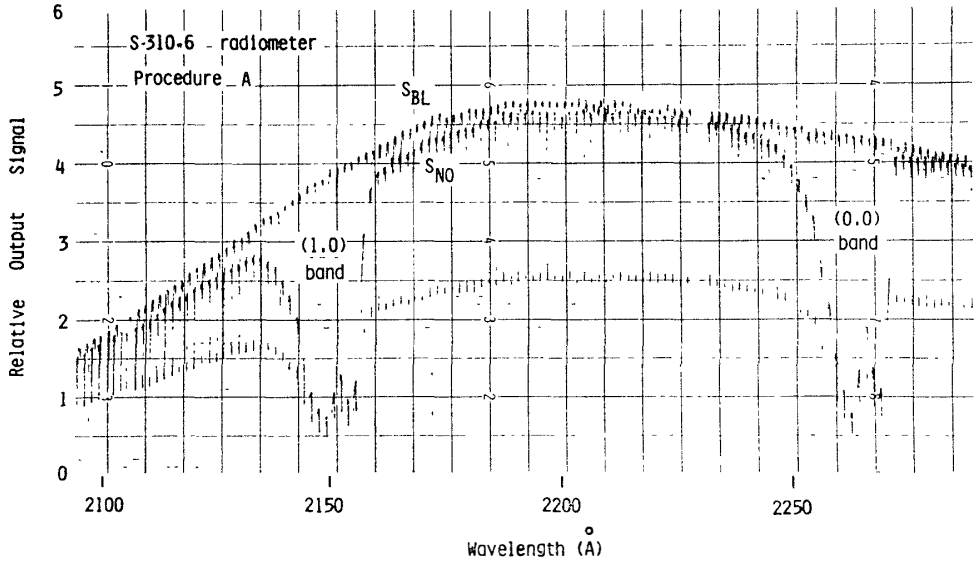

Fig. 1.5. Example of the output signal in the procedure A. S_{BL} and S_{NO} are the output signals with blank and NO cells, respectively.

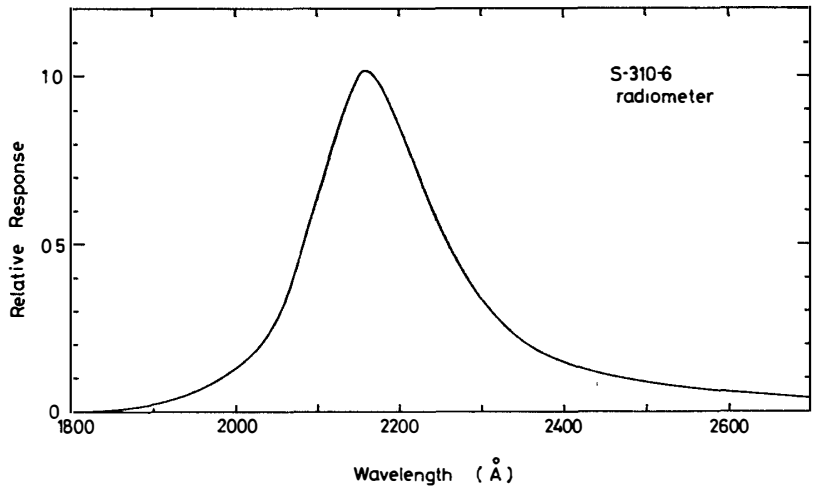

Fig. 1.6. Example of the spectral response of a radiometer normalized to its value at 2148 Å.

transmittance of the interference filter since the spectral response of the photomultiplier and the transmittance of the blank cell vary slowly over this wavelength region.

In Fig. 1.5, a little difference between S_{BL} and S_{NO} can be seen at wavelengths of no selective absorption, for example at 2200 Å. The correction factor f is given as a weighted mean of the ratios, S_{NO}/S_{BL}, at such wavelengths. The weighting function for S_{NO}/S_{BL} is η_λ. Also in the figure, the selective absorption at the wavelengths of the $\gamma(v', 0)$ bands is evident in S_{NO}. The correction factor w is given as a weighted sum of equivalent widths of these absorption bands divided by the equivalent band width of the radiometer's sensitivity. The weighting function is also η_λ.

1.5. Observation of the $\gamma(1, 0)$ Band Airglow

1.5.1. Rocket experiments

Four rocket experiments were carried out to measure the $\gamma(1, 0)$ band airglow. Rocket flight data are summarized in Table 1.1. The sounding rockets S-210-9 and S-310-6 were launched at Uchinoura (31°N); ISRO 05-31 is a Centaure IIB type rocket and was launched at Thumba (9°N) at geomagnetic equator; S-210JA-27 was launched at Syowa Station (69°S) in the auroral zone.

Table 1.1. Rocket flight data.

Sounding rocket	Launching site	Date	Time UT, LST	Solar zenith angle	Apogee (km)
S-210-9	Uchinoura (31°N, 131°E)	Aug. 19, 1973	0955, 1855	90°	115
ISRO 05-31	Thumba (9°N, 77°E)	Mar. 26, 1976	0135, 0705	82°	140
S-210JA-27	Syowa Station (69°S, 40°E)	Aug. 10, 1977	1247, 1547	92°	120
S-310-6	Uchinoura (31°N, 131°E)	Jan. 19, 1979	0850, 1750	94°	212

It must be noted that all of these rocket experiments were carried out at around the local sunset (S-210-9, S-210JA-27 and S-310-6) or at around the local sunrise (ISRO 05-31). A favorable geometry between the sun direction and the line of sight of the radiometer can be chosen under these conditions so as to avoid contamination due to direct incidence of the sunlight into the radiometer's light baffle. Therefore, these rockets were launched in the azimuthal direction opposite to the sun.

The airglow measurement took place after an ejection of the nose-cone of the rocket at around 60 to 70 km, and the photometric data were obtained until a tumbling of the rocket began when the rocket re-entered into the thick atmosphere below 90 km. Coning half-angles of the rockets S-210-9, ISRO 05-31, S-210JA-27 and S-310-6 were 5°, 9°, 4° and 14°, respectively, which were small enough to obtain good photometric data.

There was no anomalous geophysical event during or just before these four rocket experiments. Geophysical conditions during the S-210JA-27 experiment

made at Syowa Station in the auroral zone will be described in detail in Subsection 1.7.2.

1.5.2. Deduction of the $\gamma(1, 0)$ band emission rate

Figure 1.7 shows an example of raw output signals during a rocket experiment (S-310-6). Difference between S_{BL} and S_{NO} is evident in the figure, and is mainly due to the absorption of the NO $\gamma(1, 0)$ band emission by the NO molecules in the cell. Gradual decrease along the time sequence seen in both S_{BL} and S_{NO} is due to the fact that the rocket passed through an emitting layer. Dark-current level of the radiometer's output signal, which is not obvious in the figure, was determined from output signals before the ejection of the nose-cone of the rocket during the ascent.

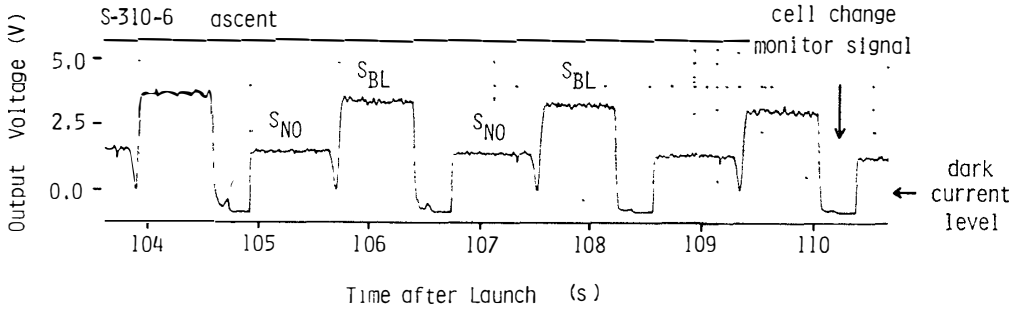

Fig. 1.7. Example of raw output signals during a rocket experiment.

S_{BL} and S_{NO} read on the strip charts were converted into the values in the zenith direction by using the relations, *e. g.*;

$$S_{BL}(\theta=0)=\cos\theta S_{BL}(\theta), \tag{1.22}$$

where θ is the angle between the zenith and the line of sight of the radiometer. Equation (1.22) is based upon a plane parallel approximation, which is valid as far as θ is smaller than 70°. Since the line of sight of the radiometer was set parallel to the spinning axis of the rocket, θ was kept less than 40° during an airglow measurement. Corrected S_{BL} and S_{NO} obtained in the S-210-9, ISRO 05-31, S-210JA-27 and S-310-6 experiments are plotted in Figs. 1.8, 1.9, 1.10 and 1.11, respectively.

An interpolation or a smoothing procedure is required to evaluate the emission rate of the $\gamma(1, 0)$ band ($4\pi I_{10}$) and the background radiations ($4\pi I_R+4\pi I_B$) since the values for S_{BL} and S_{NO} at the same altitude are necessary for evaluating these emission rates. Smoothed curves shown in Figs. 1.9 (ISRO 05-31) and 1.10 (S-210JA-27) were obtained by fitting data points with a least square method, whereas the data obtained in the S-210-9 and S-310-6 experiments shown in Figs. 1.8 and 1.11 were treated with an interpolation. $4\pi I_{10}$ and $4\pi I_R+4\pi I_B$ deduced from the data obtained in the S-210-9, ISRO 05-31, S-210JA-27 and S-310-6 experiments are shown in Figs. 1.12, 1.13, 1.14 and 1.15, respectively. In evaluating $4\pi I_{10}$ and $4\pi I_R+4\pi I_B$ from

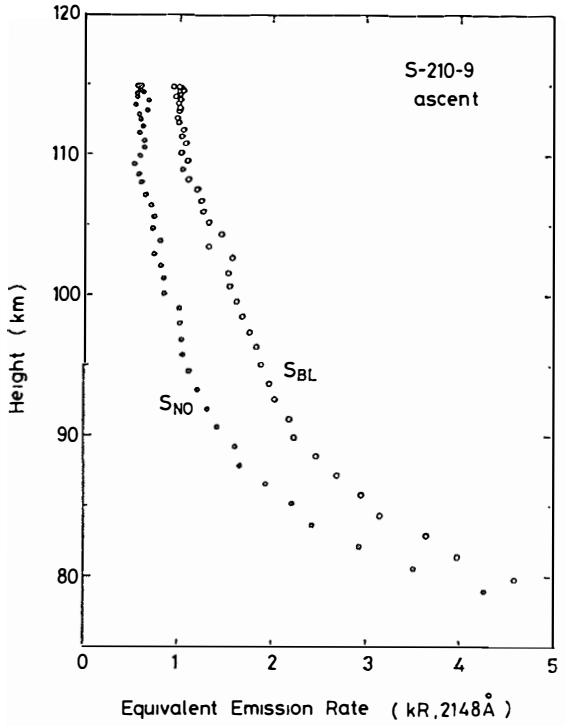

Fig. 1.8. Equivalent emission rates of the signals with a blank cell (S_{BL}) and a NO cell (S_{NO}) obtained in the S-210-9 experiment. The emission rate scale is given in equivalence to the 2148 Å radiation.

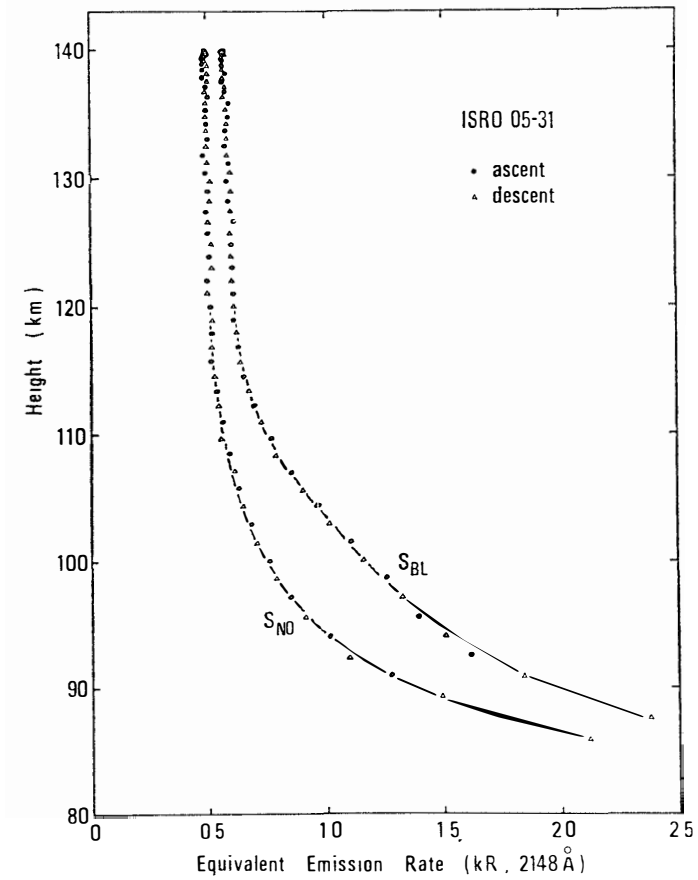

Fig. 1.9. Same as Fig. 1.8. but in the ISRO 05-31 experiment.

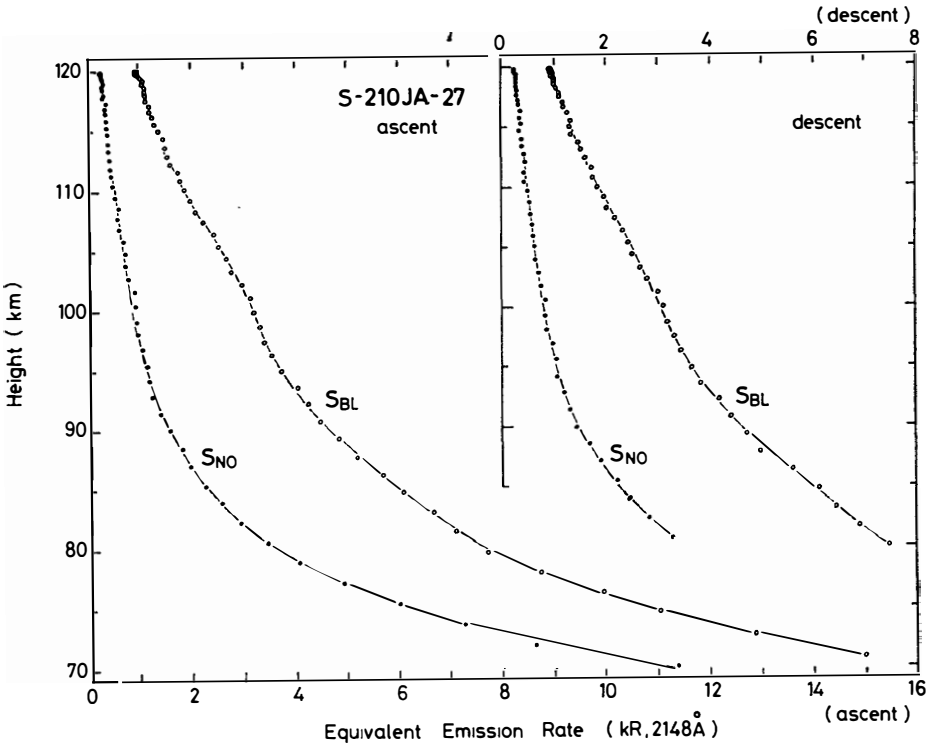

Fig. 1.10. Same as Fig. 1.8 but in the S-210JA-27 experiment.

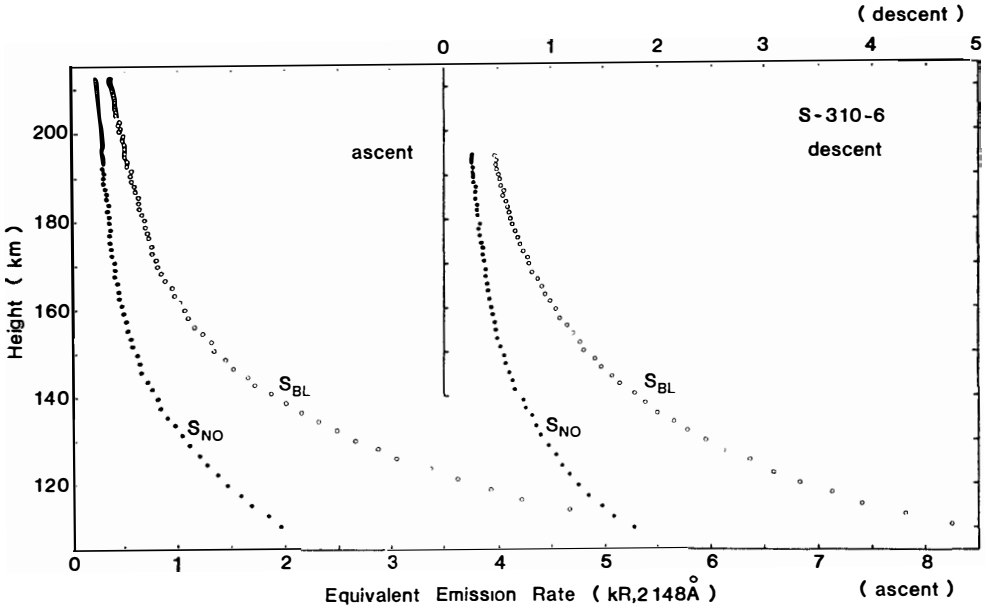

Fig. 1.11. Same as Fig. 1.8 but in the S-310-6 experiment.

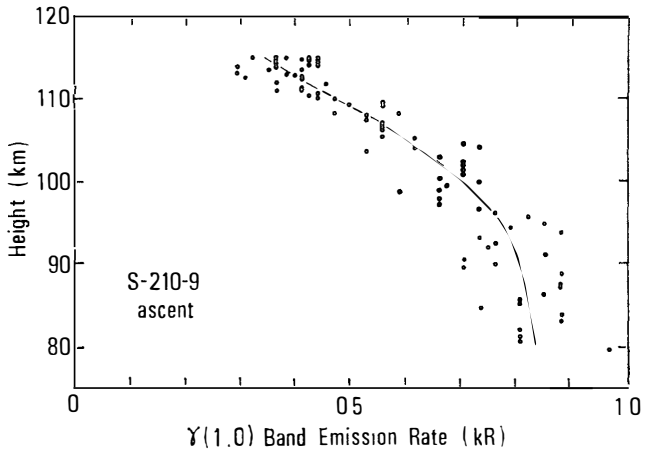

Fig. 1.12a. Emission rate of the NO $\gamma(1, 0)$ band obtained in the S-210-9 experiment.

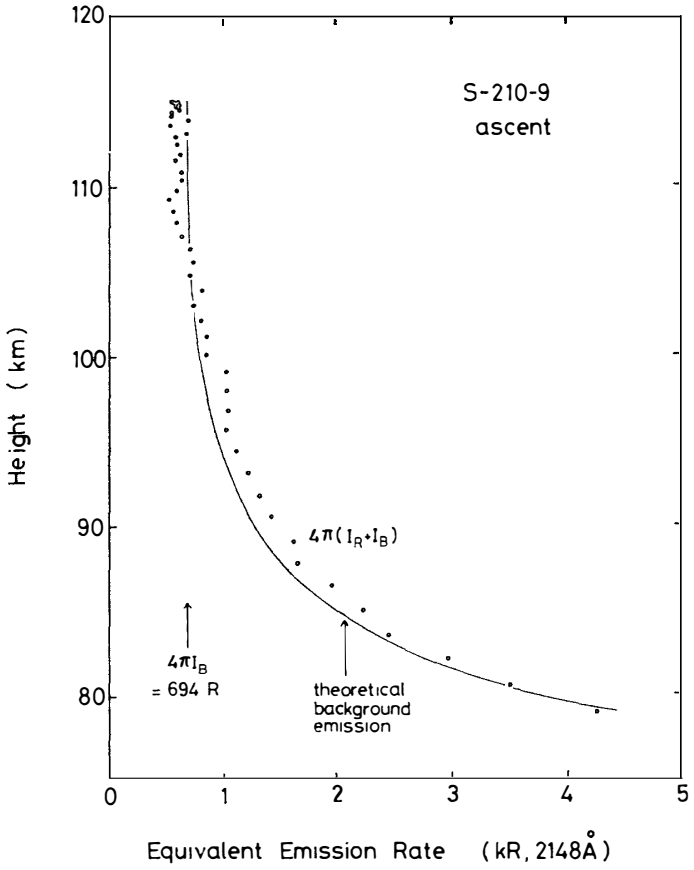

Fig. 1.12b. Equivalent emission rate of the background radiations ($4\pi I_R + 4\pi I_B$) obtained in the S-210-9 experiment. Also shown is the theoretical equivalent emission rate of the Rayleigh scattered sunlight superposed on a constant background.

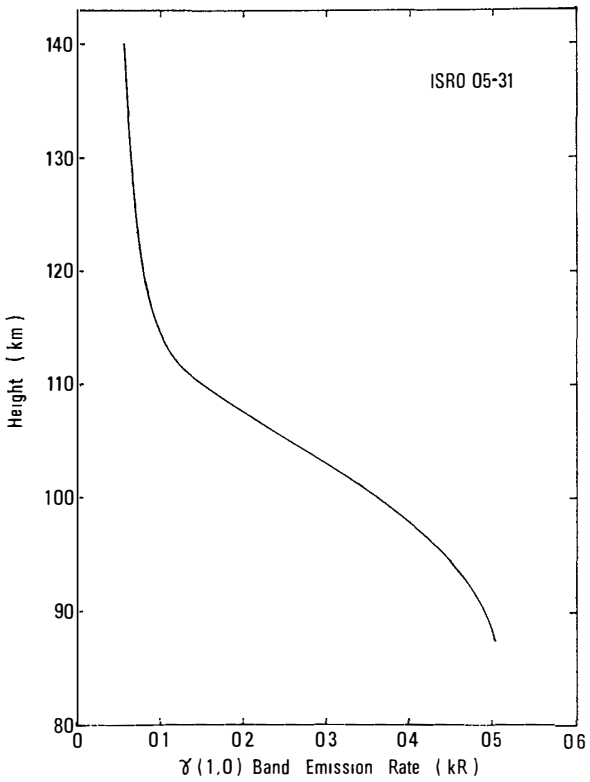

Fig. 1.13a. Same as Fig. 1.12a but in the ISRO 05-31 experiment.

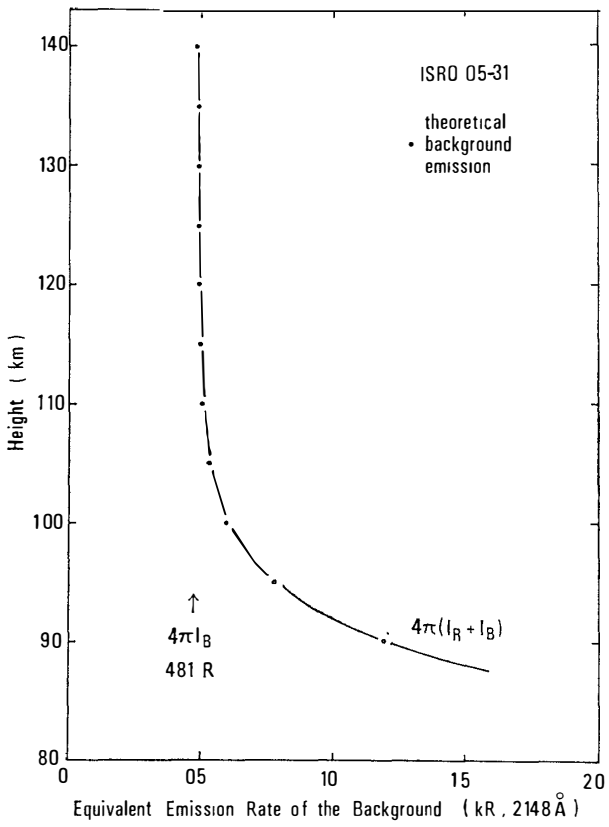

Fig. 1.13b. Same as Fig. 1.12b but in the ISRO 05-31 experiment.

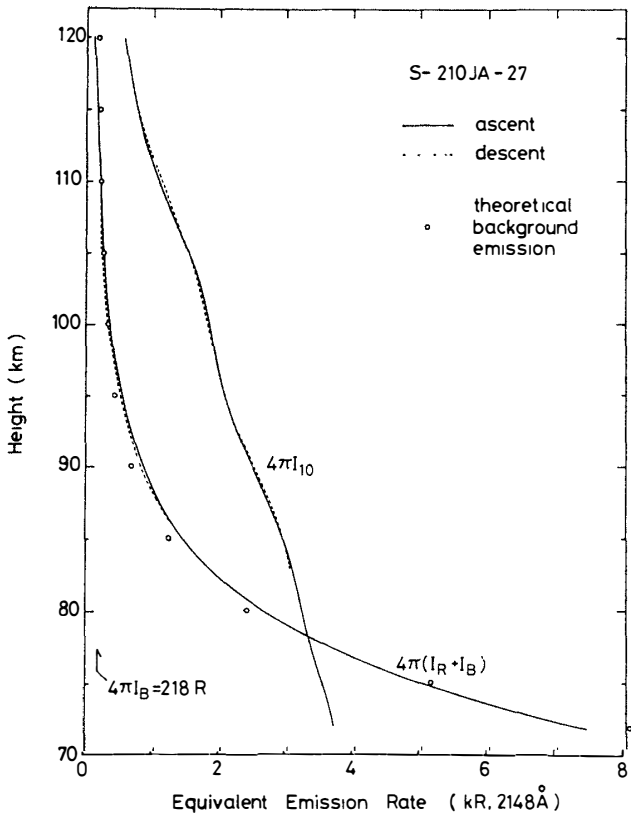

Fig. 1.14. Emission rate of the $\gamma(1, 0)$ band ($4\pi I_{10}$) and equivalent emission rate of the background radiations ($4\pi I_R+4\pi I_B$) obtained in the S-210JA-27 experiment. Also shown is the theoretical equivalent emission rate of the Rayleigh scattered sunlight superposed on a constant background.

S_{BL} and S_{NO}, eqs. (1.5) and (1.6) were used for the S-210-9 experiment and eqs. (1.14) and (1.15) for the others; interpolated values of S_{BL} and S_{NO} were used for the S-210-9 and S-310-6 experiments, and smoothed ones for the others in the evaluation of the emission rates.

Absolute values for the emission rate, except for the S-310-6 experiment, was determined so as to fit the measured emission rate of the Rayleigh scattered sunlight to the theoretical one as mentioned in Subsection 1.3.2. These theoretical emission rates of the background radiations deduced by using eqs. (1.3) and (1.16) are represented in Figs. 1.12b, 1.13b and 1.14. Model atmospheres for a suitable season and latitudes were taken from CIRA (1965, 1972) in evaluating eq. (1.16). $4\pi I_B$ was assumed so as to get the best agreement between the measured emission rate of the background radiations and the calculated one. Absolute values for the emission rate were determined by using the calibration data for the photomultiplier sensitivity in the S-310-6 experiment since the airglow signals at the altitude below 110 km could not be measured. Although the radiometer was designed to measure

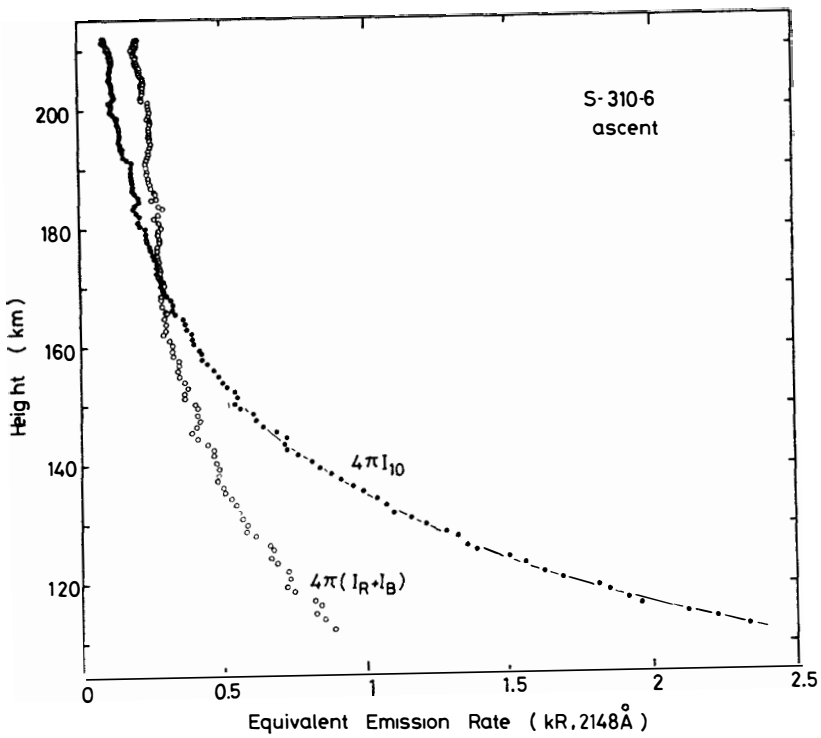

Fig. 1.15a. Same as Fig. 1.14 but in the ascent of the S-310-6 experiment.

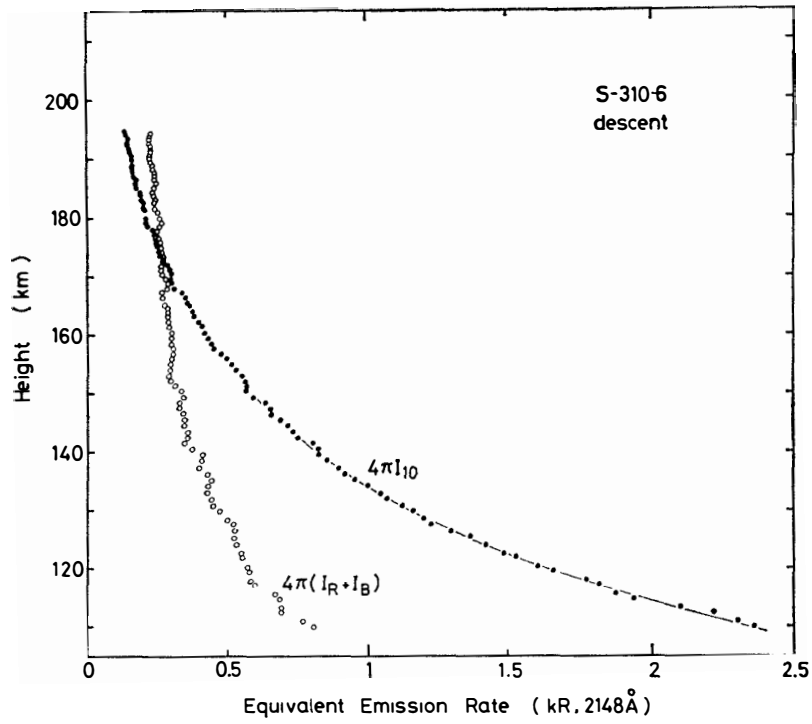

Fig. 1.15b. Same as Fig. 1.14 but in the descent of the S-310-6 experiment.

the airglow signals at the altitude as low as 90 km, unexpected large $\gamma(1, 0)$ band emission prevented the radiometer from measuring the airglow signals at the lower altitude. The emission rate of the Rayleigh scattered sunlight at the altitudes above 110 km is too small to be measured and to calibrate the $\gamma(1, 0)$ band emission rate.

Discrepancies between the observed and the theoretical emission rates for the background radiations are seen in Figs. 1.12b, 1.13b and 1.14. These discrepancies must be discussed since precision as well as accuracy in deducing the $\gamma(1, 0)$ band emission rate relate to these discrepancies. The discrepancy is apparent in Fig. 1.12b for the S-210-9 experiment. It may be due to the contribution from the $v''\neq 0$ progression of the $\gamma(v', v'')$ bands, since a simple data analysis by using eqs. (1.5) and (1.6) was adopted. On the other hand, the discrepancies appear to be smaller in the ISRO 05-31 and S-210JA-27 experiment as shown in Figs. 1.13b and 1.14, respectively, since more accurate analysis by using eqs. (1.14) and (1.15) was adopted in these cases. The discrepancies still remain; they may originate from (i) errors in the laboratory calibration, (ii) difference between the real and model atmospheres and/or (iii) unexpected airglow or auroral emissions at the wavelength of the radiometer's sensitivity. A calibration error more than a factor 2 is necessary for explaining the discrepancy, but such a large error is improbable. The second is also improbable because a temperature deviation of more than 50 K is required at around 90 km to induce the discrepancies. Even in the case of S-210JA-27 experiment, contamination of the auroral emissions such as NII 2140/2144 Å doublet (DICK, 1978; SHARP, 1978) may be neglected because of non-auroral condition. A possible explanation for these discrepancies is a contamination from the O_2 airglow in the Schumann-Runge band (HUDSON and MAHLE, 1972). However, it is hard to draw a definite conclusion at this time. The emission rate of the background radiations $(4\pi I_R + 4\pi I_B)$ obtained in the S-310-6 experiment shown in Figs. 1.15a and 1.15b may be mainly due to an instrumental contamination. In fact, the data just after the apogee were lost by a large contamination possibly due to direct incidence of the sunlight inside the radiometer's light baffle. Theoretical emission rate of the Rayleigh scattered sunlight is only a few tens Rayleighs at 120 km, and cannot explain the observed one.

1.5.3. Excitation mechanism of the $\gamma(1, 0)$ band

The observed $\gamma(1, 0)$ band emission can be attributed to resonance fluorescence of solar middle ultraviolet radiations by the atmospheric NO molecules in the processes:

$$\mathrm{NO}(X^2\Pi)+h\nu(\text{solar u.v.})\rightarrow \mathrm{NO}(A^2\Sigma^+) \tag{1.23}$$

followed by

$$\mathrm{NO}(A^2\Sigma^+)\rightarrow \mathrm{NO}(X^2\Pi)+h\nu(\gamma\text{-bands})\,. \tag{1.24}$$

Since the first excited electronic state $(A^2\Sigma^+)$ lies about 5 eV above the ground state

($X^2\Pi$), there is no significant thermal excitation to the $A^2\Sigma^+$ state at temperatures in the mesosphere and the thermosphere. Another excitation process has been suggested by WOFSY and MCELROY (1977). It is radiative recombination of atomic nitrogen and atomic oxygen:

$$\mathrm{N}+\mathrm{O}\rightarrow\mathrm{NO}(C^2\Pi) \quad \text{and} \quad \mathrm{NO}(A^2\Sigma^+) \tag{1.25}$$

followed by radiative cascading:

$$\mathrm{NO}(C^2\Pi)\rightarrow\mathrm{NO}(A^2\Sigma^+)+h\nu(1.22\ \mu\mathrm{m}) \tag{1.26}$$

and spontaneous emission (1.24). However, a contribution from this process is considered to be as small as a few Rayleighs at the relevant altitude (FELDMAN and TAKACS, 1974), and is neglected in the present study. Though many auroral excitation mechanisms for the γ-band emissions have been proposed (SHARP and REES, 1972; CALLEAR and WOOD, 1971; IMAMI and BORST, 1975; FELDMAN, 1976), the $\gamma(1, 0)$ band emission obtained in the S-210JA-27 experiment can also be attributed to resonance fluorescence mechanism. Geophysical conditions during the S-210-JA-27 experiment were so calm that the auroral excitation could not contribute to the $\gamma(1, 0)$ band emission obtained in the experiment. The γ-band arises from an allowed transition ($A^2\Sigma^+\rightarrow X^2\Pi$) with a spontaneous emission coefficient larger than $10^6\ \mathrm{s}^{-1}$. No quenching process can affect the height profile of the $\gamma(1, 0)$ band emission rate at the relevant altitude. Therefore, an observed height profile of the $\gamma(1, 0)$ band emission rate in the zenith direction should be proportional to the column density of the atmospheric NO in the zenith direction. Note that a strict proportionality is broken by the self-absorption effect (see Subsection 1.6.2).

1.6. Deduction of NO Density

1.6.1. Calculation of the emission rate factor: A simple treatment

The specific emission rate factor of the $\gamma(v', v'')$ band, $g_{v'v''}$, is defined as a number of photons emitted in the $\gamma(v', v'')$ band within a unit time interval by one NO molecule when illuminated by the solar radiation. BARTH (1966a) has already calculated some of them; however, many other emission rate factors than those included in his report are necessary in the present study. Neglecting both the rotational structure of a band and the self-absorption by the atmospheric NO molecules, $g_{v'v''}$ can be calculated by the formula (BARTH, 1966a):

$$g_{v'v''}=(\pi e^2/mc^2)f_{0v'}\bar{\Phi}_{0v'}(A_{v'v''}/\sum_{v''} A_{v'v''}) , \tag{1.27}$$

where $f_{0v'}$ is the oscillator strength of absorption for the $(v', 0)$ band; $\bar{\Phi}_{0v'}$ is the solar flux density averaged in the vicinity of $(v', 0)$ band (photons $cm^{-2}\ s^{-1}\ (cm^{-1})^{-1}$); $A_{v'v''}$ is the spontaneous emission coefficient of the (v', v'') band and $\pi e^2/mc^2=8.85\times 10^{-13}$ cm. In evaluating eq. (1.27), $f_{0v'}$ was taken from MARR (1964) and $\bar{\Phi}_{0v'}$ from BRINKMAN *et al.* (1966). $A_{v'v''}$ were calculated from $f_{0v'}$ and Franck-Condon factors, $q_{v'v''}$, given in NICHOLLS (1964) by using the formulae (CHAMBERLAIN, 1961):

Table 1.2. Physical quantities related to the γ-band emission rate.

Band $v'v''$	Wavelength (Å)	$f_{0v'}$	$\bar{\Phi}_{0v'}$ (**)	$A_{v'v''}$ (s^{-1})	$g_{v'v''}$ (photons s^{-1})
0 0	2262	4.14E–4*	6.82E11	5.42E5	2.75E–6
0 1	2362			7.53E5	3.82E–6
0 2	2470			5.91E5	3.01E–6
0 3	2586			3.47E5	1.76E–6
0 4	2712			1.69E5	8.58E–7
0 5	2848			7.32E4	3.71E–7
0 6	2998			2.89E4	1.47E–7
0 7	3171			1.06E4	5.38E–8
0 8	3349			3.71E3	1.88E–8

Table 1.2. (*Continued*).

Band $v'v''$	Wavelength (Å)	$f_{0v'}$	$\bar{\Phi}_{0v'}$ (**)	$A_{v'v''}$ (s^{-1})	$g_{v'v''}$ (photons s^{-1})
1 0	2148	7.94E–4	5.18E11	1.15E6	7.88E–6
1 1	2238			3.11E5	2.13E–6
1 2	2338			3.09E3	2.12E–8
1 3	2439			1.74E5	1.19E–6
1 4	2550			2.79E5	1.92E–6
1 5	2670			2.39E5	1.64E–6
1 6	2800			1.51E5	1.03E–6
1 7	2941			7.96E4	5.46E–7
1 8	3094			3.72E4	2.55E–7
1 9	3261			1.59E4	1.09E–7
1 10	3443			6.35E3	4.35E–8
2 0	2047	6.81E–4	1.79E11	1.09E6	2.02E–6
2 1	2128			5.95E4	1.10E–7
2 2	2215			4.61E5	8.55E–7
2 3	2309			1.85E5	3.42E–7
2 4	2410			4.02E2	7.42E–10
2 5	2516			7.48E4	1.38E–7
2 6	2630			1.59E5	2.94E–7
2 7	2757			1.62E5	3.00E–7
2 8	2888			1.17E5	2.17E–7
2 9	3032			6.99E4	1.29E–7
2 10	3189			3.64E4	6.74E–8
2 11	3360			1.72E4	3.18E–8
3 0	1956	3.54E–4	8.26E10	6.19E5	2.40E–7
3 1	2030			7.62E5	2.94E–7
3 2	2109			1.42E5	5.49E–8
3 3	2193			1.29E5	4.98E–8
3 4	2283			2.99E5	1.16E–7
3 5	2379			1.08E5	4.17E–8
3 6	2481			2.02E2	7.80E–11
3 7	2580			4.86E4	1.88E–8
3 8	2697			1.11E5	4.29E–8
3 9	2823			1.21E5	4.67E–8
3 10	2958			9.49E4	3.66E–8
3 11	3105			6.11E4	2.36E–8
3 12	3264			3.44E4	1.33E–8
3 13	3435			1.76E4	6.80E–9

* 4.14E–4 is read as 4.14×10^{-4}.

** photons $cm^{-2}\,s^{-1}\,Å^{-1}$.

$$A_{v'0}=(8\pi^2e^2/mc)f_{0v'}/\lambda_{v'0}^2 \tag{1.28}$$

and

$$A_{v'v''}=(q_{v'v''}/q_{v'0})(\lambda_{v'0}/\lambda_{v'v''})^3A_{v'0}\,, \tag{1.29}$$

where $\lambda_{v'v''}$ is the wavelength of the (v', v'') band and $8\pi^2e^2/mc=0.668$ cm^2 s^{-1}. The calculated emission rate factors and related quantities are summarized in Table 1.2.

The solar flux data used in evaluating eq. (1.27) is the same as that used in evaluating the equivalent emission rate of the Rayleigh scattered sunlight (eq. (1.16)). Since both $g_{v'v''}$ and the emission rate of the Rayleigh scattered sunlight are proportional to the solar flux, a variation of the solar flux does not affect the deduced NO density. A γ-band consists of so many rotation lines that a structure of the solar flux within the band may be averaged out. Consequently, it causes no serious error in evaluating $g_{v'v''}$ to neglect the rotational structure of a band as will be shown in the next subsection. The self-absorption effect cannot be neglected when the atmospheric abundance of NO is large as in the cases of the S-210JA-27 and S-310-6 experiments.

1.6.2. Calculation of the emission rate factor: A more accurate treatment including self-absorption effect

In this section, the emission rate factor of the $\gamma(1, 0)$ band is calculated taking into account both the self-absorption effect and the rotational structure of the band. Though a similar calculation was made by CRAVENCE (1977), his result is inconvenient for use in the present study because his calculation was made for an analysis of a satellite observation in which observation geometry is different from that of a rocket observation. The $\gamma(1, 0)$ band is made up of twelve rotational branches, and each consists of many rotation lines. Again, each rotation line has a Doppler-broadened profile. The calculation of the emission rate factor including both the rotational structure and the self-absorption effect becomes much more complex than that described in the previous section. Formulations described below are same as those adopted by PEARCE (1969) but extended to include the self-absorption effect.

The emission rate factor of the $\gamma(1, 0)$ band including both the rotational structure and the self-absorption effect can be expressed as a sum of the emission rate factor of individual rotation lines as

$$g_{10}(T, N)=\sum_{J'}\sum_{J''}g_{\mathrm{rot}}(J', J'', T, N)\,, \tag{1.30}$$

where g_{rot} is the emission rate factor of a rotation line including the self-absorption; N is the column density of NO between the sun and the point where resonance fluorescence occurs; T is the temperature and J is the quantum number for the total angular momentum. Define J for the ground state before absorption, J' for the excited state and J'' for the ground state after reradiation. The emission rate factor for an individual rotation line is

$$g_{\mathrm{rot}}(J', J'', T, N)=\tilde{\omega}(J', J'')\sum_{J} r(J, J', T)T^*[\tau_0(J, J', T, N)]\,, \tag{1.31}$$

where $\tilde{\omega}$ is the radiative branching ratio; r is the excitation rate due to a transition $J\rightarrow J'$ without self-absorption effect; $T^*(\tau_0)$ is T-function formulated by TOHMATSU and OGAWA (1966) to represent a probability that a photon can be transmitted without absorption along the path with the optical thickness τ_0, where τ_0 is the optical thickness at the wavelength of the center of a rotation line between the sun and the point where resonance fluorescence occurs. The expression for $\tilde{\omega}$ is

$$\tilde{\omega}(J', J'')=\frac{A_{10}}{\sum_{v''} A_{1v''}}\,\frac{\nu^3(J', J'')S(J', J'')}{\sum_{J''}\nu^3(J', J'')S(J', J'')}\,, \tag{1.32}$$

where ν is the wave number and S is the rotational line strength. The expression for r is

$$r(J, J', T)=\frac{\pi e^2}{mc^2}\Phi(J, J')f_{01}\frac{S(J, J')}{\sum_{J'} S(J, J')}\rho(J, i, T)\,, \tag{1.33}$$

where Φ is the solar flux density at the wavelength of the rotation line; f_{01} is the oscillator strength of absorption of the (1, 0) band; ρ is the distribution function and i is the doublet index for the ground state. ρ is calculated on the basis of the Boltzmann distribution as

$$\rho(J, i, T)=(2J+1)\exp\left[-hcF(J, i)/kT\right]/Z(T)\,, \tag{1.34}$$

where F is the rotational term value (cm^{-1}) and Z is the partition function. The expression for τ_0 is

$$\tau_0(J, J', T, N)=\frac{\sqrt{\pi}e^2}{mc^2}\,\frac{f_{01}}{\Delta\nu_D}\,\frac{S(J, J')}{\sum_{J'} S(J, J')}\rho(J, i, T)N\,. \tag{1.35}$$

The expression for T^* given by TOHMATSU and OGAWA (1966) is

$$T^*(\tau_0)=\pi^{-1/2}\int_{-\infty}^{\infty}\exp\left[-x^2-\tau_0\exp(-x^2)\right]\mathrm{d}x\,, \tag{1.36}$$

where x is the variable defined by

$$x=(\nu-\nu_0)/\Delta\nu_D \tag{1.37}$$

with

$$\Delta\nu_D=(2kT/M)^{1/2}\nu_0/c\,, \tag{1.38}$$

where ν is the wave number; ν_0 is the wave number at the center of a rotation line; $\Delta\nu_D$ is the Doppler half-width of the rotation line (cm^{-1}) and M is the mass of a NO molecule.

In the above calculation, some approximations are implicitly (or explicitly) adopted. First, the atmospheric NO molecules are assumed to lie only in the $v=0$

vibrational level of the ground electronic state ($X^2\Pi$). Since the first vibrational level $v=1$ lies about 0.24 eV above the $v=0$ level, the distribution function for the $v=1$ level is estimated to be only 10^{-4} at a temperature of 300 K. Second, the thermal equilibrium is assumed within the rotational levels. A removal frequency of a molecule in the ground electronic state by the absorption of the solar radiation is estimated to be in an order of magnitude of 10^{-3} s^{-1}, which is much smaller than the thermal collision frequency at the relevant altitude. Third, the rotation line is assumed to have a pure Doppler profile since both the collision width and the natural width are found to be much smaller than the Doppler width at the relevant altitude. And fourth, the spin-splitting of the $A^2\Sigma^+$ electronic state is neglected, since the spin-splitting is only about 0.0028 J cm^{-1} (BERGEMAN and ZARE, 1972), which is smaller than the Doppler half-width (0.063 cm^{-1} at 300 K) for main rotation lines ($J \lesssim 25$). The self-absorption along the line of sight of the radiometer may be neglected since a NO column density between the radiometer and the point where the emission occurs is usually small.

In evaluating eqs. (1.30) through (1.36), f_{01} was taken from MARR (1964), and Φ from BRINKMAN *et al.* (1966). $A_{v'v''}$ is calculated by using eqs. (1.28) and (1.29). Expression for S in $^2\Pi - ^2\Sigma$ transition was taken from EARLS (1935). Numerical evaluation of T^* is made by using its Taylor series expansion given by TOHMATSU and OGAWA (1966). The rotational term values and the wave numbers of the transitions are calculated using expressions after HILL and VAN VLECK (1928) and using molecular constants reported by HERZBERG (1950). The calculation for T^* was performed with temperatures of 200 K and 300 K. Since the self-absorption effect is usually significant at the altitudes below 90 km, these temperatures are reasonable.

The calculated ratios, $g_{10}(T, N)/g_{10}(T, N=0)$, with $T=200$ K and 300 K as a function of N are shown in Fig. 1.16. The emission rate factor of the $\gamma(1, 0)$ band

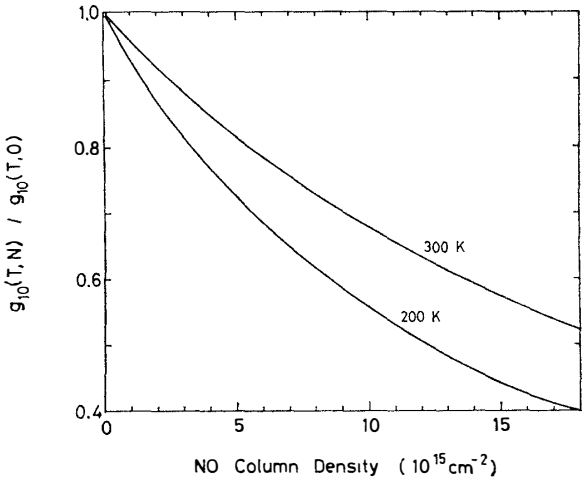

Fig. 1.16. Ratio of the emission rate factor with self-absorption, $g_{10}(T, N)$, to that without self-absorption, $g_{10}(T, N=0)$, as a function of NO column density.

allowing the rotational structure, $g_{10}(T, N=0)$, is found to be 8.20×10^{-6} photons s^{-1} at $T=200$ K and 8.15×10^{-6} photons s^{-1} at $T=300$ K. These values are about 4% larger than the value, 7.88×10^{-6} photons s^{-1}, derived by using eq. (1.27) in which the rotational structure is neglected. Since the emission rate factors of bands other than the (1, 0) band are also necessary in the data analysis, 7.88×10^{-6} photons s^{-1} is adopted as $g_{10}(T, N=0)$ for consistency. The emission rate factors of bands other than the (1, 0) band are assumed to vary in the same manner as that of the (1, 0) band shown in Fig. 1.16. This assumption may cause an error less than one percent in deriving the NO density.

1.6.3. Estimation of the error due to Doppler shift

The principle of the measurement described in Section 1.3 stands on the fact that the $\gamma(1, 0)$ band photons are completely absorbed by the NO cell. The optical thickness of the NO cell at the center of a main rotation line is estimated to be between 100 and 2000, and a line with a larger emission rate factor has a larger cross section. Consequently, the $\gamma(1, 0)$ band photons hardly pass through the NO cell. This has been confirmed by a laboratory experiment as demonstrated in Fig. 1.2. However, situations during a rocket experiment are different from those in a laboratory experiment in view of the point that the radiometer has a relative motion against the atmospheric NO molecules emitting the $\gamma(1, 0)$ band airglow. The absorption of the $\gamma(1, 0)$ band emission by the NO cell may no longer be complete during a rocket experiment because the speed of a sounding rocket at lower altitudes is generally larger than the gas kinetic speed of a NO molecule: *e. g.*, the former is about 1 km s^{-1} at 70 km and the latter is about 0.4 km s^{-1} at a temperature of 300 K. Again, the multiple scattering of the $\gamma(1, 0)$ band radiation should affect the effective transmittance of the NO cell. The collision broadening of the absorption line must also be taken into consideration since the gas pressure in the NO cell is as high as 200 Torr. A detailed analysis of this problem will be published elsewhere (IWAGAMI and OGAWA, 1981), and is briefly summarized here.

When the $\gamma(1, 0)$ band airglow enters the NO cell, the following components of the radiation flux may emerge from the NO cell: (1) the non scattered $\gamma(1, 0)$ band, Φ_1, (2) multiple scattering of the $\gamma(1, 0)$ band, Φ_2, and (3) $\gamma(1, v''\neq0)$ band fluorescence, Φ_3. Φ_1 is expected to vary with the speed of the sounding rocket considerably because of the Doppler shift of the airglow emission line. The $\gamma(1, v'\neq0)$ band fluorescence should be considered since the NO cell is transparent for the $\gamma(1, v''\neq0)$ band radiations; however, only a part of the fluorescence can enter into the photomultiplier because of the narrow aperture angle.

Based upon the radiative transfer scheme for a molecular band developed by TOHMATSU and YAMAMOTO (1976), Φ_1, Φ_2 and Φ_3 were evaluated. They were normalized with the incident flux of the $\gamma(1, 0)$ band Φ, and shown in Figs. 1.17, 1.18 and 1.19. In these figures x_R is the Doppler shift of the airglow emission line in

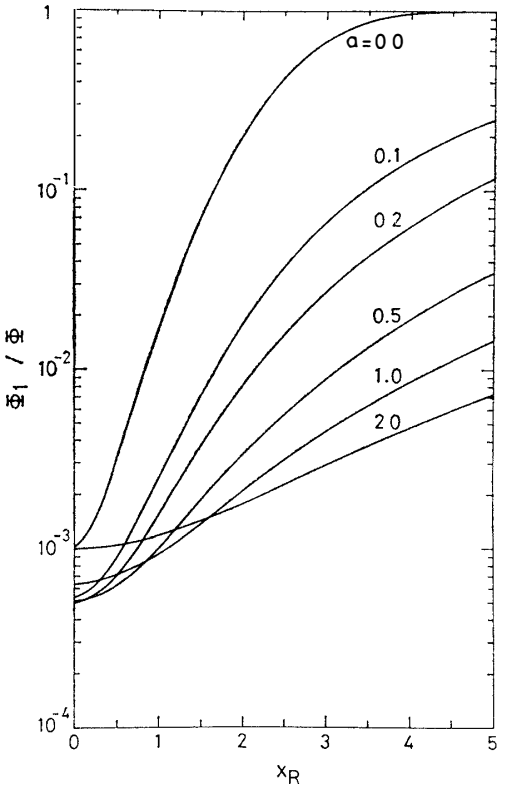

Fig. 1.17. Ratio of the transmission flux component Φ_1 to the $\gamma(1, 0)$ band incident flux Φ. a is the broadening parameter, and x_R is the Doppler shift of the emission line in units of the Doppler half-width.

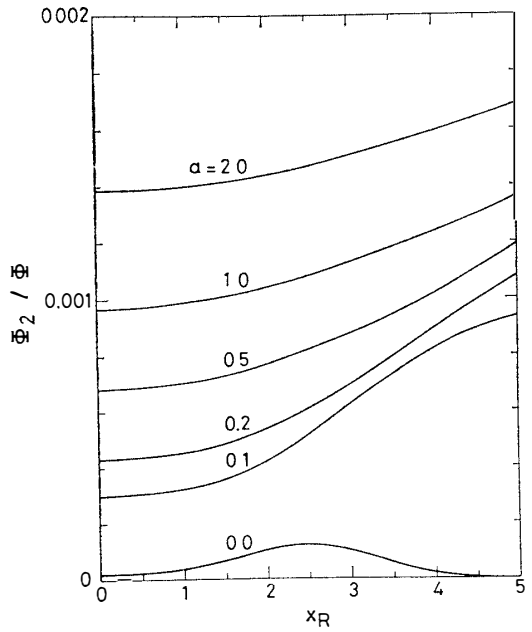

Fig. 1.18. Same as Fig. 1.17 but for the transmission flux component Φ_2.

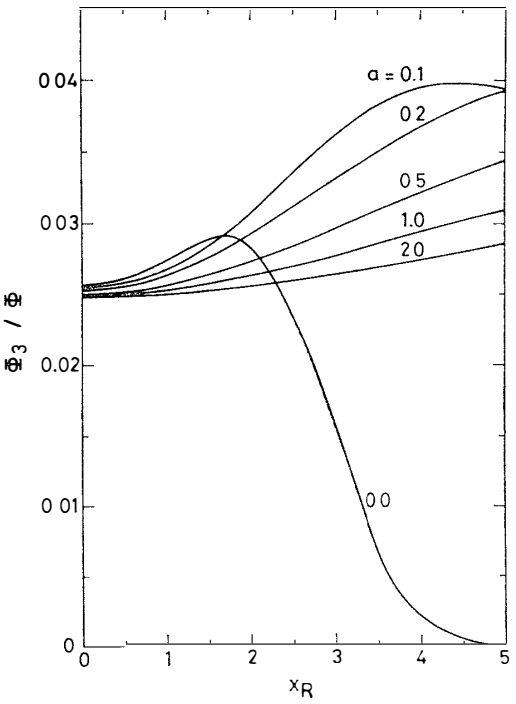

Fig. 1.19. Same as Fig. 1.17 but for the transmission flux component Φ_3.

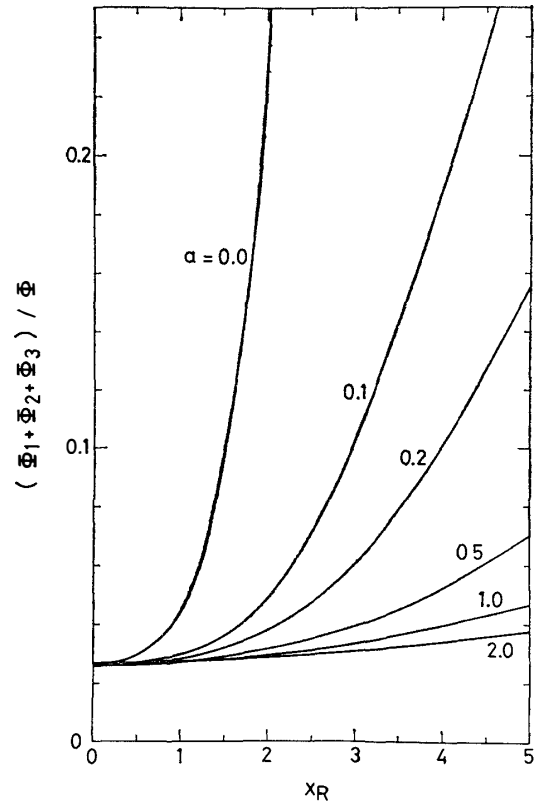

Fig. 1.20. Same as Fig. 1.17 but for the total transmission flux.

units of the Doppler halfwidth, and is equal to 2.45 when the rocket speed is 1 km s^{-1}; a is the broadening parameter for the collision broadening of the absorption line. Φ_2 and Φ_3 are found to vary a little with x_R, and Φ_3 is larger than Φ_2 by more than one order of magnitude.

The effective transmittance of the NO cell for the $\gamma(1,0)$ band airglow is given by $(\Phi_1+\Phi_2+\Phi_3)/\Phi$, and is shown in Fig. 1.20. It is found to increase monotonically with x_R, and is 3.0% and 3.5% for a=0.5 and a=2.0, respectively, at x_R=2.5. The value of the broadening parameter under the conditions in the NO cell is uncertain, but is considered to lie between 0.5 and 2.0 according to the collision diameter of a NO molecule reported by BREENE (1967), MCGREGOR *et al.* (1980) and DODGE *et al.* (1980).

Taking into account the non-zero transmittance of the NO cell, eq. (1. 11) may be revised to

$$S_{NO}=Cf[(\varepsilon+\alpha\varepsilon+\beta)I_{10}+(1-w)(I_R+I_B)]\,, \tag{1.39}$$

with

$$\varepsilon=(\Phi_1+\Phi_2+\Phi_3)/\Phi\,, \tag{1.40}$$

while eq. (1.10) remains unchanged. ε represents the effective transmittance of the NO cell for the $\gamma(1,0)$ band airglow as shown in Fig. 1.20. The following effects may contribute to the errors in the $\gamma(1,0)$ band airglow emission rate and the NO

Table 1.3. Estimated maximum errors for the $\gamma(1, 0)$ band emission rate and the NO density (units in %).

Sounding rocket	For emission rate		For density	
	$a=0.5$	$a=2.0$	$a=0.5$	$a=2.0$
S-210-9	4	3	11	4
ISRO 05-31	5	4	9	5
S-210JA-27	5	4	6	5
S-310-6	6	4	7	5

density: (i) the $\gamma(1, 0)$ band emission rate $4\pi I_{1_0}$ changes by about ε by the use of eq. (1.39) instead of eq. (1.11), (ii) an altitude dependence of ε causes a change in the NO density, (iii) the instrumental constant C may also change. All of these three effects by neglecting ε cause underestimations.

The errors in the $\gamma(1, 0)$ band emission rates and the NO densities were estimated by comparing the values obtained from eqs. (1.10) and (1.11) and those from eqs. (1.10) and (1.39), and the maximum errors in our present measurements are summarized in Table 1.3 for the cases of $a=0.5$ and $a=2.0$. The error is found to maximize its value at the lowest altitude of the measurement because of the greatest rocket speed. The rocket speed there was about 1 km s^{-1} for S-210-9, ISRO 05-31 and S-210JA-27, and was about 1.5 km s^{-1} for S-310-6. As seen in the table, the error of the $\gamma(1, 0)$ band airglow emission rate was found to be $4\sim 6\%$ for $a=0.5$ and $3\sim 4\%$ for $a=2.0$, and that of the NO density to be $6\sim 11\%$ for $a=0.5$ and $4\sim 5\%$ for $a=2.0$.

It may be concluded that the error due to the neglect of the finite transmittance of the NO cell is considerably smaller than the experimental error (see Figs. 1.22 through 1.25). The latter is of a few tens percent, whereas the former is usually less than ten percent as far as the broadening parameter is larger than 0.5. Consequently, the error due to the finite transmittance of the NO cell can be neglected.

1.6.4. Deduction of NO density

The NO $\gamma(1, 0)$ band emission is considered to arise from resonance fluorescence of solar radiation by atmospheric NO molecules as discussed in Subsection 1.5.3. Therefore, the apparent emission rate of the $\gamma(1, 0)$ band in the zenith direction at altitude z is expressed in terms of NO density by the formula:

$$4\pi I_{10}(z)=\int_z^\infty g_{10}(N[z'])n(\mathrm{NO}, z') \exp\left[-\tau_{\mathrm{M}}(z')\right] \mathrm{d}z' , \tag{1.41}$$

where the emission rate factor of the $\gamma(1, 0)$ band, g_{10}, is a function of the NO column density between the sun and the radiometer, N; $n(\mathrm{NO}, z)$ is the number density of NO and τ_{M} is the optical thickness for the 2148 Å radiation due to absorption by

atmospheric molecules other than NO between the sun and the radiometer. An explicit expression for the NO number density can be obtained by differentiating eq. (1.41) by z as

$$n(\mathrm{NO}, z)=-\frac{\mathrm{d}}{\mathrm{d}z}[4\pi I_{10}(z)]/g_{10}(N[z]) \exp[-\tau_{\mathrm{M}}(z)] . \tag{1.42}$$

If both the self-absorption effect and the attenuation of the solar radiation due to the atmospheric absorption are neglected, then eq. (1.42) can be simplified in the form:

$$n(\mathrm{NO}, z)=-\frac{\mathrm{d}}{\mathrm{d}z}[4\pi I_{10}(z)]/g_{10}(N=0) . \tag{1.43}$$

It must be noted that g_{10} in the right hand side of eq. (1.42) implicitly includes the NO number density. To deduce the NO density as corrected for the self-absorption effect, the following procedure is necessary. First, the NO density is deduced from the measured emission rate of the $\gamma(1, 0)$ band by using eq. (1.43). Second, N is numerically calculated from the NO density distribution obtained in the first step to evaluate g_{10} at each altitude by using the relation shown in Fig. 1.16. And third, the NO density with the self-absorption effect can be calculated from eq. (1.42) by using g_{10} obtained in the second step.

$\tau_{\mathrm{M}}(z)$ was evaluated from the molecular absorption of O_2 and O_3 and the attenuation due to the Rayleigh scattering, where the O_2 density distribution was taken from CIRA (1972), the O_2 absorption cross section (8.1×10^{-24} cm^2) from DITCHBURN and YOUNG (1962), the O_3 density distribution from WATANABE and TOHMATSU (1976), the O_3 absorption cross section (1.25×10^{-18} cm^2) from INN and TANAKA (1953), and for the Rayleigh scattering the atmospheric density distribution was

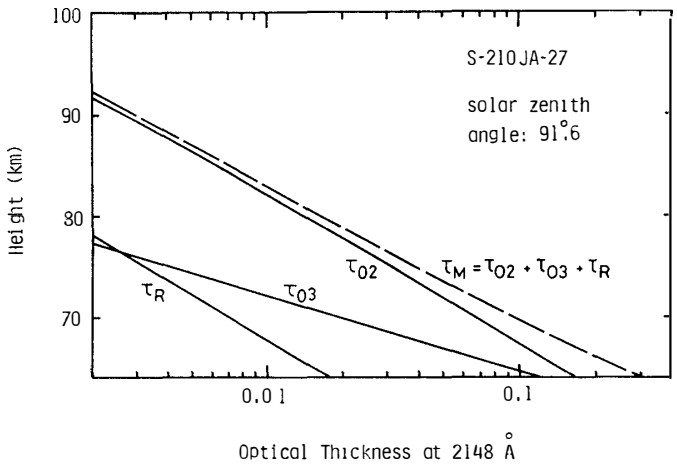

Fig. 1.21. Calculated optical thickness between the sun and the radiometer for the 2148 Å radiation (τ_M) under the conditions in the S-210JA-27 experiment. Contributions from the absorption due to O_2, O_3 and the Rayleigh scattering are indicated by τ_{02}, τ_{03} and τ_R, respectively.

taken from CIRA (1972) with the cross section of DALGARNO (1962). Figure 1.21 shows the calculated $\tau_M(z)$ for the S-210JA-27 experiment. As seen in the figure, the optical thickness for the 2148 Å radiation is found to be negligibly small above about 75 km even under the condition of large solar zenith angle (91.6°).

NO densities deduced from the measured emission rates of the $\gamma(1,0)$ band obtained in the S-210-9, ISRO 05-31, S-210JA-27 and S-310-6 experiments are shown

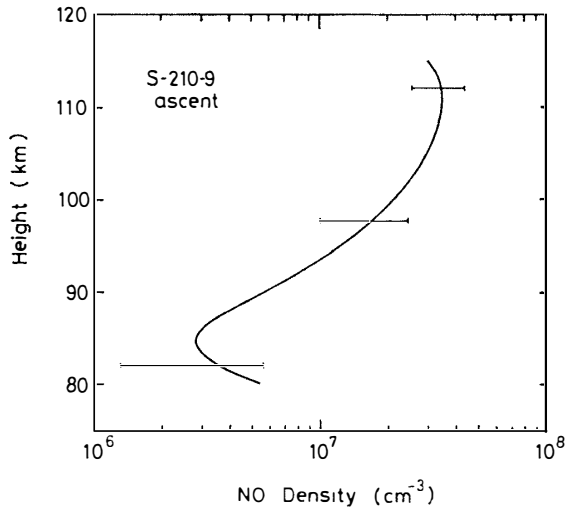

Fig. 1.22. NO density distribution obtained in the S-210-9 experiment. The horizontal bars represent the possible error in the smoothing procedure.

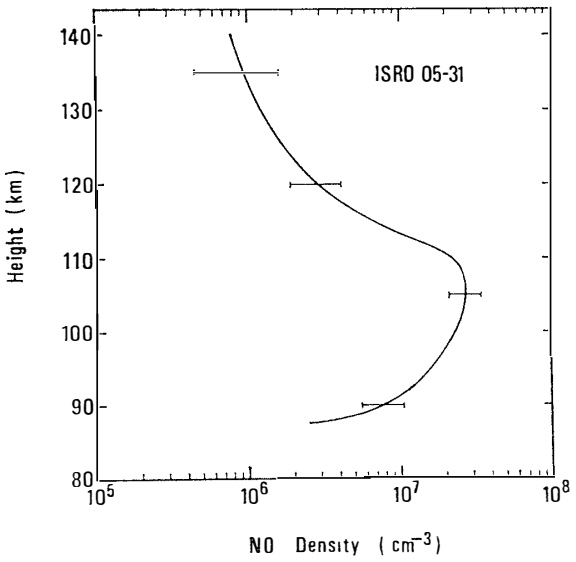

Fig. 1.23. Same as Fig. 1.22 but in the ISRO 05-31 experiment.

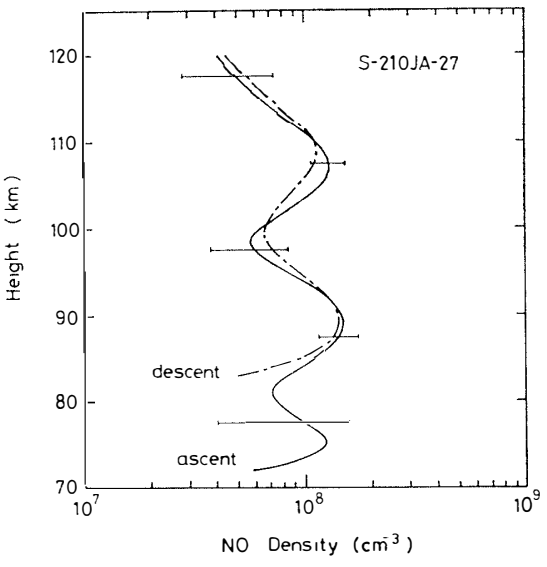

Fig. 1.24. Same as Fig. 1.22 but in the S-210-JA-27 experiment.

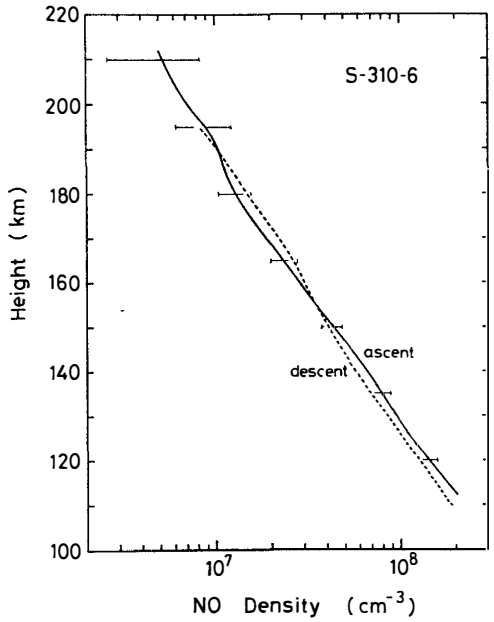

Fig. 1.25. Same as Fig. 1.22 but in the S-310-6 experiment.

in Figs. 1.22, 1.23, 1.24 and 1.25, respectively. The correction due to the self-absorption was neglected in deriving the NO density profiles obtained in the S-210-9 and ISRO 05-31 experiments since it was found to be less than 5%. In the S-210JA-27 and S-310-6 experiments, amounts of the correction found were 32% and 67%, respectively, at most. The correction for the attenuation of 2148 Å radiation due to the atmospheric absorptions was made only for the result obtained in the S-210JA-27 experiment since this experiment obtained data below 80 km.

1.7. Results and Discussions

1.7.1. Results at middle and low latitudes

Brief description of odd nitrogen chemistry

In this section the NO density distributions obtained in the S-210-9, ISRO 05-31 and S-310-6 experiments which were carried out at middle and low latitudes are discussed from a viewpoint of a current odd nitrogen chemistry in the upper atmosphere. A brief statement on the reactions producing and destructing NO seems to be instructive to understand the following discussions, which are referred from the theoretical model calculations developed by OGAWA and KONDO (1977; hereafter called OK77) and by KONDO and OGAWA (1977; hereafter called KO77). These models are revised versions of OGAWA and SHIMAZAKI (1975) in order to allow a diurnal variation of the thermospheric temperature.

According to OK77 and KO77, the following outline of the odd nitrogen chemistry can be drawn. A major part of NO in the thermosphere is produced in the reactions of metastable atomic nitrogen and O_2:

$$N(^2D)+O_2 \rightarrow NO+O\,, \tag{1.44}$$

and of atomic nitrogen in the ground state and O_2:

$$N(^4S)+O_2 \rightarrow NO+O\,. \tag{1.45}$$

Between 80 and 90 km, the production of NO through

$$O_2^+ + N_2 \rightarrow NO+NO^+ \tag{1.46}$$

is also considerable besides the productions through reactions (1.44) and (1.45). The production of NO due to reaction (1.44) is dominant below about 130 km, while that due to reaction (1.45) is dominant above the altitude.

The loss of NO, on the other hand, is governed principally by the reaction of atomic nitrogen in the ground state:

$$NO+N(^4S) \rightarrow N_2+O\,, \tag{1.47}$$

by the predissociation due to solar radiation:

$$NO+h\nu(<1908\ \text{Å})\rightarrow N(^4S)+O\,, \tag{1.48}$$

and also by the ion-molecule reaction:

$$NO+O_2^+\rightarrow NO^+ +O_2\,. \tag{1.49}$$

Almost all of the sink of NO is due to reaction (1.47) above about 115 km, whereas the sinks due to reactions (1.48) and (1.49) become important below 105 km and between 95 km and 115 km, respectively.

As seen in the above descriptions, the NO density in the upper atmosphere is highly sensitive to the density ratio of $N(^2D)$ and $N(^4S)$ especially at the altitudes below 130 km where NO is produced from $N(^2D)$ and destroyed by $N(^4S)$. $N(^2D)$ and $N(^4S)$ are produced in the thermosphere by the following processes:

(i) dissociative recombination of NO^+

$$NO^+ +e\rightarrow N(^2D,\ ^4S)+O\,, \tag{1.50}$$

(ii) ion-molecule reaction

$$N_2^+ +O\rightarrow NO^+ +N(^2D,\ ^4S)\,, \tag{1.51}$$

(iii) predissociation of N_2 by solar radiation

$$N_2+h\nu(<1000\ \text{Å})\rightarrow 2\ N(^2D,\ ^4S)\,, \tag{1.52}$$

(iv) dissociation of N_2 by electron impact

$$N_2+e^*\rightarrow 2N(^2D,\ ^4S)+e^*\,, \tag{1.53}$$

and (v) predissociation of NO by solar radiation (1.48).

In the above processes except (v), η^*, the quantum yield of $N(^2D)$ is uncertain; however, it may be larger than 0.5, and probably as large as 0.9 (KO77). Similar conclusion has been drawn by other investigators who analyzed the data from mass-spectrometric and/or photometric measurements of atmospheric constituents (Rusch *et al.*, 1975; Oran *et al.*, 1975; Torr *et al.*, 1976; Strobel *et al.*, 1976; Frederic and Rusch, 1977). Predissociation of NO by solar radiation (1.48) can only produce atomic nitrogen in the ground state. Besides the above processes, the relative abundance of $N(^2D)$ and $N(^4S)$ is regulated by the quenching process:

$$N(^2D)+O\rightarrow N(^4S)+O\,. \tag{1.54}$$

This reaction is important in determining the NO density distribution above about 120 km. The rate coefficient of reaction (1.54), k_{54}, is uncertain, but KO77 favored a value of 1×10^{-12} cm^3 s^{-1} instead of $8.5\times10^{-12}\exp(500/T)$ cm^3 s^{-1} deduced from a laboratory measurement by Davenport *et al.* (1976). Other investigators, based on the data analysis for the mass-spectrometric and/or photometric measurements, concluded $k_{54}\sim4\times10^{-13}$ cm^3 s^{-1} (Strobel *et al.*, 1976); $k_{54}\sim2\times10^{-12}$ cm^3 s^{-1} (Torr *et al.*, 1976); $k_{54}\sim4\times10^{-13}$ cm^3 s^{-1} (Frederic and Rusch, 1977) and $k_{54}\sim1\times10^{-12}$ cm^3 s^{-1} (Cravence *et al.*, 1979).

In the daytime the photochemical production and loss rates of the odd nitrogen species (NO, N(^2D), N(^4S)) are of the order of 10^3 cm^{-3} s^{-1}. They are about a factor 10 greater than the divergence term due to the eddy and molecular diffusions. At night the photochemical terms decrease to about 10^2 cm^{-3} s^{-1}, whereas the dynamical terms remain on the same order of magnitude. Therefore, the concentration of odd nitrogen is determined basically by photochemical reactions above about 90 km in the daytime, whereas the dynamical processes have an important effect during the night.

Again, an important fact pointed out by OK77 and KO77 is that the thermospheric NO density distribution is controlled by the thermospheric temperature. This is a consequence from the fact that k_{45}, the rate coefficient of reaction (1.45), is highly temperature dependent and that the O_2 number density in the thermosphere also varies with the thermospheric temperature.

Comparison of experimental and theoretical profiles

In Fig. 1.26 are illustrated the altitude profiles of the NO densities obtained in the S-210-9, ISRO 05-31 and S-310-6 experiments, and also illustrated are the NO density profiles obtained in the theoretical model calculation by OK77 at the local sunrise (06 h LT) and at the local sunset (18 h LT) for various exospheric temperatures. The S-210-9 and S-310-6 experiments were carried out at Uchinoura (31°N) at around the local sunset, and the ISRO 05-31 experiment was carried out at Thumba (9°N) about an hour after the local sunrise (see Table 1.1). The theoretical model calculation by OK77 is performed under the conditions of 45° latitude in equinox assuming $\eta^*=0.9$ and $k_{54}=1\times10^{-12}$ cm^3 s^{-1}. According to the empirical formula given by JACCHIA (1971), the exospheric temperatures for the days of the S-210-9, ISRO 05-31 and S-310-6 experiments are 930 K, 880 K and 1340 K, respectively. The S-210-9 and ISRO 05-31 experiments were carried out during a period of low solar activity ($F_{10.7}\sim80$), while the S-310-6 experiment was during a period of high solar activity ($F_{10.7}\sim180$).

Comparing the NO density profile obtained in the S-210-9 experiment with that theoretically calculated at 18 h LT with $T_\infty=900$ K, a good agreement between them is found in Fig. 1.26. A considerable difference in NO density gradient below 85 km between those observed and theoretical NO density profiles may be caused by an error due to scattering of data points or to contamination by the intense Rayleigh scattered sunlight at the lower altitude.

The NO density profile obtained in the ISRO 05-31 experiment is also found to be in agreement with that theoretically calculated at 06 h LT with $T_\infty=900$ K. Again, the smaller NO density predicted theoretically above 120 km in the morning than in the evening is evident in the observed NO density. According to OK77, this smaller NO density at around 120 km in the morning occurs as a consequence of the persistent destruction of NO and N(^4S) (reaction (1.47)) and decrease of the NO

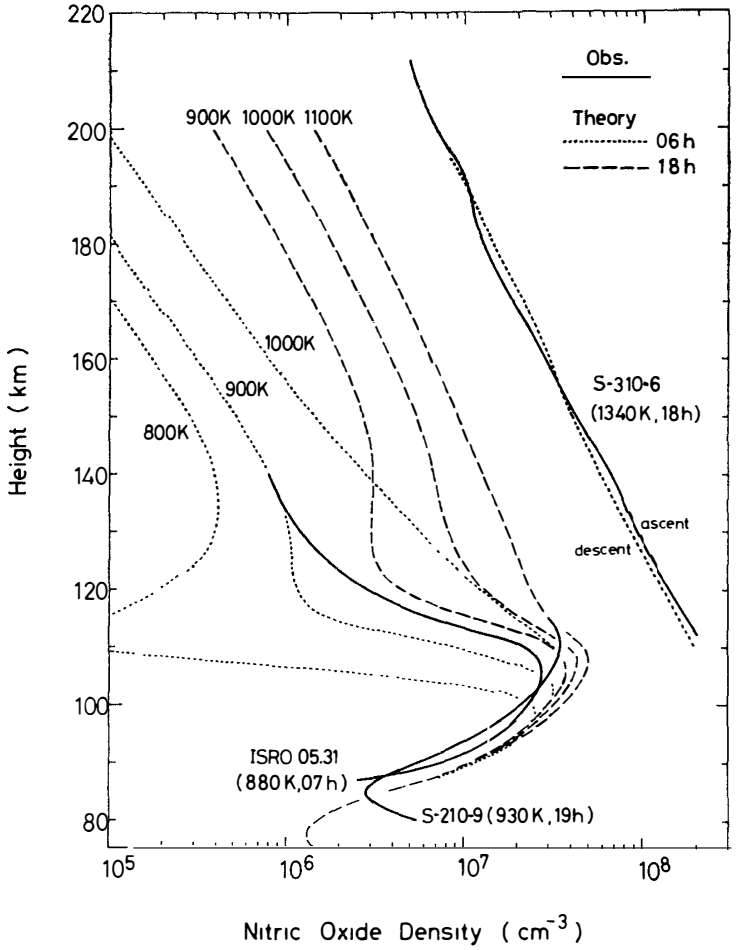

Fig. 1.26. Comparison of the NO density profiles obtained at middle and low latitudes (S-210-9, 31°N; ISRO 05-31, 9°N; S-310-6, 31°N) with those theoretically calculated by OGAWA *and* KONDO *(1977). Thick lines represent observed profiles; dashed and dotted lines represent theoretical NO density profiles at 18h LT and 06h LT, respectively, with various exospheric temperatures.*

production rate due to reaction (1.44) during night, whereas below 110 km the NO density changes a little at 18 h LT and 06 h LT because of the large time constant for chemical removal of NO. However, a little discrepancy, which is equivalent to about 50 K difference in the exospheric temperature, can be seen between those observed and theoretical NO densities at the altitudes between 110 and 130 km. This discrepancy may be caused by an error in evaluating T_∞ since the error is expected to be about 50 K at most (JACCHIA, 1971). Taking into account both the 50 K error in T_∞ and the experimental error shown in Fig. 1.23, the discrepancy may be explained. Another explanation is that the discrepancy may be caused by an error in the value of the quenching rate coefficient, k_{54} adopted in the model calculation by OK77. As shown by KO77, adoption of a smaller value for k_{54} causes a larger NO

density at only around 120 km. This is due to the fact that above 130 km the NO production through the reaction of $N(^2D)$ and O_2 (reaction (1.44)) is less important than that of reaction (1.45), and below 110 km quenching of $N(^2D)$ by O (reaction (1.54)) is no longer important owing to decrease in the ratio of O to O_2 densities. Smaller values for k_{54} than 1×10^{-12} cm^3 s^{-1} adopted by OK77 have been favored by recent researches as mentioned earlier.

Unfortunately OK77 did not show the NO density profile with T_∞ larger than 1100 K; therefore, a direct comparison of the NO density profile obtained in the S-310-6 experiment (T_∞=1340 K) with that from OK77 is impossible. However, it is possible to estimate the NO density profile with T_∞=1340 K by a simple calculation since the NO density between 150 and 190 km can be approximately described by a photochemical equilibrium. As mentioned before, the dynamical effect is less important than the chemical effect in determining the NO density below 190 km, and the NO density above 150 km is determined by the production through reaction (1.45) and the loss through reaction (1.47). Thus, the NO density between 150 and 190 km can be well approximated as

$$n(\mathrm{NO})=(k_{45}(T)/k_{47})n(\mathrm{O_2})\,, \tag{1.55}$$

where n(NO) and $n(O_2)$ are the number densities of NO and O_2, respectively; k_{45} and k_{47} are the rate coefficients for reactions (1.45) and (1.47), respectively, and T is the temperature. k_{45} is highly temperature dependent as $k_{45}(T)=1.1\times10^{-14}T$ exp $(-3150/T)$ cm^3 s^{-1} (BAULCH *et al.*, 1973). k_{47} is 2.7×10^{-11} cm^3 s^{-1} independent of temperature (BAULCH *et al.*, 1973). Substituting values for $n(O_2)$ and T taken from CIRA (1972) in eq. (1.55), the NO density between 150 and 190 km is found to increase by a factor of about 3 as the exospheric temperature increases from 1100 K to 1340 K. Consequently, the NO density between 150 and 190 km obtained in the S-310-6 experiment is also found to be consistent with the temperature dependent model of thermospheric odd nitrogen developed by OK77 and KO77. Though the NO density estimated by using eq. (1.55) is found to be still smaller than that obtained in the S-310-6 experiment by a few tens percent, the discrepancy may be explained by the experimental error and/or the error in the exospheric temperature estimation.

However, the above discussion cannot be simply extrapolated to the altitudes below 130 km, since NO is produced through reaction of $N(^2D)$ and O_2 (reaction (1.44)) instead of reaction (1.45) below the altitude, and the rate coefficient of reaction (1.44) reported by HUSAIN *et al.* (1974) is independent of temperature. On the other hand, the loss rate of NO at the altitudes below 130 km still has a temperature dependence since NO is mainly destroyed by $N(^4S)$ whose density depends on temperature. However, the degree of this temperature dependence of the loss rate of NO becomes smaller at the lower altitudes and almost negligible below 110 km because atmospheric temperature is almost independent of the exospheric tempera-

ture below the altitude. Therefore, the lowest part of the NO density profile obtained in the S-310-6 experiment cannot be explained as a consequence of the temperature dependence of NO density.

A possible explanation is that the solar extreme ultraviolet (EUV) flux in the S-310-6 experiment was larger than that used in the model calculation by OK77. The NO density is expected to increase at around 110 km with increasing solar EUV flux due to the increase in $N(^2D)$ production rate through photodissociation of N_2 (reaction (1.52)), which provides the largest source of $N(^2D)$ at around 110 km, and through the ionic reactions (1.50), (1.51) and (1.53). On the other hand, the loss rate of NO through reaction (1.47) may also increase with increase of the solar EUV flux since both $N(^2D)$ and $N(^4S)$ are produced via reactions (1.50) through (1.53). However, the increase in the production rate may overcome the increase in the loss rate for the case of $\eta^*=0.9$. Predissociation of NO (reaction (1.48)) is negligible to remove NO above 105 km.

OK77 took into account a variation in T_∞ which is closely correlated with solar activity, but did not a variation in the solar EUV flux. OK77 adopted the solar EUV flux presented by HINTEREGGER (1970). He recommended his flux to be representative of a moderate solar activity with $F_{10.7}\sim 150$, but it is now considered to correspond to that in the low solar activity with $F_{10.7}\sim 70$ (HINTEREGGER, 1976). Note that the S-210-9 and ISRO 05-31 experiment were carried out in a period of low solar activity ($F_{10.7}\sim 80$), while the S-310-6 experiment was in a period of high solar activity ($F_{10.7}\sim 180$). The NO density at around 110 km is expected to increase roughly in proportion to the EUV flux, since the production rate of $N(^2D)$ through photodissociation of N_2 (reaction (1.52)) is proportional to the EUV flux. Actually, an increase in the solar EUV flux by more than a factor of two during the rising period of solar cycle 21 has been found by a spectrometric measurement on board a satellite (TORR *et al.*, 1979).

Since the NO density calculated by OK77 under the conditions of 18 h LT with $T_\infty=1100$ K is about 5×10^7 cm^{-3} at 110 km (see Fig. 1.26), NO density is expected to be more than 10^8 cm^{-3} at 110 km when $F_{10.7}\sim 180$. Such an increase in NO density at around 110 km during the 11 years solar cycle has been inferred from mass-spectrometric measurements of ions in the ionospheric *E*-region (GOLSHAN and SECHRIST, 1975; SWIDER, 1978). Consequently, a very large NO density below about 130 km obtained in the S-310-6 experiment may be explained by the dependence of the NO density on the solar EUV flux.

1.7.2. Result in the auroral zone

In this section the NO density profile obtained in the S-210JA-27 experiment, which was carried out at Syowa Station (69°S) in the auroral zone, is discussed from a viewpoint of a current odd nitrogen chemistry under a perturbation due to auroral particle precipitations.

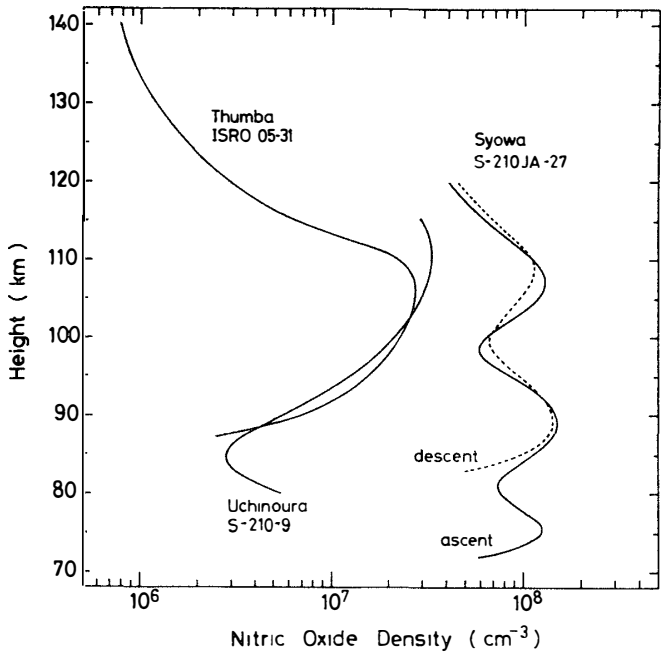

Fig. 1.27. Comparison of the NO density profiles obtained at Syowa Station (69°S), Uchinoura (31°N) and Thumba (9°N). Note that the exospheric temperatures for the days of these experiments were roughly the same.

Figure 1.27 shows the NO density profiles obtained in the S-210JA-27 experiment together with others obtained in the present work. Note that the exospheric temperatures estimated for the days of these experiments were roughly same; they were 860 K, 930 K and 880 K for the days of the S-210JA-27, S-210-9 and ISRO 05-31 experiments, respectively. These observed NO density profiles should be nearly the same unless an additional source of NO exists in the polar upper atmosphere. However, it is evident that the NO density observed at Syowa Station is much larger than those at the middle and low latitudes. Again, a remarkable feature observed at Syowa Station is a double peak structure. Another peak was observed at around 75 km in the ascent, but it may be uncertain due to large experimental errors. Two main peaks, one at around 110 km and the other at around 90 km, are evident both in the ascent and in the descent though the rocket shifted horizontally about 50 km during its flight above the 90 km altitude. Note that these two peaks correspond to the wavy structure of the observed $\gamma(1, 0)$ band emission rates shown in Fig. 1.14, and that the modulation in this structure exceeds experimental errors.

The chemistry of odd nitrogen species in the upper atmosphere under auroral perturbations has been studied theoretically by a number of people (*e. g.*, KONDO and OGAWA, 1976; HYMAN *et al.*, 1976; REES and ROBLE, 1979). According to their model calculations, precipitating auroral particles can produce odd nitrogen species, and a large NO density appears in the mesosphere and the lower thermosphere.

The increase in NO density is caused by the increase in N(^2D) density produced through impact dissociation of N_2 by auroral electrons (same form as reaction (1.53)). However, a double peak structure has never been predicted, and must require some explanation for its reality.

Before discussing the NO density profile obtained in the S-210JA-27 experiment, it seems useful to summarize the results of the numerical model calculation for the perturbation due to auroral particle precipitations by KONDO and OGAWA (1976; hereafter called KO76). Their model calculation is performed under the conditions of 70° latitude in equinox assuming that the quantum yield of N(^2D) in impact dissociation of N_2 by an auroral electron is equal to 0.9. According to KO76, the increase rate of the NO density at an altitude level is roughly proportional to the total energy deposited there. Again, the peak NO density after auroral perturbation occurs at the stopping altitude of precipitating particles, where the stopping altitude depends on the energy of the incident particles. An important point they found is that enhancement of the NO density at the altitudes between 80 km and 120 km remains for at least one day because of slow chemical removal of NO as well as of small vertical transport by eddy and molecular diffusions. Both of time constants for chemical removal of NO and for vertical transport are order of one day or more in this altitude region. They neglected the horizontal transport in their model, but it might be less effective than the vertical one.

Although it was geomagnetically quiet during the flight except the blackout in the ionogram, the disturbance which might cause the NO density enhancement can

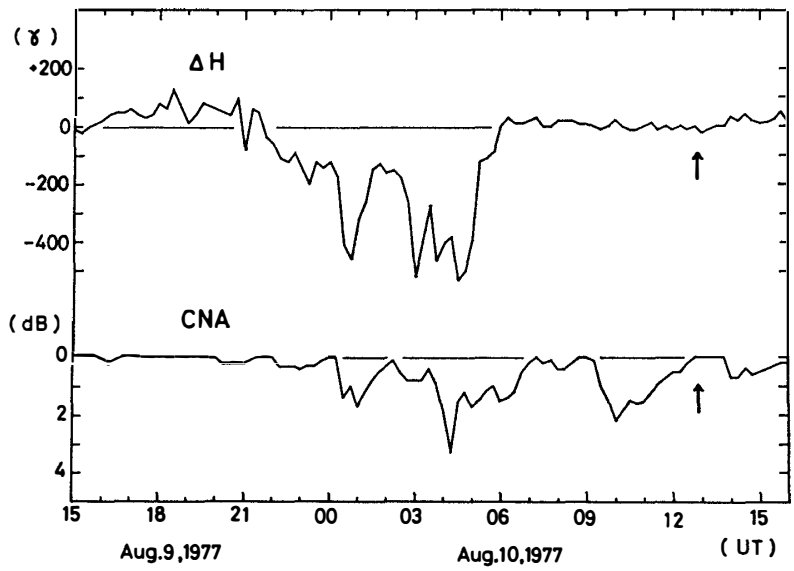

Fig. 1.28. A quarter-hourly value of ΔH (horizontal component of the geomagnetic variation) and of CNA (cosmic noise absorption at 30 MHz) observed at Syowa Station (69°S, 40°E). The time of the S-210JA-27 rocket flight is indicated by arrows.

be found within a day before the flight. As shown in Fig. 1.28, there was an auroral substorm in the last night and a CNA (cosmic noise absorption at 30 MHz) event a few hours before the flight. The blackout in the ionogram during the flight might have been caused by the particle precipitation in this CNA event. The electron precipitation with a characteristic energy of several keV is associated with a usual auroral substorm (REES, 1969), and according to KO76, a 5 keV electron precipitation can produce a NO density enhancement at around 105 km. On the other hand, CNA is usually caused by electrons with energy of several tens keV (AKASOFU, 1968). These latter electrons may produce a NO density enhancement at the altitude around 80–90 km. Based on this knowledge and the stability of the enhanced NO density found by KO76, the above two disturbances are thought to be responsible for the observed NO density peaks at around 110 km and 90 km, respectively.

Unfortunately, a semi-empirical evaluation of the electron influx by making use of measured emission rate of an optical aurora was not possible because of clouds during the substorm and sunlight during the CNA event. However, it is possible to estimate roughly the electron influx at the time of the disturbance based on the magnitude of geomagnetic disturbance during the auroral substorm and the CNA intensity.

The auroral substorm was about ΔH (horizontal component of the geomagnetic variation) $= -400\,\gamma$ in magnitude and of 4 hours duration as represented by a quarter-hourly average shown in Fig. 1.28. Using the experimental relation between ΔH and the auroral intensity in the N_2^+ 1NG (0, 1) 4278 Å band observed by the author

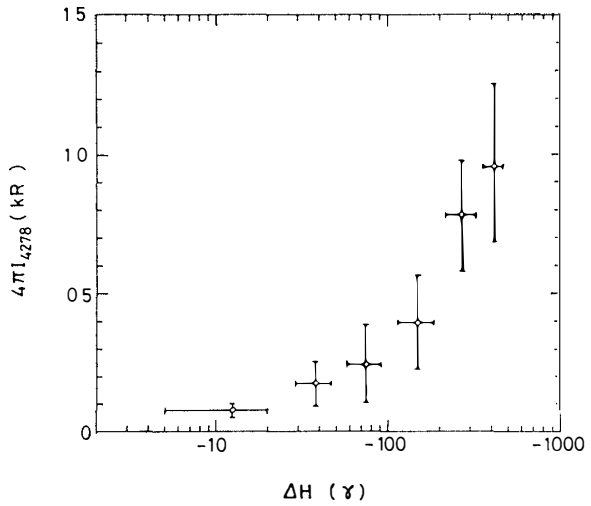

Fig. 1.29. Experimental relation between hourly averaged horizontal component of the geomagnetic variation (ΔH) and hourly averaged emission rate of the N_2^+ 1NG(0, 1) 4278 Å band ($4\pi I_{4278}$) observed at Syowa Station in 1977. Contamination in $4\pi I_{4278}$ due to stellar sources and the airglow continuum is corrected. Vertical and horizontal bars represent one standard deviation of data points.

at Syowa Station in 1977 as shown in Fig. 1.29, the average auroral intensity c about 900 Rayleighs might be expected during the substorm. Then, the energ influx was estimated to be about 5 erg cm^{-2} s^{-1} for this substorm using the relation between the energy influx of the precipitating particles and the intensity of the optical aurora obtained by McEwen and Venkatarangan (1978). According to KO76 the electron precipitation with a characteristic energy of 5 keV and with total energ influx of 25 erg cm^{-2} s^{-1} produces a peak NO density of 4×10^{8} cm^{-3} at around 105 km after 30 minutes duration of the precipitation. Since the auroral substorm in the last night continued for about 4 hours, it could have produced a peak NO density c 6×10^{8} cm^{-3} at around 105 km.

The disturbance in the CNA event a few hours before the flight was of 1.5 dB magnitude and of two hours duration. Based on the experimental relation between the CNA magnitude and the 40–80 keV electron flux observed by a satellite (Penman *et al.*, 1979), the CNA event concerned may be caused by an electron influx of about 1 erg cm^{-2} s^{-1} with a characteristic energy of several tens keV. The KO76 calculation shows the electron precipitation with a characteristic energy of 40 keV and with energy influx of 0.5 erg cm^{-2} s^{-1} between 40 and 80 keV will produce a NO density enhancement with a peak density of 5×10^{7} cm^{-3} at around 85 km after 30 minutes duration. Consequently, the observed NO density of 1.5×10^{8} cm^{-3} at around 90 km may be possibly explained by the CNA event of two hours duration. Again, the auroral substorm in the last night was accompanied by a CNA enhancement as seen in Fig. 1.28. It is highly probable that precipitating electrons, which are responsible for this CNA enhancement, might also play an important role to increase the NO density in the 80–90 km altitude region.

1.8. Conclusion

The radiometer which makes use of a self-absorbing gas cell was shown to be useful in measuring the NO $\gamma(1, 0)$ band airglow. The error arising from the Doppler shift due to rocket motion was found to be unimportant.

At middle and low latitudes, the NO densities during a period of low solar activity ($F_{10.7} \sim 80$) were observed to have their peaks of about 3×10^7 cm^{-3} at around 110 km, and were found to be in agreement with those theoretically calculated by OGAWA and KONDO (1977). However, a smaller value for the rate coefficient of N(^2D) quenching by O than used in their model calculation may be favorable to attain better agreement. The NO density in a period of high solar activity ($F_{10.7} \sim 180$) was observed to be as large as about 10^8 cm^{-3} at 120 km and about 10^7 cm^{-3} at 200 km, and was found to be explained semi-quantitatively as a consequence of the temperature dependence of thermospheric NO density as well as its dependence on the solar EUV flux.

In the auroral zone, the NO density was observed to be in the order of 10^8 cm^{-3} with two peaks at around 110 km and 90 km. The observed NO density is much larger than those observed at middle and low latitudes under the conditions of similar solar activity. Though it was geomagnetically quiet during the observation, auroral disturbances within a day before could be responsible for the enhanced NO density because of a long duration of the enhanced NO density. The observed two NO density peaks might be attributed to the two disturbances which occurred in the previous night and a few hours before the flight. The estimated characteristic energy and the total energy influx for these particle precipitation events possibly explain the observed two peak densities at around 110 and 90 km.

PART 2. GROUND OBSERVATION OF THE NI 5200 Å EMISSION IN THE AURORAL ZONE

2.1. Introduction

The NI (^2D–^4S) 5200 Å doublet has long been recognized in the airglow and aurora. However, only a little data exists on its intensity and variations because of the difficulty in measuring this faint emission. Measurements of the emission in the night airglow have been made by WEILL (1968) and HERNANDEZ and TURTLE (1969). Their measurements show that the emission is a permanent feature of the night airglow spectrum and that its behavior is similar to the OI 6300 Å emission.

The 5200 Å emission in the aurora has been measured by GÉRARD and HARANG (1973) with a tilting-filter photometer, and the similarity between the behavior of the NI and OI emissions was also found. They speculated that the excitation mechanism of the 5200 Å emission in the aurora is dissociative recombination of NO^+, but the base of their argument is obscure. EATHER and MENDE (1971) measured the 5200 Å emission with an airborne tilting-filter photometer at various locations around the auroral oval in order to investigate the characteristics of auroral particle precipitation. They found that the intensity ratio of the 5200 Å doublet to the N_2^+ 1NG 4278 Å band varies from about 0.05 in the night side of the auroral oval to 0.4 in the polar side of the oval. FREDERICK and HAYS (1978) measured the horizontal distribution of the 5200 Å and the N_2 3371 Å emissions over the polar region with satellite-borne photometers, and found that the former was more smeared than the latter which is directly corresponded to the energy influx of the precipitating particles. They concluded that this 5200 Å behavior was due to ionospheric motions induced by magnetospheric convection, but their measurements might have been subjected to contaminations due to the sunlight.

Production and loss of N(^2D) in the aurora is of special interest because of its relationship to NO. Enhancements of NO density in the polar upper atmosphere have been inferred from satellite and rocket measurements of the $\gamma(1, 0)$ band fluorescence (RUSCH and BARTH, 1975; GÉRARD and BARTH, 1977; CRAVENS and STEWART,

1978; IWAGAMI and OGAWA, 1980), and an enhancement of NO density may be caused by auroral production of N(^2D) (KONDO and OGAWA, 1976; HYMAN *et al.*, 1977; REES and ROBLE, 1979).

The purpose of Part 2 of this study is to present ground observations of the 5200 Å emission at Syowa Station (69°S) with a tilting-filter photometer, and to discuss the characteristics and excitation process of the emission in the aurora.

2.2. Instrumentation

A tilting-filter photometry was adopted in the present study in order to discriminate the faint 5200 Å doublet emission from background radiations such as an airglow continuum and a starlight. A tilting-filter photometer, which can make wavelength scanning by tilting a narrow band interference filter, has been one of the common instrumentations in the photometry of airglow and aurora since it was introduced by EATHER and REASONER (1969). Again, a tilting-filter photometer has the advantage that it can provide much higher throughput (the product of collecting area, collecting solid angle and transmittance) than a grating spectrometer. Therefore, a tilting-filter photometer may be the best instrumentation to measure the faint 5200 Å doublet emission in airglow and aurora.

Figure 2.1 shows a block-diagram of the photometer used to measure the 5200 Å emission in the present study. Its optics consists of an interference filter which is periodically tilted during measurements, a lens, a shutter, a field stop and a photomultiplier with multi alkali photocathode. With a normal incidence of light, the interference filter has a peak transmittance of 56% at 5212.0 Å (at a temperature of 16°C) with a FWHM band width of 4.6 Å, and the wavelength of peak transmission shifts toward shorter wavelength with a slant incidence of light. The characteristics of the interference filter under the conditions of the actual measurement will be described in detail in the next section. The lens has an effective diameter of 4.8 cm and a focal length of 20 cm. A field of view of the photometer is 2.5° in full-angle. The photomultiplier is sensitive over the middle ultraviolet and visual region.

Signal from the photomultiplier is sent to a pen-recorder by way of operational amplifiers. The photomultiplier is cooled at −20°C in order to reduce the noises. A stabilized voltage of 800 V was fed to the photomultiplier. A tilting controller consists of a motor and a gear system, and periodically tilts the interference filter up to 15° away from the normal. The period of the tilting (0°→15°→0°) was about 90 s. This slow tilting speed allows the amplifiers to integrate the signal with a time constant as large as 1.5 s. This integration time constant would not cause any serious error in evaluating the 5200 Å emission rate since it takes about 10 s for the transmission passband of the interference filter to pass over the 5200 Å doublet.

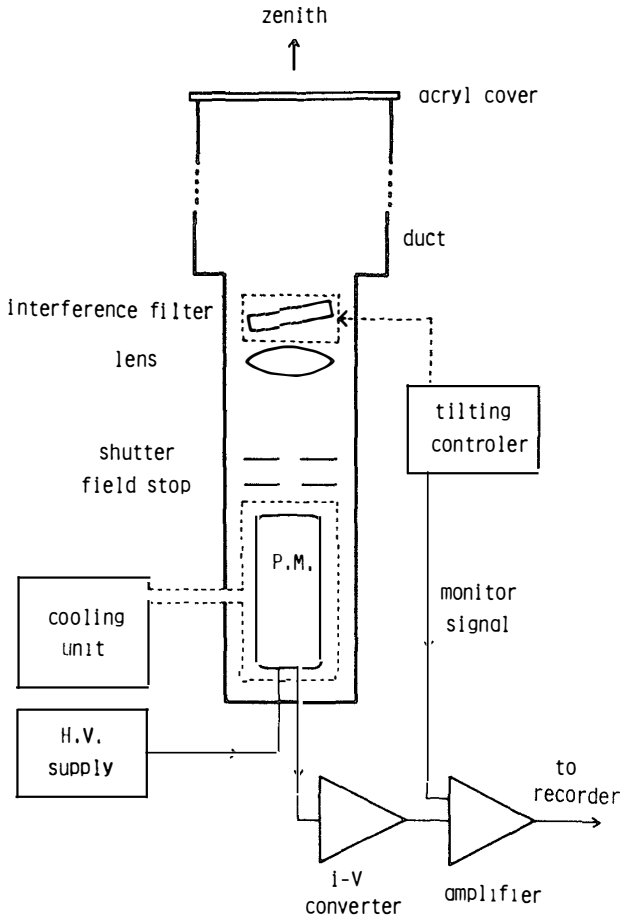

Fig. 2.1. Block-diagram of the 5200 Å tilting-filter photometer.

The whole system of the photometer except the top of a duct was set in a room with its line of sight directed toward the zenith.

An instrumentation of a 4278 Å photometer should also be noted here, for the observed characteristics of the 5200 Å will be discussed in relation to the N_2^+ 1NG (0, 1) 4278 Å band auroral emission. The 4278 Å photometer consists of an interference filter placed perpendicularly to the photometer's optical axis, a lens with an effective diameter of 4.8 cm, a shutter, a field stop, a photomultiplier with multi alkali photocathode and a D. C. amplifier. The interference filter has a peak transmittance of 59% at 4275 Å with a FWHM band width of 35 Å. A field of view of the 4278 Å photometer is 4° in full-angle. This photometer was set out of doors with its line of sight directed also toward the zenith.

2.3. Laboratory Calibration

A laboratory calibration of the photometer consists of the following two procedures. One is to determine transmission parameters of the interference filter by means of a monochromatic light source, and the other is to determine a response of the photometer for the 5200 Å doublet emission by means of a light source with known irradiance. Since spectral response of the photomultiplier and transmittance of the lens vary slowly with wavelength at around 5200 Å, the relative spectral sensitivity of the photometer is characterized by transmittance of the interference filter.

A measurement of transmittance of the interference filter was made by an optical system consisting of a halogen lamp, a monochromator (Nikon P250) and a collimation lens. This system supplied a collimated radiation with a FWHM band width of 0.6 Å. The measurement was repeated with changing the incident angle of the light beam to the filter.

In Fig. 2.2 are shown measured transmission parameters, maximum transmittance (T_M), wavelength of maximum transmission (λ_M) and a FWHM band width ($\Delta\lambda_{1/2}$), of the interference filter as a function of the tilt angle. λ_M appears to shift toward shorter wavelength as the tilt angle increases, and an amount of the shift is found to be roughly in proportion to square of the tilt angle as mentioned by EATHER and REASONER (1969). T_M and $\Delta\lambda_{1/2}$ are also found to vary with the tilt angle: the former decreases and the latter increases as the tilt angle increases, but their amounts of changes are not so much.

However, these transmission parameters of the interference filter shown in Fig. 2.2 cannot be used directly in data analysis because the photometer has a field of view of 2.5° in full-angle. These transmission parameters of the interference filter measured with a parallel light must be converted to those with a divergent light. On the polar coordinate illustrated in Fig. 2.3, this conversion can be made as

$$T_f^*(\zeta, \lambda)=\cos\zeta \int_{\phi=0}^{2\pi}\int_{\theta=0}^{\alpha} T_f(\xi, \lambda)\mathrm{d}\omega \Big/ \int_{\phi=0}^{2\pi}\int_{\theta=0}^{\alpha} \mathrm{d}\omega \tag{2.1}$$

with

$$\xi=\cos^{-1}(\cos\theta\cos\zeta+\sin\theta\sin\zeta\cos\phi) \tag{2.2}$$

and

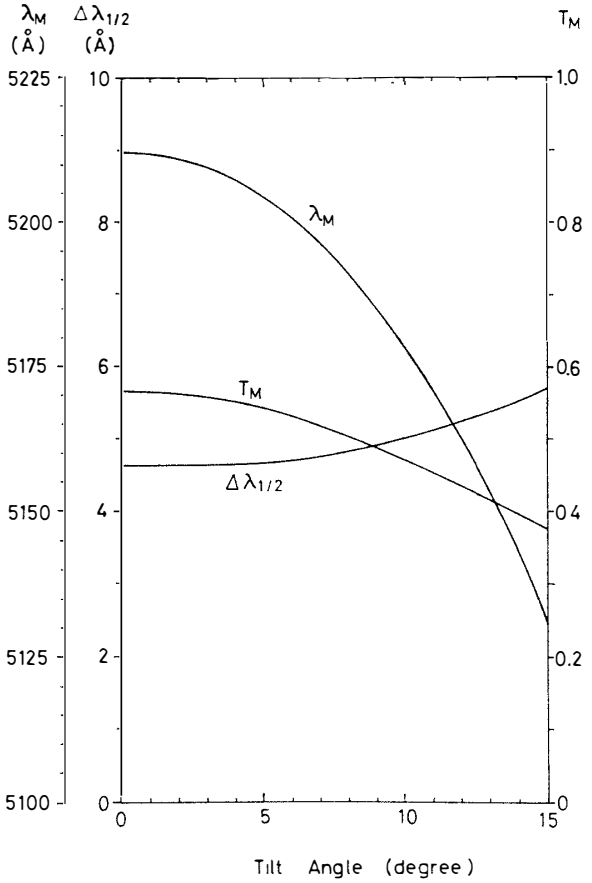

Fig. 2.2. Transmission parameters of the interference filter measured with a parallel light; maximum transmittance (T_M), wavelength of maximum transmission (λ_M) and a FWHM band width ($\Delta\lambda_{1/2}$) are given as a function of the tilt angle.

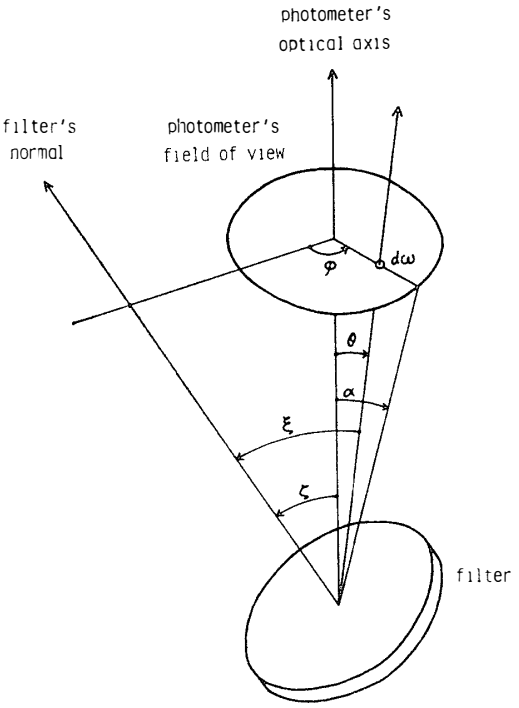

Fig. 2.3. Spatial geometry of the interference filter and the photometer's field of view. See text.

$$d\omega = \sin\theta \, d\theta \, d\phi \,, \tag{2.3}$$

where

T_f^* : transmittance of the interference filter with a divergent light,
T_f : transmittance of the interference filter with a parallel light,
$d\omega$: solid angle element,
ζ : tilt angle of the interference filter,
λ : wavelength,
α : half-angle of a field of view of the photometer,
ξ : angle between the filter's normal and the direction of the solid angle element,
θ and ϕ: variables.

cos ζ in eq. (2.1) represents a change in the detecting area and may be approximated

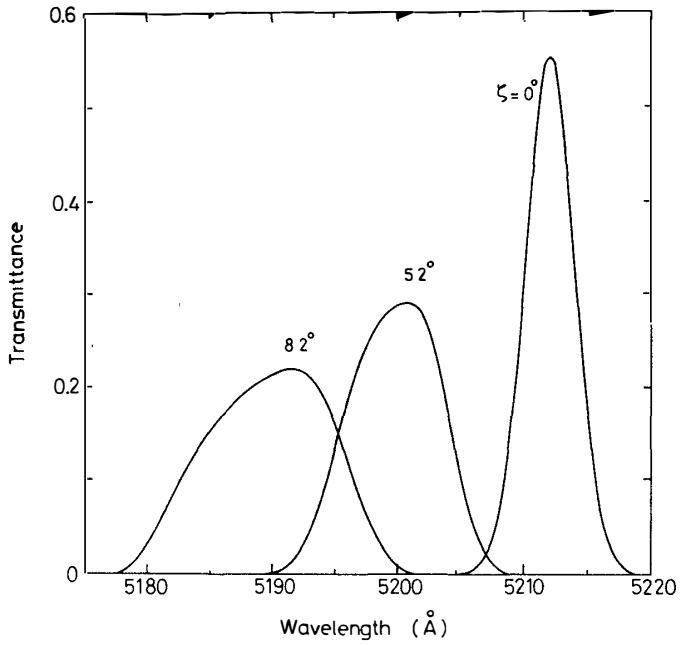

Fig. 2.4. Transmission profiles of the interference filter calculated taking into account the photometer's field of view. ζ is the tilt angle.

to be unity. In order to evaluate T_f^* numerically with eq. (2.1), $T_f(\xi=\text{constant})$ was approximated as a Gaussian function of wavelength with transmission parameters shown in Fig. 2.2.

Figure 2.4 shows examples of transmission profiles of the interference filter deduced with a divergent light of $\alpha=1.25°$ at tilt angles of 0°, 5.2° and 8.2°. It is evident in the figure that the decrease in maximum transmittance and increase in a FWHM band width with increase of the tilt angle is more considerable than in the case with a parallel light shown in Fig. 2.2. Yet, at the tilt angle of 0° the transmission profile appears to be almost identical to that with a parallel light. An equivalent band width changes little by the conversion $T_f \rightarrow T_f^*$ via eq. (2.1); therefore, a response of the photometer for a continuum radiation is independent of parallelism of an input radiation. On the other hand, a response of the photometer for the 5200 Å doublet emission is in proportion to the peak value of T_f^*. Figure 2.5 shows wavelength of the peak transmission of the filter as a function of the time after the normal position.

Determination of a response of the photometer was performed by means of a tungsten-filament quartz halogen lamp as a standard light source. The light source was placed about 30 m away from the photometer, and the tilt angle was 0°. Therefore, the input light was almost parallel and the filter's transmission profile had its peak at 5212 Å. The output current signal of the photomultiplier for the incident irradiance (i_L) can be expressed in units of ampere as

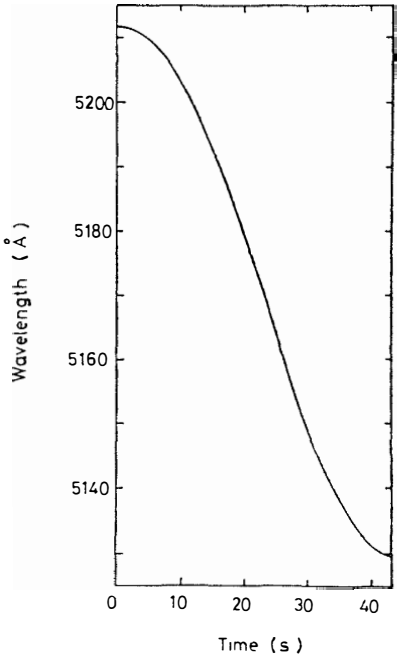

Fig. 2.5. Wavelength of peak transmission of the interference filter as a function of the time after the normal position.

$$i_L = SeA_p T_l \Phi_L \int T_f(\zeta=0, \lambda)\mathrm{d}\lambda \,, \tag{2.4}$$

where

S : detecting area,
e : charge of an electron,
A_p : response of the photomultiplier at 5212 Å (electrons photon^{-1}),
T_l : transmittance of the lens,
Φ_L : photon flux of the light source at 5212 Å (photons cm^{-2} s^{-1} Å^{-1}).

The last factor of the right hand side of eq. (2.4) represents an equivalent band width of the interference filter, and is 2.9 Å. A_p can be determined by the equation, since other factors are known.

The output current signal of the photomultiplier for the 5200 Å doublet emission in the aurora (i_{5200}) can be expressed in units of ampere as

$$i_{5200} = 10^6(4\pi I_{5200})(\omega/4\pi)SeA_p T_l T_f^*(\zeta=\zeta', \lambda=5200\ \text{Å}) \,, \tag{2.5}$$

where

$4\pi I_{5200}$: emission rate of the 5200 Å doublet (Rayleighs),
ω : solid angle of the photometer's field of view,
ζ' : tilt angle when the peak of T_f^* coincides with the 5200 Å doublet.

An effective transmittance of the filter for the 5200 Å doublet emission is $T_f^*(\zeta=\zeta',$

$\lambda=5200$ Å)$=0.28$. The instrumental constant C_{5200} which converts the 5200 Å emission rate to the output current can be calculated by the equation:

$$C_{5200}=10^6(\omega/4\pi)SeA_pT_1T_f^*(\zeta=\zeta', \lambda=5200 \text{ Å}) . \tag{2.6}$$

2.4. Results and Discussions

2.4.1. Observed 5200 Å emission rate

Observation of the 5200 Å emission was performed at Syowa Station (69°S, 40°E) over 145 nights from March to October 1977. However, the number of nights with a clear sky all night long and without the bright moon was only 13. Results and discussions described hereafter are based on the data obtained in these 13 nights. In order to know the instantaneous auroral activity, the N_2^+ 1NG (0, 1) 4278 Å band emission was also measured by a photometer. The excitation mechanism of this band emission in the aurora is considered to be the simultaneous ionization and excitation of N_2 by precipitating electrons (CHAMBERLAIN, 1961); therefore, its emission rate has been used as an indicator for the instantaneous energy input by precipitating electrons. The moonlight causes no serious error in measuring the 5200 Å emission rate since the 5200 Å photometer adopts a tilting-filter photometry, which enables subtraction of background continuum radiation. However, a moonlight contamination in the 4278 Å data is considerable since the photometer is equipped with a fixed filter. The 5200 Å photometer was carried back to Japan in 1978, and was used to measure the 5200 Å night airglow at Kakioka (36°N, 140°E) for comparison. The observation at Kakioka was performed from December 1978 to March 1979 over four clear and moonless nights.

Figures 2.6a and 2.6b show examples of raw output signals of the 5200 Å photometer; the former represents a case of a high auroral activity and the latter represents a case of no visual aurora in the vicinity of the photometer's field of view. The 5200 Å doublet is easily identified in Fig. 2.6a, though its doublet structure cannot be resolved. Also it is recognized in Fig. 2.6b where the 5200 Å emission rate is about 2 Rayleighs (hereafter written as R). The detection limit of this photometer for the 5200 Å emission is about 1 R. A background continuum radiation around 5200 Å under the non-auroral condition consists of an airglow continuum and of starlight. When auroral activity is high, a wing of the N_2^+ 1NG (0, 3) 5228 Å band and the N_2^+ 1NG (1, 4) 5150 Å band are superimposed on the continuum background as seen in Fig. 2.6a. Output signals of the 5200 Å photometer were read on strip charts

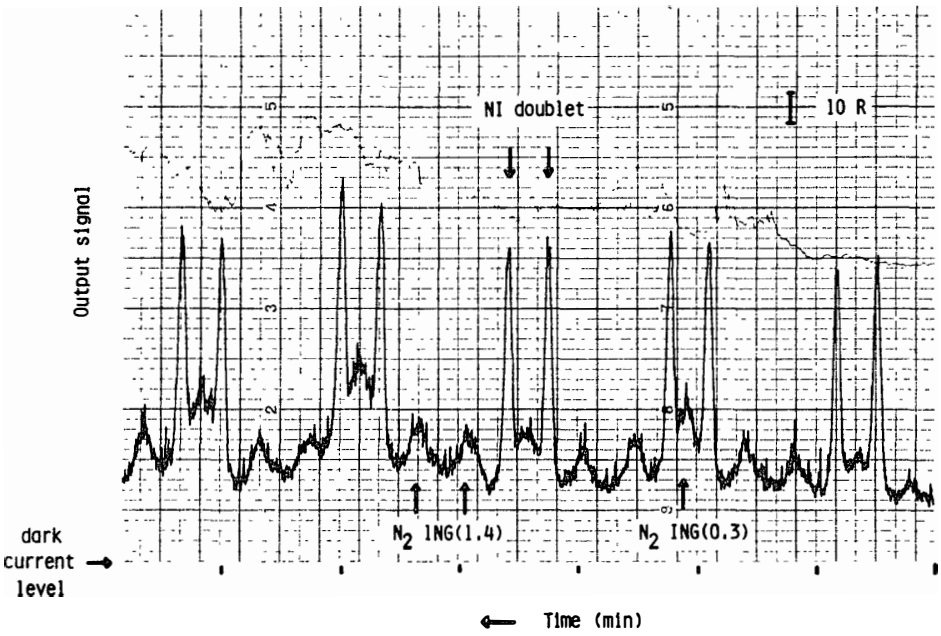

Fig. 2.6a. Example of a raw output signal of the 5200 Å photometer with a high auroral activity. Wavelength is being swept periodically between 5130 and 5212 Å. Besides the NI 5200 Å doublet, the N_2^+ 1NG(1, 4) 5150 Å band and a wing of the N_2^+ 1NG (0, 3) 5228 Å band can be identified.

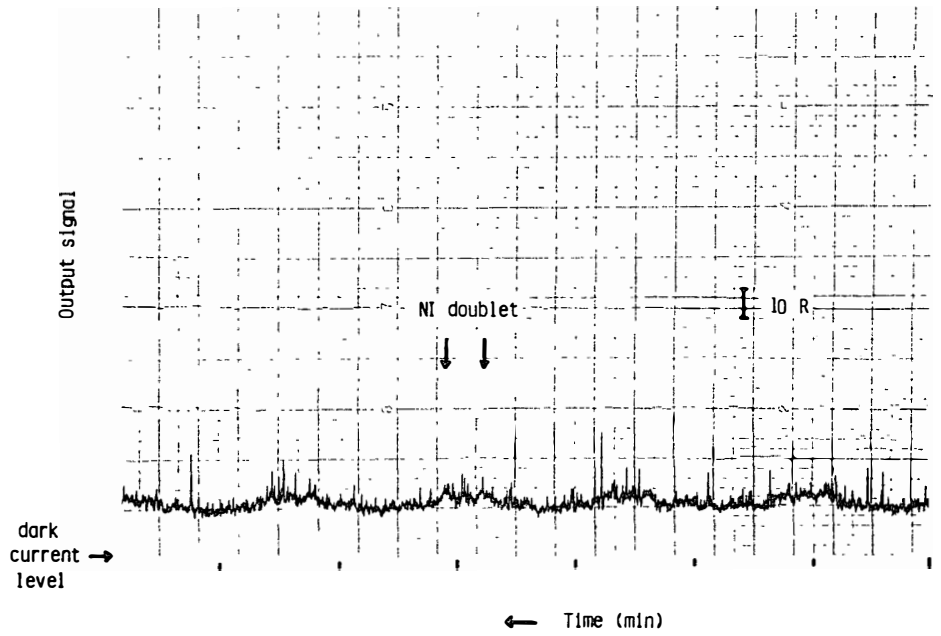

Fig. 2.6b. Same as Fig. 2.6a but with little auroral activity.

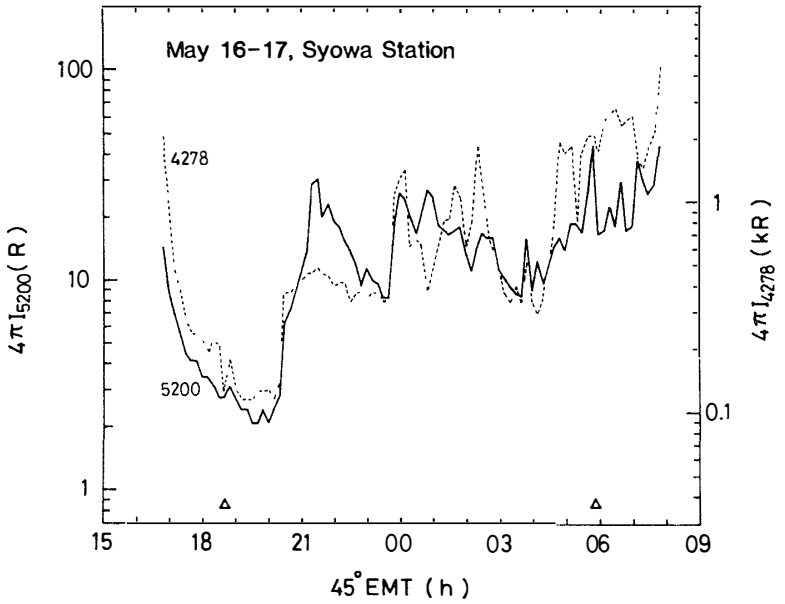

Fig. 2.7a. Nighttime variations of the 5200 Å emission rate ($4\pi I_{5200}$: real line) and 4278 Å emission rate ($4\pi I_{4278}$: dotted line) observed at Syowa Station on May 16–17, 1977. The beginning and the end of data correspond to the times of the solar zenith angle of about 100°, and the times of the solar zenith angle of 110° are indicated by triangles. 45°EMT= UT+3 hours.

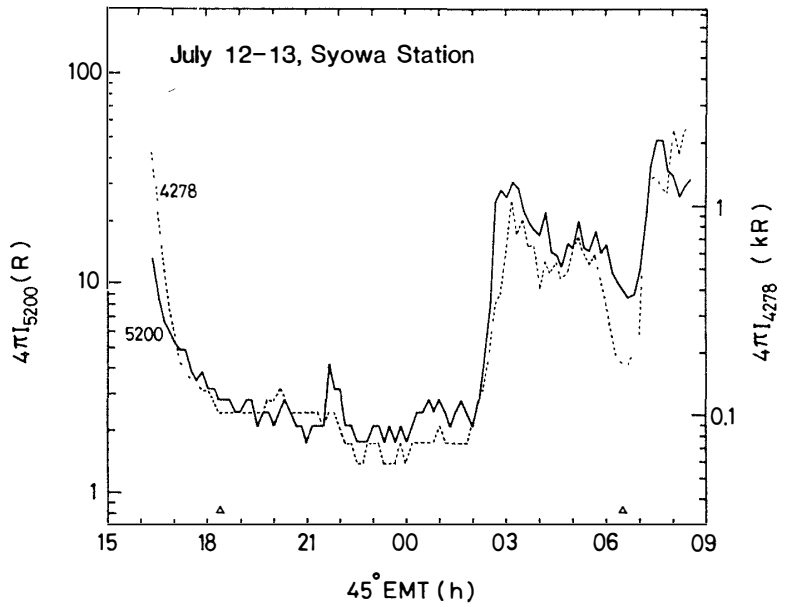

Fig. 2.7b. Same as Fig. 2.7a but on July 12–13, 1977. A small enhancement in the 5200 Å emission rate observed around 22 h is due to a nebula.

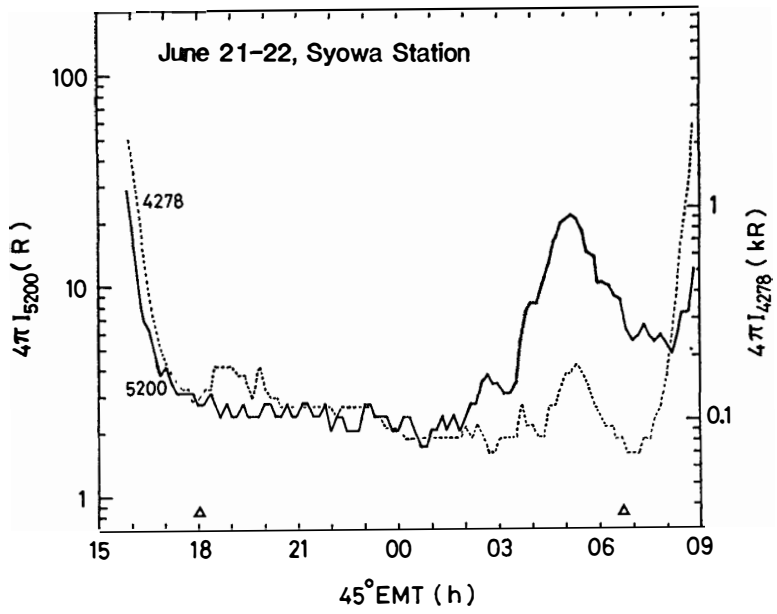

Fig. 2.7c. Same as Fig. 2.7a but on June 21–22, 1977.

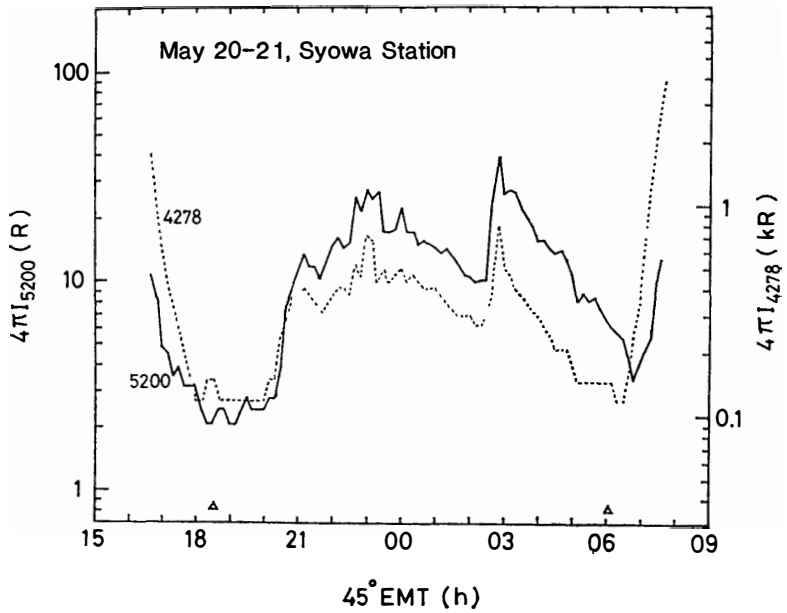

Fig. 2.7d. Same as Fig. 2.7a but on May 20–21, 1977.

averaging four samples every ten minutes. The time span for four samples is about three minutes.

Figures 2.7a through 2.7d show examples of nighttime variations of the 5200 Å doublet and the 4278 Å band emission rates. The time is 45° EMT (=UT+3 hours), which is the local standard time at Syowa Station. It must be noted here that the

emission rates of the 5200 Å doublet and the 4278 Å band shown in these figures include contaminations. The contamination is estimated to be about 1 R for the 5200 Å emission and about 50 R for the 4278 Å emission. Consequently, it may be neglected when auroral activity is high. A detailed discussion on the contamination will be given in the next subsection.

Figure 2.7a shows a case of an active night: a diffuse aurora (20–23 h), active discrete arcs (00–03 h) and a pulsating aurora (05–08 h) were seen. Figure 2.7b shows one of the moderate cases: active discrete arcs (02–06 h) were seen, but no visual aurora before 02 h. Figure 2.7c shows a case of a quiet night: a dim and diffuse aurora was seen only after 04 h. Figure 2.7d shows a case of a diffuse aurora all night long. Since Syowa Station is located in the auroral zone, an aurora was seen every night from there in spite of low solar activity in 1977. As seen in these examples, the 5200 Å emission is found to be one of the common spectral features of

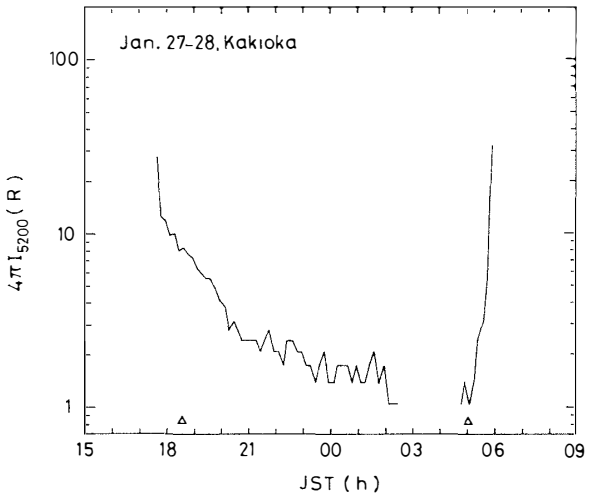

Fig. 2.8a. Nighttime variation of the 5200 Å emission rate ($4\pi I_{5200}$) observed at Kakioka on January 27–28, 1979. The beginning and the end of data correspond to the times of the solar zenith angle of about 100°, and the times of the solar zenith angle of 110° are indicated by triangles. JST = UT + 9 hours.

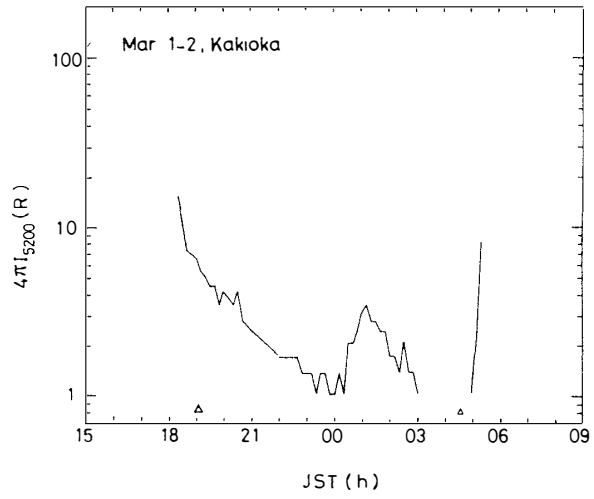

Fig. 2.8b. Same as Fig. 2.8a but on March 1–2, 1979.

aurora. When the 4278 Å emission is enhanced, the 5200 Å emission is found to be also enhanced.

Figures 2.8a and 2.8b show examples of nighttime variation of the 5200 Å emission rate observed at Kakioka. The 5200 Å emission should consist of only an airglow component in these cases. A midnight enhancement of the emission, as seen in Fig. 2.8b, was found in two nights among four nights.

2.4.2. Estimation of the contamination

It has been pointed out that the contamination due to the OH(9,2) band is serious in measuring the 5200 Å night airglow (*e. g.*, HERNANDEZ and TURTLE, 1969; BURNSIDE *et al.*, 1977). Since the spectral band width of the present 5200 Å photometer is about 10 Å when its peak response occurs at the 5200 Å doublet (see Fig. 2.4), some rotation lines of the OH(9, 2) band inevitably contribute to the apparent signals of the 5200 Å emission.

Measurement of the OH(9, 2) band night airglow is scarce because of its weakness, and its emission rate at middle latitude is theoretically estimated to be 5 R (LLEWELLYN *et al.*, 1978) to 10 R (CHAMBERLAIN, 1961; VALLANCE JONES, 1973). The OH emissions over the wide latitude range were measured with a photometer on board an aircraft by DICK *et al.* (1970), and no latitude dependence of the emission was found. An enhancement of the OH emissions associated with an aurora was investigated by MOREELS *et al.* (1976) with airborne photometers, and was found to

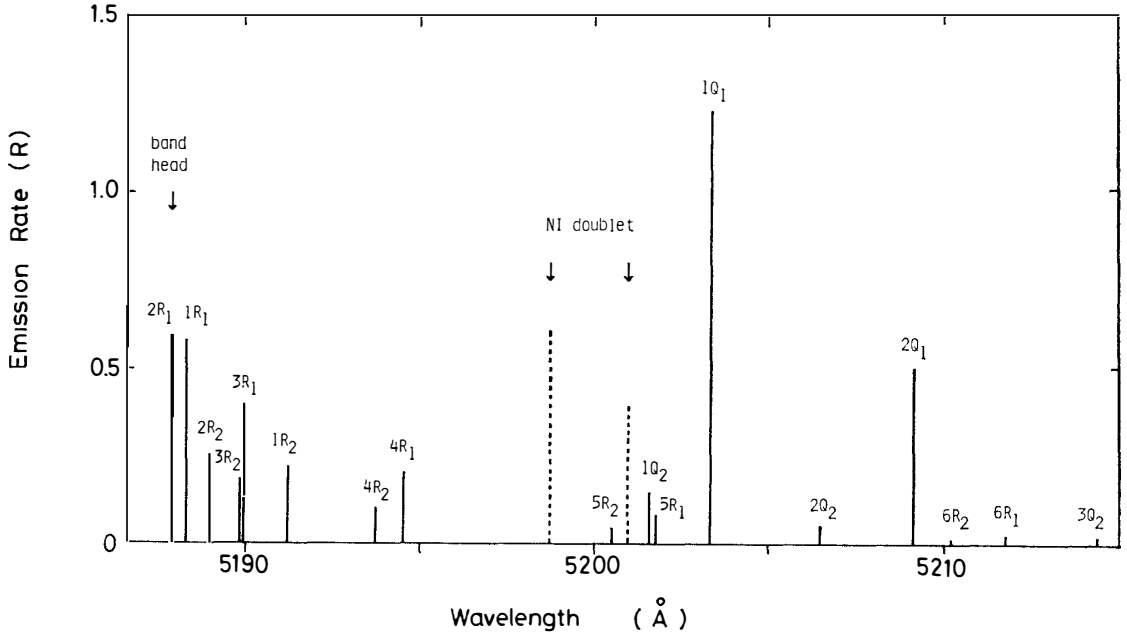

Fig. 2.9. Rotational structure of the OH(9, 2) band around the NI 5200 Å doublet. The total emission rates of the OH band and the NI doublet are assumed to be 10 R and 1 R, respectively.

be less than a factor of two. Therefore, the nighttime emission rate of the OH(9,2) band at Syowa Station may be 10 R or less in quiet times and up to 20 R even under the active auroral conditions.

Figure 2.9 represents the rotational structure of the OH (9, 2) band, and the NI doublet is also shown in the same figure. The total emission rates of the OH(9, 2) band and the NI lines are assumed to be 10 R and 1 R, respectively, in this figure. The wavelengths of rotation lines of the (9, 2) band were calculated with the molecular constants of OH given by KRASSOVSKY *et al.* (1962), and their relative intensities were calculated from Hönl-London factors of BENEDICT *et al.* (1953) assuming the rotational temperature of 200 K. Since the calculated wavelengths of these rotation lines may have some uncertainty, the wavelengths of the NI lines were adjusted so that the intervals between the NI lines and the $1Q_1$ rotation line of the OH(9, 2) band may be those measured by HERNANDEZ and TURTLE (1969) with a Fabry-Perot spectrometer.

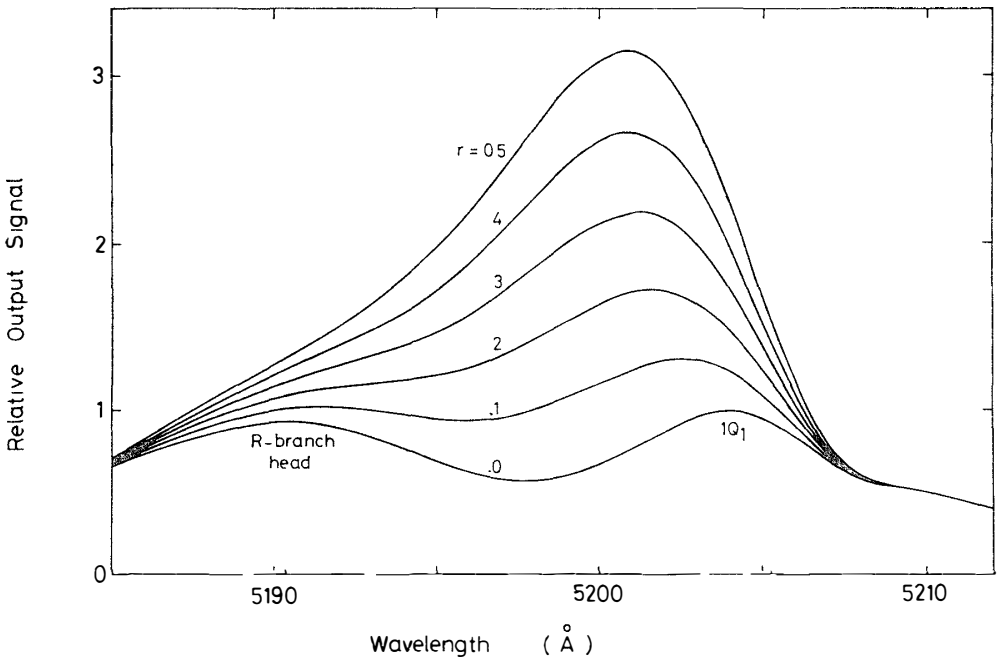

Fig. 2.10. Output signals of the 5200 Å photometer calculated by modifying the rotational structure of the OH(9, 2) band and the NI doublet with the photometer's instrumental function T_f^*. r is the ratio of the total emission rate of the NI lines to the OH (9, 2) band.

Figure 2.10 shows the calculated output signals of the 5200 Å photometer for the rotation lines of the OH band and the NI doublet as modified by the photometer's instrumental function (T_f^*) with the ratio of the total emission rate of the NI lines to the OH band as a parameter. The $1Q_1$ rotation line is the strongest of the OH

(9, 2) band, and contributes more than ten percent of the total emission rate of the OH (9, 2) band. This line is so close to the NI doublet that it cannot be resolved. Other rotational structures except for the R-branch head are found to be averaged out and will be observed as a continuum background. As seen in Fig. 2.10, about ten percent of the total emission rate of the OH band is expected to contaminate the apparent output signal of the NI doublet. Since the total emission rate of the OH (9, 2) band is considered to be about 10 R, the NI doublet emission rate observed at Syowa Station under the quiet auroral condition is estimated to include the OH contamination of about 1 R.

The output signal of the 4278 Å photometer is also ascribed to some contaminations such as the airglow continuum and starlight. The airglow continuum has been observed to be about 0.5 R/Å around the wavelength region (BROADFOOT and KENDALL, 1968), and the starlight in the direction of the photometer's line of sight varies with local time from 100 to 300 S_{10} according to ROACH and MEGILL (1961). Assuming a G2 type spectrum for the starlight, 100 S_{10} is equivalent to 0.3 R/Å at 4278 Å. Since the 4278 Å photometer's filter has an equivalent band width of 25 Å and a transmission of 0.5 at 4278 Å, the continuum radiation of 1 R/Å is equivalent to the 4278 Å band emission rate of 50 R. Therefore, the contamination in the 4278 Å band emission rate due to the airglow continuum (0.5 R/Å) and the starlight (0.3–0.9 R/Å) is estimated to vary between 40 and 70 R.

2.4.3. Observed characteristics of the 5200 Å emission

By examining the observed nighttime variations of the NI 5200 Å emission at Syowa Station, the following characteristics of the emission are deduced.

i) The 5200 Å emission rate is well correlated with the 4278 Å emission rate, and its typical value is about 30 R when discrete auroral arcs are seen. The 4278 Å emission rate is about 1 kR in such a case.

ii) The ratio of the 5200 Å emission rate to the 4278 Å emission rate decreases as the 4278 Å emission rate increases.

iii) The 5200 Å emission rate including the OH contamination never becomes smaller than about 2 R at Syowa Station, whereas it becomes smaller than 2 R at Kakioka.

The first means that the NI 5200 Å emission is enhanced by auroral particles at Syowa Station. The 5200 Å emission may be excited by dissociative recombination of NO^+ in the ionospheric *F* region (TORR *et al.*, 1976):

$$NO^+ + e \rightarrow N(^2D, {}^4S) + O\,, \tag{2.7}$$

where NO^+ is supplied by the ion-atom interchange reaction of O^+ and N_2:

$$O^+ + N_2 \rightarrow NO^+ + N(^4S)\,. \tag{2.8}$$

This process may be promoted under the auroral condition where the electron and ion

densities are enhanced by precipitating particles. The production rate of the $N(^2D)$ through reaction (2.7) increases with increase in the electron density. As mentioned in Subsection 1.7.1, the quantum yield of $N(^2D)$ in reaction (2.7) is estimated to be close to unity.

On the other hand, the observed enhancement of the 5200 Å emission associated with an aurora might be caused by the dissociation and excitation of N_2 by the auroral electron impact:

$$N_2+e^*\rightarrow 2N(^2D, {}^4S)+e^* , \tag{2.9}$$

where e* represents an energetic electron, and the quantum yield of $N(^2D)$ in the reaction is considered to be more than 0.5 (see Subsection 1.7.2). Since the dissociation rate of N_2 is expected to be larger than the total ionization rate under an auroral perturbation (KONDO and OGAWA, 1976), reaction (2.9) may be the dominant excitation process of the 5200 Å emission in the aurora.

The dissociative recombination (reaction (2.7)) has been proposed as the dominant excitation mechanism of the 5200 Å emission in the aurora by GÉRARD and HARANG (1973); however, their argument is merely based upon a proportionality between the NI 5200 Å emission rate and the OI 6300 Å emission rate. It is also likely that the electron impact excitation induces the proportionality between the NI and OI emission rates.

In order to confirm whether or not the dissociative recombination can explain the observed enhancement of the 5200 Å emission in the aurora, a simple evaluation of the volume emission rate due to the dissociative recombination was executed for the altitudes between 110 and 300 km with the chemical equilibrium assumption as follows:

a) $N(^2D)$ is produced only through reaction (2.7), where NO^+ is supplied by reaction (2.8),

b) $N(^2D)$ is lost through reactions with electron, O, O_2 and the spontaneous emission,

c) electron is lost only through reaction (2.7),

d) ionic species are only O^+ and NO^+.

Since other reactions than reaction (2.7) are involved in removing electrons in the real ionosphere, this evaluation gives an upper limit on the 5200 Å emission rate due to the dissociative recombination.

According to the chemical equilibrium for NO^+, the production rate of $N(^2D)$ can be expressed as

$$P=k_7[NO^+][e]=k_8[O^+][N_2] , \tag{2.10}$$

where k_7 and k_8 are the rate coefficients of reactions (2.7) and (2.8), respectively, and brackets denote the number densities. By using the charge neutrality:

$$[e]=[O^+]+[NO^+] , \tag{2.11}$$

eq. (2.10) can be reformed as

$$P=\frac{k_7k_8[e]^2[N_2]}{k_7[e]+k_8[N_2]} . \tag{2.12}$$

The loss rate of $N(^2D)$ can be written in the form:

$$L=(k_{14}[e]+k_{15}[O]+k_{16}[O_2]+A_{5200})[N(^2D)] , \tag{2.13}$$

where A_{5200} is the transition probability of the NI 5200 Å doublet; k_{14}, k_{15} and k_{16} are the rate coefficients of the following reactions, respectively:

$$N(^2D)+e\rightarrow N(^4S)+e , \tag{2.14}$$

$$N(^2D)+O\rightarrow N(^4S)+O \tag{2.15}$$

and

$$N(^2D)+O_2\rightarrow NO+O . \tag{2.16}$$

The volume emission rate of the 5200 Å doublet can be written as

$$\varepsilon_{5200}=A_{5200}(P/L). \tag{2.17}$$

To evaluate eq. (2.17) numerically, the following values for the coefficients were used (T is the temperature in K):

$k_7=4.6\times10^7(300/T)$ cm^3 s^{-1} (BIONDI, 1969),
$k_8=1.2\times10^{-12}(300/T)$ cm^3 s^{-1} (MCFARLAND *et al.*, 1973),
$k_{14}=1.0\times10^{-9}(T/300)^{1/2}$ cm^3 s^{-1} (RUSCH *et al.*, 1975),
$k_{15}=1.0\times10^{-12}$ cm^3 s^{-1} (KONDO and OGAWA, 1977),
$k_{16}=5.2\times10^{-12}$ cm^3 s^{-1} (HUSAIN *et al.*, 1974),
$A_{5200}=1.06\times10^{-5}$ s^{-1} (GARSTANG, 1956).

The number densities of major neutral species, $[N_2]$, $[O_2]$ and $[O]$, and temperatures were taken from CIRA (1972). The calculations were made for $[e]=10^5$, 3×10^5 and 10^6 cm^{-3} over the whole altitude region with the exospheric temperatures of 800 K and 1200 K. The electron densities in the ionospheric E and F_1 region under auroral perturbations are enhanced to be about 10^5, 3×10^5 and 10^6 cm^{-3} corresponding to IBC I, II and III aurorae (*e. g.*, KAMIYAMA, 1966; JONES and REES, 1973; KONDO and OGAWA, 1976).

Figure 2.11 shows an example of the calculated reaction frequencies in the case of $[e]=10^5$ cm^{-3} with the exospheric temperature of 800 K, and the calculated volume emission rates and the column emission rates of the 5200 Å doublet are shown in Fig. 2.12. The 5200 Å column emission rates are hardly affected by the change in the exospheric temperature and are about 2.6 R, 9.2 R and 33 R corresponding to $[e]=10^5$, 3×10^5 and 10^6 cm^{-3}, respectively. As mentioned earlier, the 4278 Å emission rate was about 1 kR when the 5200 Å emission rate was 30 R. The 4278 Å emission rate of 1 kR corresponds to an intermediate case of IBC I and II. Therefore,

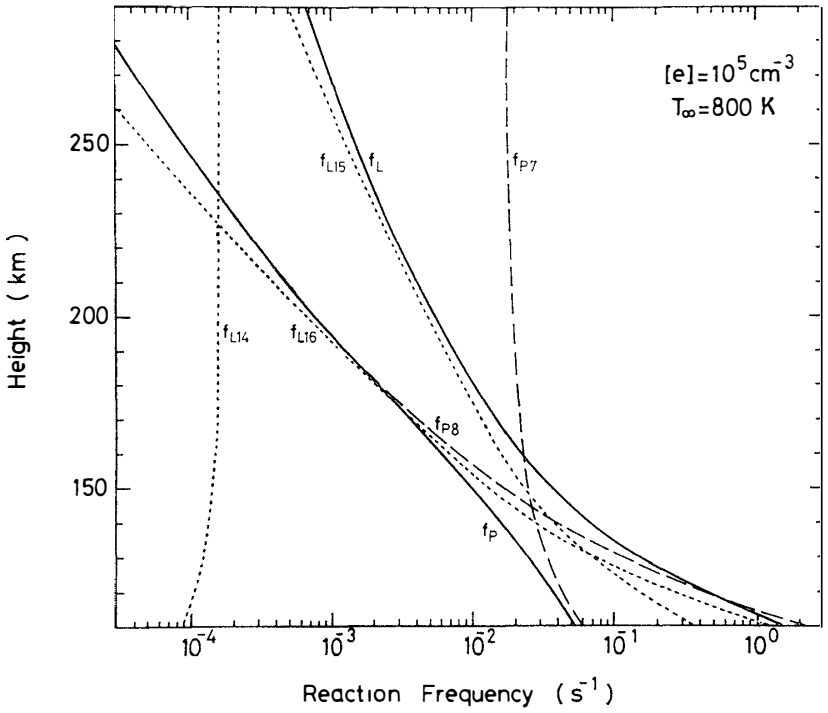

Fig. 2.11. Calculated reaction frequencies related to the 5200 Å emission due to the dissociative recombination in the case of $[e]=10^5\ cm^{-3}$ *with the exospheric temperature of 800 K; dotted lines:* $f_{L14}=k_{14}[e]$, $f_{L15}=k_{15}[O]$ *and* $f_{L16}=k_{16}[O_2]$; *dashed lines:* $f_{P7}=k_7[e]$ *and* $f_{P8}=k_8[N_2]$; *real lines:* $f_L=f_{L14}+f_{L15}+f_{L16}$ *and* $f_P=f_{P7}f_{P8}/(f_{P7}+f_{P8})$. *See text.*

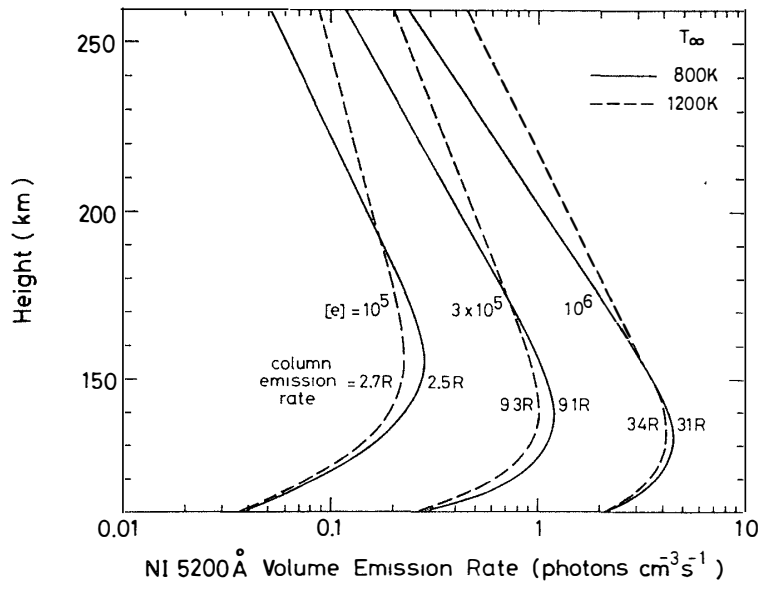

Fig. 2.12. Calculated volume emission rate of the 5200 Å doublet due to the dissociative recombination in cases of $[e]=10^5$, 3×10^5 *and* $10^6\ cm^{-3}$ *with the exospheric temperature of 800 K and 1200 K. The column emission rates are also noted.*

the dissociative recombination yields only 5 R or so within the observed 5200 Å emission rate of 30 R. Note that this is an upper limit for the 5200 Å emission rate due to the dissociative recombination process.

ROBLE and REES (1977) calculated the density distribution of odd nitrogen species in the thermosphere under auroral perturbations. According to their results, an enhancement in the 5200 Å emission rate may be expected to be 130 R after 10^3 s duration of an IBC II$^+$ aurora with 8 keV electrons. Since the dissociative recombination provides the 5200 Å emission rate of about 15 R in an IBC II$^+$ aurora, the electron impact may be responsible for about 90% of the 5200 Å emission rate in this case. Another case calculated by ROBLE and REES (1977) shows that the 5200 Å emission rate is enhanced to 140 R under an IBC I$^-$ aurora with 0.2 keV electrons. This remarkable dependence of the 5200 Å emission rate on the mean energy of precipitating electrons is a natural consequence of the highly metastable nature of N(^2D). Since the mean energy of precipitating electrons associated with discrete auroral arcs is usually a few keV (MENG, 1978), the 5200 Å emission rate of 30 R in the middle of IBC I and II may be excited by the electron impact. Therefore, it may be concluded that the 5200 Å emission in the aurora is mainly excited by the dissociation and excitation of N_2 by the electron impact.

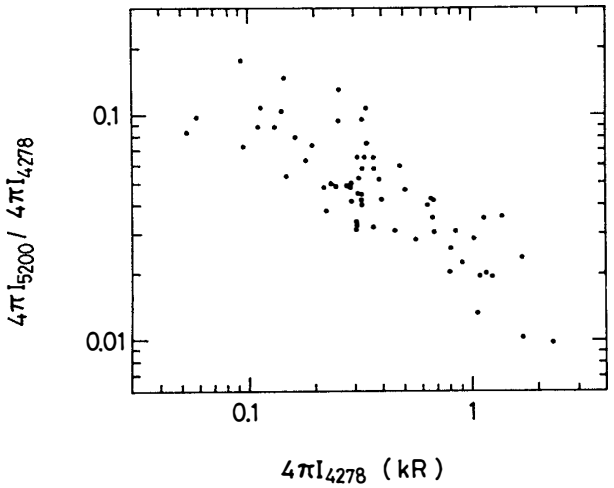

Fig. 2.13. Observed relation between the hourly averaged 5200 Å emission rate ($4\pi I_{5200}$) and the hourly averaged 4278 Å emission rate ($4\pi I_{4278}$). The ratio $4\pi I_{5200}/4\pi I_{4278}$ is plotted against $4\pi I_{4278}$. The contaminations are corrected.

The second is demonstrated in Fig. 2.13, where the 5200 Å and 4278 Å emission rates have been corrected for the contaminations: 1 R for the former and 50 R for the latter (see Subsection 2.4.2). And data points shown in the figure were taken in the periods when the solar zenith angle was larger than 105° and some auroral activity was evident. Therefore, data in a quiet period, *e.g.*, before 02h on July 12–13 (Fig. 2.7b), are not included in the figure. A similar characteristic of the 5200 Å

auroral emission has already been reported by GÉRARD and HARANG (1973), but they gave no explanation for it. This characteristic might be explained if the 5200 Å auroral emission were mainly excited by the dissociative recombination. As seen in Fig. 2.12 the 5200 Å emission rate due to the dissociative recombination increases more gradually than the increase in the total energy influx of precipitating particles (the total energy influx associated with an IBC II aurora is one order of magnitude larger than that with an IBC I aurora), whereas the 4278 Å emission rate is believed to be nearly in proportion to the total energy influx. However, the dissociative recombination has been found to be insufficient to explain the observed 5200 Å emission rate.

A possible explanation is that the total energy influx of precipitating particles increases as their mean energy increases. It is well known that an auroral particle with higher mean energy can penetrate into the lower altitude in the atmosphere. Since the 5200 Å emission arises from a forbidden transition with a very small transition probability ($\sim 10^{-5}$ s^{-1}), the efficiency for $N(^2D)$ to emit a photon becomes smaller at lower altitude because of the deactivation processes (2.14) through (2.16) (see Fig. 2.11). On the other hand, the 4278 Å emission is affected little by deactivation processes because of its large transition probability, and its emission rate is considered to be proportional to the total energy influx of precipitating particles. Therefore, if the mean energy of the auroral electrons increases with their total energy, then 5200 Å emission rate increases more gradually than the 4278 Å emission rate. Actually, such a characteristic has been known for the precipitating electrons associated with a discrete auroral arc (MENG, 1978). A recent simultaneous observation of electron precipitations and optical aurorae by using a satellite (MENG, 1979) shows that it is also the case in the diffuse aurora.

The third that the 5200 Å emission rate including the OH contamination never becomes smaller than 2 R at Syowa Station may be explained in two ways. One is the OH contamination which amounts to 1 R (see Subsection 2.4.2). Another is a continuous particle drizzle even in a quiet period. Such a continuous particle drizzle has been inferred from ionospheric or optical measurements (WALKER *et al.*, 1968; EATHER and MENDE, 1972). However, it seems difficult to draw a definite conclusion at this time, because 2 R is close to the detection limit of the photometer (~ 1 R).

2.5. Conclusion

From the ground observations at Syowa Station in the auroral zone, the NI 5200 Å doublet is found to be one of the common spectral features of the aurora. The 5200 Å emission is always found to be enhanced when the N_2^+ 1NG(0, 1) 4278 Å band emission is enhanced.

The excitation mechanism for the 5200 Å emission in the aurora is investigated with a simple model calculation assuming chemical equilibrium. The dissociative recombination of NO^+, which is believed to be the main excitation mechanism for the 5200 Å night airglow at middle latitude, is found to be able to explain only a few tens percent of the observed emission rate of the 5200 Å doublet in the aurora. Therefore, the dissociation and excitation of N_2 by the direct impact of auroral electrons may be the dominant excitation mechanism for the 5200 Å emission in the aurora.

The ratio of the 5200 Å emission rate to the 4278 Å emission rate is found to have a tendency to decrease with increase of the 4278 Å emission rate. This tendency may be due to the characteristics of the precipitating particles that their mean energy increases with their total energy, as well as to the highly forbidden nature of the NI 5200 Å emission.

Acknowledgments

This research could not have been accomplished without the supports rendered by many people. Special thanks are due to late Prof. T. TOHMATSU, Prof. T. OGAWA, Drs. K. SUZUKI and K. SHIBASAKI. The author thanks late Prof. T. TOHMATSU for his encouragement and guidance in preparing this study. He thanks Prof. T. OGAWA for his continuing guidance and encouragement in planning and executing this study. He thanks Drs. K. SUZUKI and K. SHIBASAKI for their careful reading of the manuscript. He also wants to thank Profs. N. FUKUSHIMA and S. KOKUBUN and Dr. E. KANEDA who encouraged him by discussions with interest. And he thanks Miss Y. SHINDO for typing the manuscript. Thanks are also due to the other members of the Geophysics Research Laboratory, University of Tokyo.

The rocket experiments at Uchinoura were conducted by the Institute of Space and Aeronautical Science, University of Tokyo. The rocket experiment at Thumba was conducted by the Indian Space Research Organization. The rocket experiment and the ground observation of the auroral emissions at Syowa Station were made as an activity of the 18th Japanese Antarctic Research Expedition, which was supported by the National Institute of Polar Research. Thanks are also due to the other members of JARE-18 for their helpful cooperations.

References

AKASOFU, S.-I. (1968): Polar and Magnetospheric Substorms. Dordrecht, D. Reidel, 73–109 (Astrophys. Space Sci. Lib., Vol. 11).

BAKER, K. D., NAGY, A. F., OLSEN, R. O., ORAN, E. S., RANDHAWA, J., STROBEL, D. F. and TOHMATSU, T. (1977): Measurement of nitric oxide altitude distribution in the mid-latitude mesosphere. J. Geophys. Res., **82**, 3281–3286.

BARTH, C. A. (1964): Rocket measurement of nitric oxide dayglow. J. Geophys. Res., **69**, 3301–3303.

BARTH, C. A. (1966a): Nitric oxide in the upper atmosphere. Ann. Géophys., **22**, 198–207.

BARTH, C. A. (1966b): Rocket measurement of nitric oxide in the upper atmosphere. Planet. Space Sci., **14**, 623–630.

BAULCH, D. L., DRYSDALE, D. D., HORNE, D. G. and LLOYD, A. C. (1973): Evaluated kinetic data for high temperature reactions, 2, Homogeneous gas phase reactions of the H_2–N_2–O_2 system. Cleveland, Chemical Rubber Company Press.

BEITING, E. J. and FELDMAN, P. D. (1978): A search for nitric oxide gamma band emission in an aurora. Geophys. Res. Lett., **5**, 51–53.

BENEDICT, W. S., PLYLER, E. K. and HUMPHREYS, C. J. (1953): The emission spectrum of OH from 1.4 to 1.7 μ. J. Chem. Phys., **21**, 398–402.

BERGEMAN, T. H. and ZARE, R. N. (1972): Hyperfine structure of the $A^2\Sigma^+$ state of nitric oxide. Bull. Am. Phys. Soc., **17**, 149.

BIONDI, M. A. (1969): Atmospheric electron-ion and ion-ion recombination processes. Can. J. Chem., **47**, 1711–1719.

BREENE, R. G. (1967): Spectral line broadening in air molecule systems. Appl. Opt., **6**, 141–147.

BRINKMANN, R. T., GREEN, A. E. S. and BARTH, C. A. (1966): A digitalized solar ultraviolet spectrum. JPL Tech. Rep., No. 32–951, Jet Propulsion Laboratory.

BROADFOOT, A. L. and KENDALL, K. R. (1968): The airglow spectrum, 3100–10000 Å. J. Geophys. Res., **73**, 426–428.

BURNSIDE, R. G., MERIWETHER, J. W. and TORR, M. R. (1977): Contamination of groundbased measurements of OI (6300 Å) and NI (5200 Å) airglow by OH emissions. Planet. Space Sci., **25**, 985–988.

CALLEAR, A. B. and WOOD, P. M. (1971): Rates of energy transfer from $N_2(A^3\Sigma_u^+)$ to various molecules. Trans. Faraday Soc., **67**, 272–288.

CHAMBERLAIN, J. W. (1961): Physics of the Aurora and Airglow. New York, Academic Press, 704p.

CIRA (1965): COSPAR International Reference Atmosphere, 1965. Amsterdam, North Holland.

CIRA (1972): COSPAR International Reference Atmosphere, 1972. Berlin, Akademie.

CRAVENS, T. E. (1977): Nitric oxide gamma band emission rate factor. Planet. Space Sci., **25**, 369–372.

CRAVENS, T. E. and STEWART, A. I. (1978): Global morphology of nitric oxide in the lower E region. J. Geophys. Res., **83**, 2446–2452.

CRAVENS, T. E., GERARD, J. C., STEWART, A. I. and RUSCH, D. W. (1979): The latitudinal gradient of nitric oxide in the thermosphere. J. Geophys. Res., **84**, 2675–2680.

DALGARNO, A. (1962): Spectral reflectivity of the earth's atmosphere, III. The scattering of light by atomic system. GCA Report, No. 62–68.

DAVENPORT, J. E., SLANGER, T. G. and BLACK, G. (1976): The quenching of $N(^2D)$ by $O(^3P)$. J. Geophys. Res., **81**, 12–16.

DICK, K. A. (1978): The auroral 2150 Å feature: A contribution from lines of singly ionized atomic nitrogen. Geophys. Res. Lett., **5**, 273–274.

DICK, K. A., SIVJEE, G. G. and CROSSWHITE, H. M. (1970): Aircraft airglow intensity measurements: Variations in OH and OI (5577). Planet. Space Sci., **18**, 887–894.

DITCHBURN, R. W. and YOUNG, P. A. (1962): The absorption of molecular oxygen between 1850 and 2500 Å. J. Atmos. Terr. Phys., **24**, 127–139.

DODGE, L. G., DUSEK, J. and ZABIELSKI, M. F. (1980): Line broadening and oscillator strength measurements for the nitric oxide $\gamma(0, 0)$ band. J. Quant. Spectrosc. Radiat. Transfer, **24**, 237–249.

DONAHUE, T. M., ZIPF, E. C. and PARKINSON, T. D. (1970): Ion composition and ion chemistry in an aurora. Planet. Space Sci., **18**, 171–186.

DUYSINX, R. and MONFILS, A. (1972): Auroral spectra recorded between 2000 and 3000 Å with a fast scanning spectrometer. Ann. Géophys., **28**, 109–110.

EARLS, L. T. (1935): Intensities in $^2\Pi$–$^2\Sigma$ transitions in diatomic molecules. Phys Rev., **48**, 423–424.

EATHER, R. H. and REASONER, D. L. (1969): Spectrophotometry of faint light sources with a tilting-filter photometer. Appl. Opt., **8**, 227–242.

EATHER, R. H. and MENDE, S. B. (1971): Airborne observations of auroral precipitation patterns. J. Geophys. Res., **76**, 1746–1755.

EATHER, R. H. and MENDE, S. B. (1972): Systematics in auroral energy spectra. J. Geophys. Res., **77**, 660–673.

FELDMAN, P. D. (1976): Nitric oxide gamma band emission in an aurora. Geophys. Res. Lett., **3**, 9–12.

FELDMAN, P. D. and TAKACS, P. Z. (1974): Nitric oxide gamma and delta band emission at twilight. Geophys. Res. Lett., **1**, 169–171.

FREDERICK, J. E. and RUSCH, D. W. (1977): On the chemistry of metastable atomic nitrogen in the *F* region deduced from simultaneous satellite measurements of the 5200 Å airglow and atmospheric composition. J. Geophys. Res., **82**, 3509–3517.

FREDERICK, J. E. and HAYS, P. B. (1978): Magnetic ordering of the polar airglow. Planet. Space Sci., **26**, 339–345.

GARSTANG, R. H. (1956): Transition probabilities of auroral lines. The Airglow and the Aurorae, ed. by E. B. ARMSTRONG and A. DALGANO. London, Pergamon Press, 324 p.

GÉRARD, J.-C. and HARANG, O. E. (1973): Observation of O(^1D) and N(^2D) emission in the polar aurora. Physics and Chemistry of Upper Atmospheres, ed. by B. M. MCCORMAC, Dordrecht, D. Reidel, 241–247.

GÉRARD, J.-C. and BARTH, C. A. (1977): High-latitude nitric oxide in the lower thermosphere. J. Geophys. Res., **82**, 674–680.

GOLSHAN, N. and SECHRIST, C. F. (1975): Seasonal and solar cycle variation of *E*-region nitric oxide. Radio Sci., **10**, 305–315.

HERNANDEZ, G. and TURTLE, J. P. (1969): The NI(^4S–^2D) transitions in the upper atmosphere at night. Planet. Space Sci., **17**, 675–684.

HERZBERG, G. (1950): Molecular Spectra and Molecular Structure I. Spectra of Diatomic Molecules. New York, Van Nostrand Reinhold, 558 p.

HILL, E. and VAN VLECK, J. H. (1928): On the quantum mechanics of the rotational distortion of multiplets in molecular spectra. Phys. Rev., **32**, 250–272.

HINTEREGGER, H. E. (1970): The extreme ultraviolet solar spectrum and its variation during a solar cycle. Ann. Géophys., **26**, 547–554.

HINTEREGGER, H. E. (1976): EUV fluxes in the solar spectrum below 2000 Å. J. Atmos. Terr. Phys., **38**, 791–806.

HUDSON, R. D. and MAHLE, S. H. (1972): Photodissociation rates of molecular oxygen in the mesosphere and lower thermosphere. J. Geophys. Res., **77**, 2902–2914.

HUNTEN, D. M. and MCELROY, M. B. (1968): Metastable $O_2(^1\Delta)$ as a major source of ions in the *D* region. J. Geophys. Res., **73**, 2421–2428.

HUSAIN, D., MITRA, S. K. and YOUNG, A. N. (1974): Kinetic study of electronically excited nitrogen atoms, $N(^2D, ^2P)$, by attenuation of atomic resonance radiation in the vacuum ultraviolet. J. Chem. Soc. Faraday Trans., II **70**, 1721–1731.

HYMAN, E., STRICKLAND, E. J., JULIENNE, P. S. and STROBEL, D. F. (1976): Auroral NO concentrations? J. Geophys. Res., **81**, 4765–4769.

IMAMI, M. and BORST, W. L. (1975): Electron impact excitation of the gamma bands of nitric oxide. J. Chem. Phys., **63**, 3602–3605.

INN, E. C. Y. and TANAKA, Y. (1953): Absorption coefficient of ozone in the ultraviolet and visible regions. J. Opt. Soc. Am., **43**, 870–873.

IWAGAMI, N. and OGAWA, T. (1980): An Antarctic NO density profile deduced from the gamma band airglow. Planet. Space Sci., **28**, 867–873.

IWAGAMI, N. and OGAWA, T. (1981): NO γ band airglow radiometer with a self-absorbing gas cell. to be published in Appl. Opt., **20**.

JACCHIA, L. G. (1971): Revised static models of the thermosphere and exosphere with empirical temperature profiles. Smithson. Astrophys. Obs., SP-332.

JONES, R. A. and REES, M. H. (1973): Time dependent studies of the aurora–I. Ion density and composition. Plancet. Space Sci., **21**, 537–557.

KAMIYAMA, H. (1966): Ionization and excitation by precipitating electrons. Rep. Ionos. Space. Res. Jpn, **20**, 171–187.

KONDO, Y. and OGAWA, T. (1976): Odd nitrogen in the lower thermosphere under auroral perturbations. J. Geomagn. Geoelectr., **28**, 253–282.

KONDO, Y. and OGAWA, T. (1977): A temperature dependent model of the thermospheric distribution of odd nitrogen. J. Geomagn. Geoelectr., **29**, 65–82.

KRASSOVSKY, V. I., SHEFOV, N. N. and YARIN, V. I. (1962): Atlas of the airglow spectrum 3000–12400 Å. Planet. Space Sci., **9**, 883–915.

LIN, C. L. and KAUFMAN, F. (1971): Reactions of metastable nitrogen atoms. J. Chem. Phys., **55**, 3760–3770.

LLEWELLYN, E. J., LONG, B. H. and SOLHEIM, B. H. (1978): The quenching of OH* in the atmosphere. Planet. Space Sci., **26**, 525–531.

MARR, G. V. (1964): Electronic transition moments and their effects on the band strengths and absorption oscillator strengths of the NO β and γ systems. Proc. Phys. Soc., **83**, 293–300.

MCEWEN, D. J. and VENKATARANGAN, P. (1978): Electron flux and auroral intensity measurements in situ. Geophys. Res. Lett., **5**, 1051–1054.

MCFARLAND, M., ALBRITTON, D. L., FEHSENFELD, F. C., FERGUSON, E. E. and SCHMELTEKOPF, A. L. (1973): Flow-drift technique for ion mobility and ion-molecule reaction rate constant measurements 2. Positive ion reactions of N^+, O^+, and N_2^+ with O_2 and O^+ with N_2 from thermal to $\sim$2 eV. J. Chem. Phys., **59**, 6620–6628.

MCGREGOR, W. K., FEW, J. D., KEEFER, D. R., LOWRY, H. S. and DAVIS, M. G. (1980): Note of the correction: Broadening of NO γ-band lines. J. Quant. Spectrosc. Radiat. Transfer, **23**, 527–530.

MEIRA, L. G. (1971): Rocket measurements of upper atmospheric nitric oxide and their consequences to the lower ionosphere. J. Geophys. Res., **76**, 202–212.

MENG, C.-I. (1978): Electron precipitations and polar auroras. Space Sci. Rev., **22**, 223–230.

MENG, C.-I. (1979): Electron precipitation of evening diffuse aurora and its conjugate electron fluxes near the magnetospheric equator. J. Geophys. Res., **84**, 2545–2558.

MOREELS, G., CHAHROKHI, D. and BLAMONT, J. E. (1976): OH emission intensity measurements during the 1969 NASA airborne auroral expedition. J. Geophys. Res., **81**, 5476–5478.

NARCISI, R. S., SHERMAN, C., WLODYKA, L. E. and ULWICK, J. C. (1974): Ion composition in an IBC class II aurora 1. Measurements. J. Geophys. Res., **79**, 2843–2847.

NICHOLLS, R. W. (1964): Frank-Condon factors to high vibrational quantum numbers IV: NO band systems. J. Res. Nat. Bur. Stand., **68A**, 535–540.

NICOLET, M. (1945): Contribution á l'étude de la structure de l'ionosphére. Inst. R. Météorol. Belg. Mém., **19**, 169.

NICOLET, M. (1960): Aeronomic chemical reactions. Physics and Medicine of the Atmosphere and Space, ed. by O. O. BENSON and H. STRUGHOLD. New York, John Wiley.

NICOLET, M. (1965a): Nitrogen oxides in the chemosphere. J. Geophys. Res., **70**, 679–689.

NICOLET, M. (1965b): Ionospheric processes and nitric oxide. J. Geophys. Res., **70**, 691–701.

NORTON, R. B. and BARTH, C. A. (1970): Theory of nitric oxide in the earth's atmosphere. J. Geophys. Res., **75**, 3903–3909.

OGAWA, T. and SHIMAZAKI, T. (1975): Diurnal variations of odd nitrogen and ionic densities in the mesosphere and lower thermosphere: Simultaneous solution of photochemical-diffusive equations. J. Geophys. Res., **80**, 3945–3960.

OGAWA, T. and KONDO, Y. (1977): Diurnal variability of thermospheric N and NO. Planet. Space Sci., **25**, 735–742.

ORAN, E. S., JULIENNE, P. S. and STROBEL, D. F. (1975): The aeronomy of odd nitrogen in the thermosphere. J. Geophys. Res., **80**, 3068–3076.

PEARCE, J. B. (1969): Nitric oxide gamma band emission rate factor. J. Quant. Spectrosc. Radiat. Transfer, **9**, 1593–1602.

PENMAN, J. M., HARGREAVES, J. K. and MCILWAIN, C. E. (1979): The relation between 10 to 80 keV electron precipitation observed at geosynchronous orbit and auroral radio absorption observed with riometers. Planet. Space Sci., **27**, 445–451.

POLAND, H. M. and BROIDA, H. P. (1971): Fluorescence of the γ, ε and δ systems of nitric oxide: Polarization and use of calculated intensities for spectrometer calibration. J. Quant. Spectrosc. Radiat. Transfer, **11**, 1863–1876.

REES, M. H. (1963): Auroral ionization and excitation by incident energetic electrons. Planet. Space Sci., **11**, 1209–1217.

REES, M. H. (1969): Auroral electrons. Space Sci. Rev., **10**, 413–441.

REES, M. H. and ROBLE, R. G. (1979): The morphology of N and NO in auroral substorms. Planet. Space Sci., **27**, 453–462.

ROACH, F. E. and MEGILL, L. R. (1961): Integrated starlight over the sky. Astrophys. J., **133**, 228–242.

ROBLE, R. G. and REES, M. H. (1977): Time-dependent study of the aurora: Effects of particle precipitation on the dynamic morphology of ionospheric and atmospheric properties. Planet. Space Sci., **25**, 991–1010.

RUSCH, D. W. (1973): Satellite ultraviolet measurements of nitric oxide fluorescence with a diffusive transport model. J. Geophys. Res., **78**, 5676–5689.

RUSCH, D. W. and BARTH, C. A. (1975): Satellite measurements of nitric oxide in the polar region. J. Geophys. Res., **80**, 3719–3721.

RUSCH, D. W., STEWART, A. I., HAYS, P. B. and HOFFMAN, J. H. (1975): The NI (5200 Å) dayglow. J. Geophys. Res., **80**, 2300–2304.

SAMSON, J. A. R. (1967): Techniques of Vacuum Ultraviolet Spectroscopy. New York, John Wiley, 212–224.

SHARP, W. E. (1978): The ultraviolet aurora: The spectrum between 2100 Å and 2300 Å. Geophys. Res. Lett., **5**, 703–705.

SHARP, W. E. and REES, M. H. (1972): Auroral spectrum between 1200 and 4000 Å. J. Geophys. Res., **77**, 1810–1819.

SMITH, F. L. and SMITH, C. (1972): Numerical evaluation of Chapman's grazing incidence integral $ch(X, \chi)$. J. Geophys. Res., **77**, 3592–3597.

STEWART, A. I. and CRAVENS, T. E. (1978): Diurnal and seasonal effects in E region low-latitude nitric oxide. J. Geophys. Res., **83**, 2453–2456.

STROBEL, D. F., HUNTEN, D. M. and MCELROY, M. B. (1970): Production and diffusion of nitric oxide. J. Geophys. Res., **75**, 4307–4321.

STROBEL, D. F. (1971): Diurnal variation of nitric oxide in the upper atmosphere. J. Geophys. Res., **76**, 2441–2452.

STROBEL, D. F. (1972): Nitric oxide in the D region. J. Geophys. Res., **77**, 1337–1339.

STROBEL, D. F., ORAN, E. S. and FELDMAN, P. D. (1976): The aeronomy of odd nitrogen in the thermosphere 2. Twilight emissions. J. Geophys. Res., **81**, 3745–3752.

SWIDER, W. (1978): Daytime nitric oxide at the base of the thermosphere. J. Geophys. Res., **83**, 4407–4410.

THEKAEKARA, M. P. (1974): Extraterrestrial solar spectrum, 3000–6100 Å at 1–Å intervals. Appl. Opt., **13**, 518–522.

THOMAS, R. J. (1978): A high-altitude rocket measurement of nitric oxide. J. Geophys. Res., **83**, 513–516.

TISONE, G. C. (1973): Measurement of NO densities during sunrise at Kauai. J. Geophys. Res., **78**, 746–750.

TOHMATSU, T. and OGAWA, T. (1966): Theoretical studies of the airglow resonant emission transfer. Rep. Ionos. Space Res. Jpn, **20**, 418–438.

TOHMATSU, T. and IWAGAMI, N. (1975): Measurement of nitric oxide distribution in the upper atmosphere. Space Res., **15**, 241–245.

TOHMATSU, T. and IWAGAMI, N. (1976): Measurement of nitric oxide abundance in equatorial upper atmosphere. J. Geomagn. Geoelectr., **28**, 343–358.

TOHMATSU, T. and YAMAMOTO, H. (1976): Radiative transfer of atomic and molecular resonant emissions in the upper atmosphere I. Basic theories in Doppler-broadening atmosphere. J. Geomagn. Geoelectr., **28**, 437–460.

TORR, M. R., BURNSIDE, R. G., HAYS, P. B., STEWART, A. I., TORR, D. G. and WALKER, J. C. G. (1976): Metastable ^2D atomic nitrogen in the midlatitude nocturnal ionosphere. J. Geophys. Res., **81**, 531–537.

TORR, M. R., TORR, D. G., ONG, R. A. and HINTEREGGER, H. E. (1979): Ionization frequencies for major thermospheric constituents as a function of solar cycle 21. Geophys. Res. Lett., **6**, 771–774.

TRINKS, H., VON ZAHN, U., BARTH, C. A. and KELLY, K. K. (1978): A joint nitric oxide measurement by rocket-borne ultraviolet photometer and mass spectrometer in the lower thermosphere. J. Geophys. Res., **83**., 203–206.

VALLANCE JONES, A. (1973): The infrared spectrum of the airglow. Space Sci. Rev., **15**, 355–400.

WALKER, J. C. G., BRACE, L. H. and REES, M. H. (1968): Langmuir probe evidence for a nocturnal ionization source at Fort Churchill. J. Geophys Res., **73**, 7285–7290.

WALLACE, L. and MCELROY, M. B. (1966): The visual dayglow. Planet. Space Sci., **14**, 677–708.

WATANABE, T. and TOHMATSU, T. (1976): An observational evidence for the seasonal variation of ozone concentration in the upper stratosphere and the mesosphere. Rep. Ionos. Space Res. Jpn, **30**, 47–50.

WEILL, G. M. (1968): NI(^4S–^2D) radiation in the night airglow and low latitude aurora. Atmospheric Emissions, ed. by M. B. MCCORMAC and A. OMHOLT. New York, Van Nostrand Reinhold, 440–470.

WITT, G., DYE, J. E. and WILHELM, N. (1976): Rocket-borne measurements of scattered sunlight in the mesosphere. J. Atmos. Terr. Phys., **38**, 223–238.

WOFSY, S. C. and MCELROY, M. B. (1977): Auroral recombination of N and O: A possible source for emission in the γ and δ bands of NO. Planet. Space Sci., **25**, 1021–1026.

ZIPF, E. C., BORST, W. L. and DONAHUE, T. M. (1970): A mass spectrometer observation of NO in an auroral arc. J. Geophys. Res., **75**, 6371–6376.

(*Manuscript received February 14, 1981;*
Revised manuscript received April 2, 1981)